Predictive analytics and multimodal imaging-guided decision-making in neurosurgery

Jeremy T. Moreau

Integrated Program in Neuroscience

Department of Neurology and Neurosurgery

Faculty of Medicine, McGill University, Montreal

February 2020

A thesis submitted to McGill University in partial fulfilment of the requirements of the degree of Doctor of Philosophy

Contents

Abstract

Neurosurgical decision-making is guided by surgical experience and supported by a vast array of tools used in the presurgical evaluation. In this thesis, I examine how predictive analytics and multimodal imaging can contribute to diagnosis and prognosis in neuro-oncology and to the presurgical evaluation for drug-resistant epilepsy. I present new machine learning models and a practical app for predicting meningioma malignancy and survival (chapter 2). I additionally discuss some key ethical issues relating to the application of artificial intelligence (AI) in medical diagnostics (chapter 3), including how AI systems remain biased by the same sociocultural biases that shape the datasets these systems are trained on. In relation to multimodal imaging in epilepsy surgery, in chapter 4 I introduce a new open-source software application for computing subtraction ictal single-photon emission CT coregistered to MRI (SISCOM). In chapter 5, I discuss the analysis and interpretation of ictal magnetoencephalography (MEG) in two case reports of the first patients we recorded sleeping overnight in the MEG. Finally, in chapter 6 I present the results of a study investigating the potential of a series of imaging modalities (PET, SPECT, diffusion-weighted MRI, and MEG) in helping localise and differentiate a recently characterised histopathological entity, oligodendroglial hyperplasia, from focal cortical dysplasia. These studies together offer new hypotheses and directions of investigation that could lead to more quantitative tools to guide neurosurgical decision-making and improved patient outcomes.

Résumé

La prise de décision en neurochirurgie est guidée par l'expérience chirurgicale et soutenue par une vaste gamme d'outils utilisés dans l'évaluation préchirurgicale. Dans cette thèse, j'examine comment l'analyse prédictive et l'imagerie multimodale peuvent contribuer au diagnostic et au pronostic en neuro-oncologie et à l'évaluation préchirurgicale de l'épilepsie pharmacorésistante. Je présente de nouveaux modèles d'apprentissage statistique et une application pour la prédiction de la malignité des méningiomes et les statistiques de survie associées (chapitre 2). J'aborde également certains enjeux éthiques liés à l'application de l'intelligence artificielle (IA) aux diagnostics médicaux (chapitre 3), notamment la manière dont les systèmes d'IA peuvent être biaisés par les mêmes préjugés socioculturels qui façonnent les ensembles de données sur lesquels ces systèmes sont entraînés. En ce qui concerne l'imagerie multimodale appliquée à la chirurgie pour l'épilepsie, je présente dans le chapitre 4 une nouvelle application logicielle à code source ouvert pour l'étude individuelle de la tomographie par émission monophonique critique–intercritique (SISCOM). Dans le chapitre 5, j'aborde l'analyse et l'interprétation de la magnétoencéphalographie (MEG) critique dans les deux premiers patients que nous avons enregistrés au cours d'une nuit pendant qu'ils dormaient dans la MEG. Finalement, dans le chapitre 6, je présente les résultats d'une étude sur le potentiel d'une approche basée sur l'imagerie multimodale (TEP, TEMP, IRM de diffusion et MEG) pour aider à localiser et à différencier une entité

histopathologique récemment caractérisée, l'hyperplasie oligodendrogliale, de la dysplasie corticale focale. Ensemble, ces études offrent de nouvelles hypothèses et directions de recherche qui pourraient conduire à des outils plus quantitatifs pour guider la prise de décision en neurochirurgie et améliorer les résultats chirurgicaux.

Original contributions

Chapters 2, 3, 4, 5, and 6 constitute original scholarship and are published (chapter 2) or have been submitted for publication and are currently under review (Chapters 3-6).

In chapter 1, I introduce the rationale for this thesis and discuss the relevant literature. I further provide a concise overview of the background knowledge relating to the work presented in this thesis.

Chapter 2 describes original work on new machine learning models designed to assist with the diagnosis and prognosis of meningiomas. The study represents, to our knowledge, the first application of these methods to the meningioma cases from the Surveillance, Epidemiology, and End Results population-based US registry (>60,000 patients). I additionally extended previous work on balanced ensemble classifiers with the Balanced Logistic Regression-Random Forests (BLR-RF) model presented in this paper. Finally, I programmed a new smartphone web app to accompany the manuscript. The code of this app is made freely available under an open-source licence (https://github.com/jeremymoreau/meningioma).

Chapter 3 is a commentary on ethical issues relating to some less discussed aspects of the application of artificial intelligence (AI) to medical diagnostics. In this chapter, I report original statistics on geographical disparities in funding and publication output in the field of AI-assisted medical diagnostics. I also provide theoretical case examples and discuss recent notable instances of possible systemic bias in machine learning classifiers used in this context.

Chapter 4 describes a new software program I wrote for computing subtraction ictal single-photon emission CT coregistered to MRI (SISCOM). SISCOM is a well-established technique for quantitative analysis of ictal vs interictal SPECT images [1], but the implementation of the software is entirely new and is intended to offer a user-friendly tool to perform these analyses. The code of this app is made freely available under an open-source licence (https://github.com/jeremymoreau/mnisiscom).

Chapter 5 presents two new case reports of children with drug-resistant epilepsy in whom we recorded seizures while they underwent an overnight magnetoencephalography (MEG) recording. This is to our knowledge, the first published report of ictal recordings in children who spent a night sleeping in the MEG.

Chapter 6 describes original results from a study on multimodal imaging performed in a group of drug-resistant epilepsy patients in whom we identified a newly characterised histopathological entity, oligodendroglial hyperplasia (OH). In this study we provided the first evidence, to our knowledge, that OH can be radiologically differentiated from focal cortical dysplasia type II using diffusion-weighted MRI. We further demonstrate that fluorodeoxyglucose positron emission tomography (FDG PET) and MEG imaging of focal slowing could also be particularly valuable in localising OH.

Finally, chapter 7 provides a general discussion of the results in chapters 2-6. I discuss the overall objectives met in the thesis as well as potential paths for future developments. I also provide a brief summary of the overall findings presented in the thesis and final conclusions on the aggregate body of work.

Contribution of authors

Chapter 2: Individual-patient prediction of meningioma malignancy and survival using the Surveillance, Epidemiology, and End Results database

JTM: Conception and design, data and statistical analyses, app development, figures, drafting the manuscript, critically revising the manuscript. TCH: Supervision, critically revising the manuscript. SB: Supervision, funding and administration, critically revising the manuscript. RWRD: Conception and design, supervision, drafting the manuscript, funding and administration, critically revising the manuscript.

Chapter 3: Biased intelligence: on the subjectivity of digital objectivity

JTM: Drafting the manuscript, literature review, data analysis, figures. S.B: Supervision, funding and administration, critically revising the manuscript. R.W.R.D: Supervision, funding and administration, critically revising the manuscript.

Chapter 4: MNI SISCOM: An open-source tool for computing subtraction ictal single-photon emission CT coregistered to MRI

JTM: Conception and design, app development, figures, drafting the manuscript, critically revising the manuscript. CSM: Supervision, critically revising the manuscript. SB: Supervision, funding and administration, critically revising the manuscript. RWRD: Conception and design, supervision, drafting the manuscript, funding and administration, critically revising the manuscript.

Chapter 5: Overnight Ictal Magnetoencephalography

JTM: Design and conceptualisation of the study, major role in the acquisition of data, analysis and interpretation of the data, drafted and revised the manuscript for intellectual content. EST: Analysis and interpretation of the data, revised the manuscript for intellectual content. SA: Analysis and interpretation of the data, revised the manuscript for intellectual content. BR: Design and conceptualization of the study, revised the manuscript for intellectual content. SB: Design and conceptualization of the study, revised the manuscript for intellectual content. RWRD: Design and conceptualization of the study, major role in the acquisition of data, analysis and interpretation of the data, drafted and revised the manuscript for intellectual content.

Chapter 6: Localisation of oligodendroglial hyperplasia and differentiation from focal cortical dysplasia type II with multimodal imaging

JTM wrote the first draft and made the figures. JTM and RWRD designed the project and experimental design. JTM, RV, EST, SA, CSM, and RWRD participated in data acquisition, analysis, or interpretation of data. All authors participated in critically revising the article with respect to intellectual content and approved the final manuscript version to be published. JTM was supervised by SB and RWRD.

Acknowledgements

The contributions of the people involved in each of the manuscripts composing this thesis is given in the "Contribution of authors" section above. All the work conducted as part of this thesis has been supervised by Dr Roy Dudley and Dr Sylvain Baillet.

I would like to thank Dr Dudley for being an amazing supervisor, a friend, and all-around great guy. It has probably been the greatest to stroke of luck of my PhD to meet Dr Dudley early on in the course of my degree. I thank him for inspiring me in all my work, for replying to my emails at 3am in the morning, and for always being so encouraging. I would not be where I stand today if not for his guidance and support. I am truly and forever grateful to have been able to work with Dr Dudley.

I thank Dr Baillet for being another great guy, for his energy and enthusiasm, and for the supportive lab environment he created. Dr Baillet always backed me up in my endeavours and has provided me with so many opportunities throughout my PhD. I thank him for going along with all the crazy ideas (and generating more!) and for all the great fun in these past few years at the lab.

I thank Dr Elisabeth Simard-Tremblay for teaching me to read EEG and for all the time she volunteered reviewing MEG and EEG with me. I thank her for her kindness and for always supporting me in my goals.

I am thankful to Elizabeth Bock and Marc Lalancette for saving the day every time I ran into problems with the MEG and in general for being fun people to be around.

I thank François Tadel and Martin Cousineau for all the bugs they fixed, features they added, and help they gave me with Brainstorm.

I thank my committee members Sébastien Jacquemont and Alexandre Lehmann for all their advice at my yearly advisory meetings.

I thank Dr Christine Saint-Martin for the time she spent reviewing imaging with me and Dr Bernard Rosenblatt for getting me started on the path of EEG. I thank Dr Wilson and Dr Hadeel Eid for the many useful conversations. I thank Dr Guiomar Niso for her help at the beginning of my PhD and on the many collaborations. I thank Patricia Tomaszewski for her help in acquiring MEG data. I thank Dr Jean Gotman for letting me attend his lab meetings and teaching me many things about epilepsy. I thank Dr François Dubeau for the time he spent reviewing cases with me and for the many useful discussions. I thank Dr Hui Ming Khoo for her help with reviewing SEEG. I thank Dr Eliane Kobayashi for inviting me to her EEG and Epilepsy seminars and for what she has taught me. I thank Nassima Addour for her help in scheduling patients. I am thankful to the patients and families I met at the Montreal Children's and Montreal Neurological Institute who have volunteered their time and taught me so much over the years.

I am thankful to the *Fonds de recherche du Québec – Santé*, the Foundation of Stars, the Healthy Brains, Healthy Lives initiative, Dr Bruce Williams, and Joan Chippindale for funding the PhD fellowships and awards that have supported my work.

Finally, I am thankful to my family who has always been there for me and to all my friends in the lab who have made these past years such an enjoyable and unforgettable time!

List of figures and tables

Figures

Supplementary figures

Tables

List of abbreviations

ADC	apparent diffusion coefficient
AED	antiepileptic drug
AI	artificial intelligence
AMT	α-[(11)C]-methyl-L-tryptophan
AP	average precision
AUC	area under the receiver operating characteristic curve
BLR	balanced logistic regression
BRF	balanced random forest
CI	confidence interval
CNS	central nervous system
CT	computerised tomography
DICOM	digital imaging and communications in medicine (image format)
DKI	diffusion kurtosis imaging
DTI	diffusion tensor imaging
DWI	diffusion-weighted imaging
ECD	ethyl cysteinate dimer
EEG	electroencephalogram
EMSI	electromagnetic source imaging
ESI	electrical source imaging
EZ	epileptogenic zone
FCD	focal cortical dysplasia
FDG	fluorodeoxyglucose
FDZ	functional deficit zone
FLAIR	fluid-attenuated inversion recovery
FSL	FMRIB Software Library
GRE	gradient echo
HARDI	high angular resolution diffusion imaging
HS	hippocampal sclerosis
Hz	hertz (1/s)
ICD	international classification of diseases
IED	interictal epileptiform discharges
IQ	intelligence quotient

IZ	irritative zone
KHz	kilohertz (1000/s)
KNN	k-nearest neighbours
LR	logistic regression
LZ	lesional zone
MEG	magnetoencephalography
MRI	magnetic resonance imaging
MSI	magnetic source imaging
NIfTI	neuroimaging informatics technology initiative (image format)
NOS	not otherwise specified
NPV	negative predictive value
OH	oligodendroglial hyperplasia
OLC	oligodendroglial-like cells
OR	odds ratio
PACS	picture archiving and communication system
PET	positron emission tomography
PPV	positive predictive value
QOL	quality of life
RF	random forests
ROC	receiver operating characteristic
SD	standard deviation
SEEG	stereoelectroencephalography
SEER	surveillance, epidemiology, and end results program
SISCOM	subtraction ictal single-photon emission CT coregistered to MRI
SMA	supplementary motor area
SOZ	seizure onset zone
SPECT	single-photon emission computed tomography
SPM	statistical parametric mapping
STATISCOM	statistical ictal SPECT coregistered to MRI
WHO	world health organisation

1

Chapter 1 – Introduction

I would like to see the day when somebody would be appointed surgeon somewhere who had no hands, for the operative part is the least part of the work.

– Harvey W. Cushing

The first task of neurosurgery is to identify which patients to operate, and which patients not to operate. Then, one must decide what needs to be resected, and indeed, what must not be resected. While conceptually simple, these two tasks require considerable preparation and forethought. This decision-making process is made based on the surgeon's experience and informed by an increasingly sophisticated armamentarium of tools including multimodal preoperative imaging [2,3], intraoperative imaging [4] and neurophysiological monitoring [5], and neuronavigation [6,7]. The range of available instruments continues to advance, and new developments in artificial intelligence (AI) [8–10] and novel applications of imaging [3,11] are improving patient outcomes and helping streamline preoperative neurosurgical planning. The overarching aim of this thesis is to assist with this decision-making process. I focus specifically on applications of these methods to the presurgical evaluation in neuro-oncology (chapter 2) and epilepsy surgery (chapters 4-6).

The thesis is structured in two major parts. The first discusses applications of machine learning to basic clinical data to aid with the diagnosis and prognosis of meningiomas, as well as some of the ethical considerations involved with the application of AI to medical diagnostics. The second deals specifically with novel approaches in applying multimodal imaging in the presurgical evaluation of children with drug-resistant epilepsy. A major aim of the thesis is also to provide a path to translatability by providing software tools to aid with the presurgical evaluation, whenever relevant. In the next sections, I provide some general context and background on prior work investigating ways in which AI and multimodal imaging can assist in the presurgical evaluation. These topics are necessarily broad in scope and I therefore aim in particular to reference key developments in the field and provide background knowledge of fundamental concepts discussed in later chapters.

Predictive analytics

The term "predictive analytics" encompasses a broad range of statistical techniques including machine learning, deep learning, AI, as well as more traditional methods such as linear and logistic regression [12]. In general terms, the overall aim of predictive analytics is to use past data to make predictions about the future [12]. As applied to medical diagnostics, purpose of predictive analytics is to provide health outcome predictions for individual patients (or groups of patients in the case of public health) based on a body of historical patient data [13]. The terms machine learning, deep learning, and

AI are frequently used somewhat interchangeably, but there are some notable differences. It could be said that AI is the broadest category which encompasses both machine learning and deep learning, while deep learning itself represents a subset of techniques falling under the category of machine learning.

AI refers simply to any computer-based decision-making system. Early AI systems relied on pre-programmed directives manually written by a human programmer (e.g. if tumour size > 50 mm, diagnosis = "malignant"). So-called "expert systems" were initially the subject of great enthusiasm in the 1960s and early 1970s [14], but failed to live up to initial expectations in applications to healthcare [15] and many other fields [16]. Different explanations for this failure have been discussed, including social factors and technological limitations [15], but one major drawback of these early AI systems was the inability of rule-based decision-making to successfully account for and adapt to the uncertain, incomplete, and "messy" data that characterise real-world clinical problems. The dampening of this initial enthusiasm led to the first "AI winter" in the 1980s, which was characterised by funding cuts and diminished research output in the field of artificial intelligence research [17].

In contrast to these early developments, the recent resurgence of interest in AI has for the most part been characterised by the application of automated "machine learning" algorithms. Unlike rule-based decision-making systems, these algorithms are never explicitly instructed on how to solve a problem, but rather are designed to learn solutions from vast numbers of case examples [10]. Deep learning refers to a subset of machine learning methods, artificial neural networks with many intermediary layers,

that have been found to be particularly suitable for dealing with large datasets of unstructured data [18]. The decision on whether "deep learning" or other machine learning methods are more suitable for any given problem depends mostly on the type of data one needs to work with. For instance, deep learning would be a better choice if the input data consisted of thousands of MRI scans of patients with a brain tumour. On the other hand, more classical machine learning methods, such as support vector machines or random forests [12], are typically preferable when dealing with more structured information. The basic clinical variables used in the models discussed in chapter 2 (e.g. tumour size and location, age, type of surgery) are an example of these kinds of more structured datasets. In either case, machine learning algorithms for the most part fall under two general categories based on the type of question they are used to answer, supervised and unsupervised learning.

Supervised machine learning

As an analogy, take a first-year radiology resident. Throughout their residency they will be exposed to thousands of scans and will be required to dictate reports under the supervision of a staff radiologist. The staff radiologist will tell the resident when they are right or wrong, thus shaping and gradually improving the resident's internal diagnostic "model". Supervised machine learning works around the same principle. The model is trained on thousands of examples for which the correct answer is known (e.g. 1000 images of dogs and cats, with labels indicating whether the image is of a dog or a cat), and then asked to make predictions for unlabelled examples. The performance of the model is then judged based on the accuracy of these predictions. Supervised

learning represents the bulk of the research on applications of machine to medical diagnostics [19], and is also the type of machine learning discussed in chapter 2.

Unsupervised machine learning

Returning, to our analogy, take again our first-year radiology resident who is this time tasked with looking at 1000 MRIs of patients with a meningioma and then grouping them into 3 different categories based on appearance. There are many ways they could decide to perform this task. They could decide to classify the tumours based on size, on localisation, or any other imaging characteristics. The only defining characteristic of each of the 3 groups is that the meningiomas within each group would be similar to each other in some way. Unsupervised machine learning is as the name suggests, "unsupervised", in the sense that no labelled training examples are provided. Unsupervised learning can help find natural groupings in datasets and is often also used as a method of selecting relevant features (i.e. predictor/independent variables) of interest to be used in further analyses [20]. As an example of unsupervised learning in practice, one study used these methods to find general groupings of research topics (e.g. clinical, pain, tumour, complications) in spine surgery by automatically clustering 38 years of spine-related literature [21].

Applications of machine learning in neurosurgery

Research interest in applications of machine learning in medicine has grown exponentially in the past 5-years (see chapter 3, Fig. 3-1 for reference). Neurosurgery has been no exception. Applications in neurosurgery have included diagnosing and grading

brain tumours [22–26], localising epileptogenic cortex [27–31], evaluating surgical performance [32], and predicting post-surgical outcomes [9,33–35]. Particularly exciting recent developments include one study that used machine learning to provide near real-time intra-operative brain tumour diagnosis that was non-inferior to pathologists' interpretations of standard histological images [26]. Another study developed an AI-system designed to analyse CT images to help triage acute neurological events, such as stroke and hydrocephalus, in order to predict urgency and reduce time to diagnosis and treatment [36]. While human radiologists still had greater accuracy, the AI in this study was 150 times faster in providing an interpretation of the CT study (1.2s vs. 177s on average) [36]. With continued model refinements and increasingly large datasets on which to train machine learning systems, we can expect that these kinds of tools will start making progressively greater impact in everyday neurosurgical care within the next decade [9,37–39]. It is most likely that this contribution will come in the form of a partnership between human and machine, whereby AI can help provide rapid and accurate diagnostic and prognostic workflows, thereby freeing time for human physicians and surgeons to focus on other tasks [8].

AI already contributes to timesaving in small everyday tasks such as by enabling the speech-to-text conversion in dictation software or by sorting out junk email messages from our inboxes. One key characteristic of many of the already successful real-world applications of machine learning has been the very big datasets available to train these models. For instance, AlphaGo, the first AI to beat the human world champion at the game of Go, was initially trained on a database of over 29 million positions from

160,000 games played by high-ranking human players [40]. A similar trend can be observed in studies applying machine learning in neurosurgery. The AI models trained in the first study on intraoperative brain tumour diagnosis cited above for example was trained using over 2.5 million histological specimen samples, while the second study on CT-based triaging of acute neurological events was trained on a dataset of over 30,000 CT images. While AI can be successful without "big data" [41], large datasets do often improve model performance. Indeed, in many practical scenarios, simply collecting more—and more diverse—data often yields better results than what can be achieved by algorithmic tweaking alone. Thankfully, healthcare data is not a scarce resource. One estimate put the total volume of healthcare data in 2013 at 153 exabytes (1 exabyte = 1 million terabytes, 1 terabyte ≈ 100,000 1mm isotropic T1 MRIs) and projected that that number could reach 2,314 exabytes by 2020 [42]. The challenge, however, remains in curating these data in usable and accessible formats to enable AI research. Much of healthcare data consists of unstructured information (notes, charts, etc.) stored on a vast array of various, often incompatible, electronic health records and picture archiving and communication systems [10,43,44]. Some of the early work I contributed to in this PhD [45–48] had for aim to help in this data consolidation effort, but still larger-scale collaborations and policy discussions will need to be had in order to unlock the maximum potential for impact of these data.

Finally, I feel we must consider the ethical implications of machine learning and big data as applied to neurosurgery and healthcare in general. While the development

of new AI has tremendous potential to impact patient care, reduce wait times, and improve outcomes, there have been valid criticisms of how some of this new technology is being introduced [49–51]. Concerns have been raised around issues of consent [52,53], privacy [54,55], and data ownership [55–57]. A more in-depth discussion of some of these aspects is given in chapter 3.

Paediatric epilepsy surgery

Epilepsy affects over 10 million children worldwide, and about a third of those requiring therapy will fail to respond to pharmacological treatment [58]. Resection of epileptogenic tissue can eliminate or decrease seizure frequency [59] in many of these patients. Moreover, early treatment in children is associated with better cognitive and developmental outcomes [60,61]. Quick and accurate presurgical evaluation is thus crucial.

Definitions

A number of terms are commonly used in discussing the presurgical evaluation for drug-resistant epilepsy. First, drug-resistance is typically defined as having failed two or more appropriately-selected antiepileptic drugs (AED), after which the chances of a third AED controlling seizures is greatly reduced [62]. Key concepts also include the epileptogenic zone, seizure onset zone, and irritative zone, which are illustrated in Fig. 1-1 below.

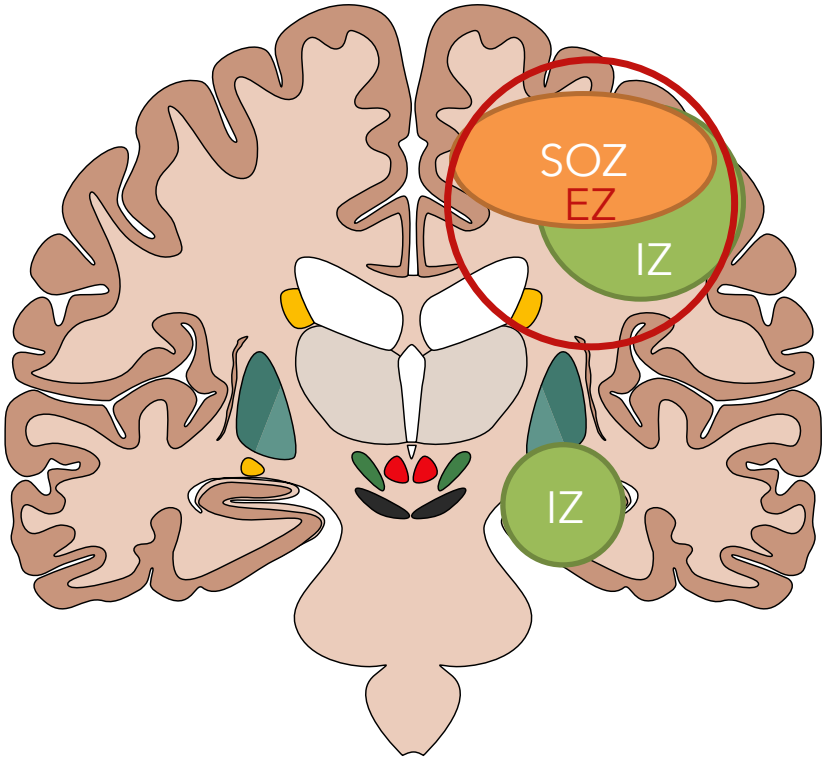

Fig. 1-1 The epileptogenic, seizure onset, and irritative zones. EZ: Epileptogenic zone, SOZ: Seizure Onset Zone, IZ: Irritative zone. Original illustration based on anatomical photographs by Crawford & McBurney [63]

The epileptogenic zone (EZ) is defined as the area of cortex that needs to be resected in order for the patient to achieve seizure freedom [64]. It is a theoretical concept in the sense that there is presently no perfect way of delineating the EZ [64]. Whether or not an EZ truly exists in all focal epilepsy patients remains a matter of debate, and ongoing research on the concept of epileptic "networks" [65-68] may provide further insight into why some patients fail to achieve seizure freedom post-surgery. In the present day,

however, the aphorism, "you can't resect a network" still holds and the EZ provides a practical, if perhaps limited, conceptual framework in guiding the presurgical evaluation. While the EZ remains a theoretical concept, the seizure onset zone (SOZ) corresponds, more tangibly, to the area of cortex from which seizures arise [64]. The SOZ can be grossly localised on the basis of ictal scalp EEG or, more precisely, with the help of invasive stereo-EEG (SEEG) or subdural grids [64]. Ictal magnetoencephalography, discussed in chapter 6, could also be a way to more precisely define the SOZ noninvasively [69]. Similarly to the SOZ, the irritative zone (IZ) corresponds to area of cortex from which interictal epileptiform discharges (IEDs, "spikes") arise. While the IZ generally overlaps with the SOZ, it can involve a more extensive area of cortex or, at times, even include secondary areas at a distance from the SOZ [70]. The IZ is still valuable in approximating the EZ, but the SOZ is generally considered the gold standard [64]. In addition to the SOZ and IZ, two additional zones worth mentioning are the lesional zone (LZ) and the functional deficit zone (FDZ). The LZ corresponds to the area in which a structural lesion is visible (typically as viewed on MRI), whereas the FDZ relates to the area of cortex that is functionally abnormal in the interictal period (typically as measured by ^{18}F-FDG PET hypometabolism or SPECT hypoperfusion). Finally, the expression "eloquent cortex" is often used to refer to areas of cortex which if resected would lead to severe neurological deficits (e.g. language, vision, motor function, etc.) [64,71,72].

Outcomes

The first randomised control trial of surgery in children with drug-resistant epilepsy showed that patients who underwent epilepsy surgery had, at 12 months postop,

higher rates of seizure freedom (77%) than patients in the medical-therapy group (7%) and also scored significantly better on measures of behaviour and quality of life [73]. This is consistent with the results of a recent systematic review and meta-analysis, which included 258 studies, and concluded that the odds ratio (OR) of seizure freedom for surgery vs. medical therapy was 6.49 [74]. This meta-analysis reported seizure freedom rates of 64.8% at 1-year postop and 60.3% at 5-years postop [74]. Seizure freedom rates were greater for hemispheric surgery (74.7%) and temporal lobe surgery (73.3%) than for extratemporal surgical cases (60.2%). Likewise, tumours (79.8%) and mesial temporal sclerosis (77.9%) had the highest rates of seizure freedom, while malformations of cortical development had reported seizure-free percentages of 57.1% [74].

While seizure-freedom remains the most reported outcome, a growing number of studies have recognised the importance of measuring the impact of surgery on cognition, behaviour, and quality of life (QOL). One recent meta-analysis found that children who achieved seizure-freedom had significantly improved QOL post-operatively or as compared to medically treated controls [75]. The study further found an average 2.26-point intelligence quotient (IQ) increase postop as compared to preop and a 10.61-point increase as compared to medically treated controls (pooled OR of 9.51 for IQ improvement in surgically vs. medically treated patients) [75]. Further studies have reported that earlier surgical treatment in children is associated with better cognitive and developmental outcomes [60,61,70]

Multimodal imaging & electrophysiology in drug-resistant epilepsy

On October 1st, 1971 at Atkinson Morley's Hospital in London, England, a woman with a suspected brain tumour underwent the first human CT scan on an experimental scanner devised by British engineer Godfrey Hounsfield [76,77]. The acquired image was only 80 × 80 pixels in size and took almost five minutes to produce, but this event would mark the beginning of a new era in neurology and neurosurgery. The first large case-series of CT in epilepsy were reported by Gastaut et al. in 1975 [78]. Of the 1,702 patients with epilepsy included in these studies, atrophic lesions were reported in 56% of cases [78]. The introduction of the x-ray by Roentgen in 1895 [79], of pneumo-encephalography by Dandy in 1918 [80,81], of EEG by Berger in 1924 [82,83], of PET by Sweet & Brownell in 1953 [84,85], and finally of MRI by Mansfield in 1977 [86] are some other noteworthy landmarks in the history of neuroimaging in epilepsy [76]. In most centres today, a combination of EEG, MRI, PET, SPECT, and occasionally MEG forms the standard of care in terms of noninvasive studies used in the presurgical evaluation for drug-resistant epilepsy [3].

MRI

MRI remains the primary method used to outline the lesional zone [3]. T1, T2, and FLAIR sequences form part of standard dedicated MRI epilepsy protocols [87]. Seizure freedom rates have been reported to be higher in children with a visible lesion on standard MRI (OR = 0.54), though this is also dependent on pathology [74]. For instance, patients with a nonlesional MRI had on average higher seizure freedom rates (51.5%) than patients with a hypothalamic hamartoma (45.9%) [74]. Additional advanced MRI techniques in-

cluding diffusion-weighted MRI (water diffusion/white matter) [88–90], arterial spin labelling (blood perfusion) [91–94], MRI spectroscopy (metabolism) [95], and EEG-functional MRI (EEG-fMRI, interictal spikes) [96–98] are also the target of ongoing research, but are not presently as broadly utilised across most centres. Another exciting development going forward will be the application of ultra-high field 7T MRI. In one study, 7T MRI (including 0.25 x 0.25 x 2mm T2*W GRE and 0.7mm isotropic FLAIR sequences) identified a structural lesion in 6/21 (21%) patients who had no visible lesions on a previous conventional MRI [99]. Nonetheless, presently with routine clinical MRI protocols, 15-30% of patients with drug-resistant focal epilepsy do not have visible lesions on MRI [3]. Yet, 51.5% of these "nonlesional" cases still achieve seizure freedom following surgery [74]. In these cases, as well as in the even greater proportion of patients who have only poorly defined/subtle lesions on MRI, additional imaging is critically important in helping to define a good presurgical hypothesis [3].

PET

^{18}F-Fluorodeoxyglucose (FDG) is the most commonly used radiotracer in PET studies for the presurgical evaluation of drug-resistant epilepsy [100]. Hypointensities on FDG PET indicate lower glucose uptake/metabolism and are used as a marker of the functional deficit zone [100]. In one study of 54 children with drug-resistant epilepsy who underwent both FDG PET and SISCOM (see SPECT section below), FDG PET was localising in 31/54 (57%) of patients, as compared to 36/54 (67%) for SISCOM and 21/54 (39%) for MRI [101]. In the 33 MRI-negative cases, FDG PET or SISCOM were found to be concordant with the presumed epileptogenic zone in 22/33 (67%) patients [101]. While

FDG PET remains the standard of care, a number of studies have explored the use of other radiopharmaceuticals including ^{11}C-ABP688 [102] and ^{11}C-AMT [103,104], which could be superior to standard FDG PET in some cases. While these newer tracers have the potential to lead to better diagnostic yields for PET imaging in epilepsy, the requirement for an on-site cyclotron due to the short half-life of carbon-11 (20 minutes) is a current barrier to broader adoption [103].

SPECT

SPECT measures blood flow (perfusion) using a gamma-emitting radiotracer (e.g. ^{99m}Technetium-ECD) [105]. It is typically the only imaging modality used in the presurgical evaluation for which attempts are made to obtain both interictal and ictal scans [3,105]. Seizures are generally associated with increased blood flow (hyperperfusion) within epileptic cortex, while the interictal state is characterised by hypoperfusion [106]. Observed interictal hypoperfusion is, however, often more subtle than ictal hyperperfusion [106]. When both interictal and ictal SPECT scans are available, a technique called subtraction ictal single-photon emission CT coregistered to MRI (SISCOM) [1] has been shown to be particularly valuable in helping to localise the epileptogenic zone [101,107–109]. In one prospective study, SISCOM was found to be concordant with the site of surgery in 23/28 (82%) of patients [108]. Timing of the tracer injection however remains an important determinant of the localisation sensitivity of SISCOM [107,108]. Continuous video-EEG monitoring and auto-injectors have been proposed as a method of reducing injection latencies [110,111].

EEG & MEG

EEG and MEG both measure the weak electric potentials (EEG) or magnetic fields (MEG) generated principally by the summated postsynaptic potentials of large ensembles of synchronously firing pyramidal neurons [112,113]. Unlike imaging methods like MRI or PET, the spatial resolution of EEG and MEG is not uniform, with deeper sources of electrical activity being more difficult to detect [114]. In the context of epilepsy, it has been estimated that detection of an interictal epileptiform discharge with MEG requires about 3-4 cm^2 of synchronously firing cortex, as compared to 6-20 cm^2 for EEG [115]. Beyond the raw traces obtained from MEG or EEG (see chapter 5, Fig. 5-1 for example), a technique called EEG/MEG source imaging (ESI or MSI) allows for the functional data from a high-density EEG (~64 or more channels/electrodes) or MEG to be combined with a model of an individual's head derived from an anatomical MRI [116]. Using this model and by solving a so called *inverse problem* [112], it is possible to estimate the location of a neural source (e.g. an interictal spike) within the brain.

In a retrospective study of 455 patients with drug-resistant epilepsies, Stefan et al. reported that MEG source imaging of interictal spikes accurately localised the treated lobe in 89% of 131 patients who underwent surgery [117]. They further reported that MEG provided information beyond routine clinical investigations (video-EEG, MRI, SPECT, PET) in 35% of a subgroup of 104 cases, with "crucial" information being provided in 11%. Similarly, a more recent case-series of 132 surgical epilepsy patients reported a 66% rate of concordance of MEG with the resection. In this case series, 85% of patients in whom MEG was concordant with the resection volume achieved seizure

freedom, as compared to 70% of patients overall [118]. One recent prospective study also looked at combined EEG/MEG source imaging (EMSI) in 141 patients and reported a localisation accuracy of 44-57%, which was not significantly different from MRI (49-76%) or PET (54-86%) [119]. EMSI also provided new clinically-useful information in 34% of patients [119]. While patients are frequently admitted for long-term video-EEG recordings to capture seizures on scalp EEG [64], ictal MEG is rarely captured because of the relatively short duration of these recordings. When available, however, there is early evidence that these ictal MEG recordings can provide reliable localisation of the SOZ with greater spatial resolution than scalp EEG [69].

Invasive EEG (SEEG/subdural grids)

Finally, while noninvasive imaging can lead directly to a resection, a second phase investigation with invasive EEG is sometimes required, especially in MRI-negative cases, to verify and refine the presurgical hypothesis [70]. SEEG, first popularised by Talairach and Bancaud in the 1960s [120], and subdural strips/grids, introduced by Wyler et al. in the 1980s [121], are the two main types of invasive EEG. Long the standard in many European centres (and the MNI), SEEG has recently been rapidly gaining in popularity in North America as well [122], in part due to the lower rate of complications [123] and the advent of robot-guided SEEG [124]. In one recent meta-analysis, the pooled rate of any complications for SEEG was 1.3% [125]. This compares favourably to the pooled rate of 4.0% for only haemorrhagic complications reported in another meta-analysis of complications related to subdural grid implantation [126]. In another recent systematic review, SEEG was associated with lower morbidity (4.8% vs. 15.5%) and mortality (0.2% vs.

0.4%) as compared to subdural grids [127]. In terms of seizure-freedom, however, there is insufficient evidence to favour either SEEG or subdural grids, and further research is needed to identify which patients might more specifically benefit from either of these two techniques [127–129].

2

Chapter 2 – Individual-patient prediction of meningioma malignancy and survival using the Surveillance, Epidemiology, and End Results database

All models are wrong, but some are useful.

– George E. P. Box

Preface

The manuscript in this chapter describes the application of machine learning methods to the diagnosis and prognosis of meningiomas. It touches on two main themes of the thesis, how predictive analytics applied to big datasets can aid decision-making in neurosurgery and how apps can help translate these tools to real-world practice. The manuscript was published as:

> **Moreau JT**, Hankinson TC, Baillet S, Dudley RWR. Individual-patient prediction of meningioma malignancy and survival using the Surveillance, Epidemiology, and End Results database. *npj Digital Medicine*. 2020;3(1):12.
> www.nature.com/articles/s41746-020-0219-5

Abstract

Meningiomas are known to have relatively lower aggressiveness and better outcomes than other CNS tumours. However, there is considerable overlap between clinical and radiological features characterizing benign, atypical, and malignant tumours. In this study, we developed methods and a practical app designed to assist with the diagnosis and prognosis of meningiomas. Statistical learning models were trained and validated on 62,844 patients from the Surveillance, Epidemiology, and End Results database. We used balanced logistic regression-random forest ensemble classifiers and proportional hazards models to learn multivariate patterns of association between malignancy, survival, and a series of basic clinical variables—such as tumour size, location, and surgical procedure. We demonstrate that our models are capable of predicting meaningful individual-specific clinical outcome variables and show good generalizability across 16 SEER registries. A free smartphone and web application is provided for readers to access and test the predictive models (www.meningioma.app). Future model improvements and prospective replication will be necessary to demonstrate true clinical utility. Rather than being used in isolation, we expect that the proposed models will be integrated into larger and more comprehensive models that integrate imaging and molecular biomarkers. Whether for meningiomas or other tumours of the CNS, the power of these methods to make individual-patient predictions could lead to improved diagnosis, patient counselling, and outcomes.

Keywords: meningioma, oncology, brain, CNS, neuro-oncology, predictive analytics, epidemiology, machine learning, SEER Program

Introduction

Meningiomas are the most common primary CNS tumour, with an incidence of 8.14 per 100,000 population [130]. They typically present with gradual onset of symptoms in the later decades of life and have generally favourable outcomes relative to other CNS tumours [131]. However, there is a great deal of variability in both aggressiveness and outcomes [132]. The decision to opt for a 'watch-and-wait' approach is made in around half of patients [133], but the process leading to this decision making remains challenging and often relies on simple heuristics, which may or may not be based on up to date evidence. The ability to precisely predict meningioma malignancy and survival beyond this standard would therefore be of clinical significance.

Many efforts to date in applying machine learning methods to the detection and grading of meningiomas have focussed on MRI imaging characteristics in small samples of patients. In this study, we develop and validate new predictive models using a set of basic clinical variables available in the Surveillance, Epidemiology, and End Results (SEER) database to predict meningioma malignancy and survival after specific treatments. The models are trained and tested on 62,844 patients included in SEER, an authoritative population-based cancer dataset with ~28% coverage of the US population [134]. A new smartphone and web app was also developed to accompany this manuscript (www.meningioma.app).

Rather than being used in isolation, we expect that the proposed models will be integrated into larger and more comprehensive models that will integrate imaging and molecular biomarkers. The source code of the meningioma.app also provides an easy entry-point for future investigators to translate predictive models for broader dissemination.

Results

Malignancy

Descriptive univariate statistical results of features initially included in the Balanced Logistic Regression-Random Forests (BLR-RF) model are presented in. No inferential statistical tests were performed as the goal of these exploratory analyses was solely to identify features with potential discriminatory value in relation to the outcome variables. Younger patients, and patients below the age of 20 especially, had relatively more malignant and borderline malignant meningiomas than older patients (Fig. 2-1a). Conversely, the relative prevalence of benign meningiomas was higher in older patients. In absolute numbers, however, benign meningiomas were much more frequent than borderline malignant or malignant meningiomas (Fig. 2-1c). Larger tumours were more malignant than smaller tumours (Fig 2-1b), especially those larger than 30mm, but with considerable overlap. Specifically, 66% of benign meningiomas in this sample were smaller than 3 cm (94% <6 cm), whereas 82% of malignant and borderline malignant ones were larger than 3 cm (22% > 6 cm).

Meningiomas were 2.8 times more frequent in females than in males, but the proportion of borderline malignant and malignant meningiomas was twice as great in men (Fig. 2-1e). Relative frequency of borderline malignant and malignant meningiomas was slightly higher in patients identified as black or "other" than in patients identified as white (Fig. 2-1f). The proportion of malignant or borderline malignant tumours was greater for tumours categorized as bilateral than for midline or unilateral tumours (Fig. 2-1d). This is likely an effect of tumour size, as discussed below. Meningiomas categorized as localizing to "other" regions were more malignant than those localizing exclusively to the cerebral or spinal meninges (Fig. 2-1g). 84.7% of meningiomas in this "other" group were from ICD-O-3 topography code 71.x (Brain), whereas 13.5% were coded as 72.x (Spinal Cord and Other Central Nervous System), and 1.8% (10 patients) fell under 75.1/75.3 (Pituitary/Pineal glands). In total, 86.3% of 62,844 meningiomas in this sample localized to the cerebral meninges (C70.0), 3.2% to spinal meninges (C70.1), 9.6% to meninges not otherwise specified (C70.9), and only 0.9% to the "other" group. Given the more aggressive behaviour of intraparenchymal meningiomas [135] and the large proportion of meningiomas in this group localizing to C71.x ICD-O-3 topography codes ("Brain", as opposed to C70.x, "Cerebral Meninges") we can speculate

that this "other" group could, at least in part, consist of intraparenchymal meningiomas.

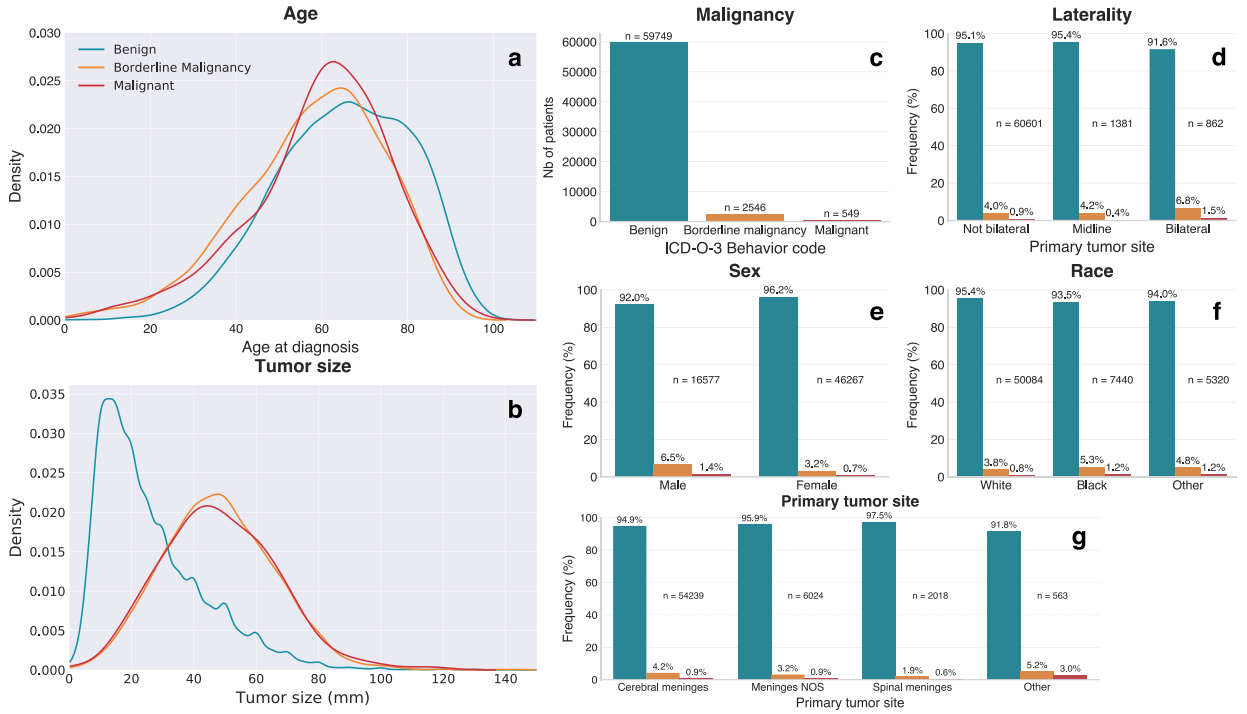

Fig. 2-1 Descriptive statistics for the malignancy outcome variable. Kernel density plots illustrate the distribution of benign, borderline malignant, and malignant meningiomas according to age at diagnosis (**a**) and tumour size (**b**). These kernel density plots are conceptually equivalent to histograms, but illustrate density (i.e. relative number of patients) as a continuous function of age/tumour size. Total number of meningiomas by WHO ICD-O-3 behaviour codes are shown in **c**. Absolute numbers and percentages of patients with benign, borderline malignant, and malignant meningiomas by subgroup are shown for laterality (**d**), sex (**e**), race (**f**), and primary tumour site (**g**).

Survival

The log hazard ratios of the survival model are presented in Fig. 2-2. There was an expected effect of age at diagnosis on probability of survival and increased tumour size was associated with worse survival. Malignant tumours predicted worse survival than borderline malignant tumours, and borderline malignant tumours worse survival than benign tumours. At the time of censoring, 76% of patients with a benign meningioma were alive (median age at diagnosis: 66) as compared to 80% of patients with a borderline malignant tumour (median age at diagnosis: 60) and 61% of patients with a

malignant tumour (median age at diagnosis: 61). Surgeries coded as "55: Gross total resection", "30: Radical", and "22: Resection (spinal cord or nerve)" predicted the greatest improved survival relative to no surgery. Patients who underwent a "40: Partial resection of lobe", "21: Subtotal resection (brain)", or other surgery had a relatively smaller improvement in survival. Amongst patients who did not undergo surgery, patients for whom the surgery was contraindicated due to another condition and patients who refused surgery had worse survival relative to patients for whom surgery was not recommended. Patients identified as black had worse survival than non-black patients, males had worse survival than females, and uninsured patients worse survival than insured patients. In the initial analyses, age at diagnosis, tumour size, sex, race, primary tumour site, and laterality were selected as features for both the malignancy and survival models. Additionally, surgical procedure, tumour behaviour (if available), insurance status, and reason for no cancer-directed surgery were included in the survival

model alone.

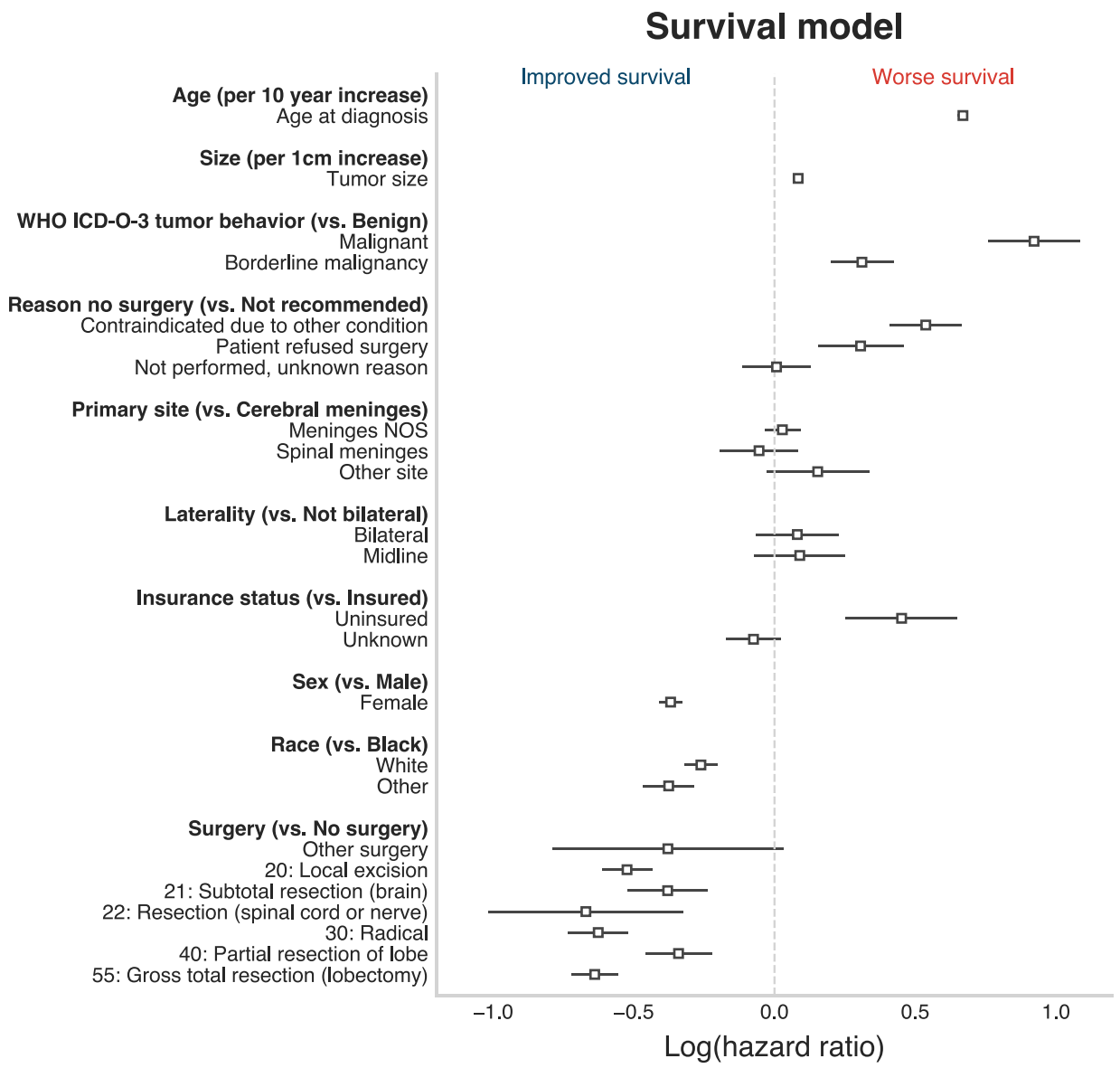

Fig. 2-2 Log hazard ratios for each of the features of the survival model. Negative values indicate proportionally lower probability of death. Positive values indicate proportionally higher probability of death. Error bars represent 95% confidence intervals.

Classifier scoring

Illustration of the performance of the malignancy classifier is presented in Fig. 2-3. The model was scored on the test dataset consisting of 18,854 randomly assigned patients initially set aside, and a weighted F1 score of 0.82 was obtained. Fig. 2-3a is a confusion

matrix showing predicted vs. true class labels, normalized by row, at the selected thresholds used in the app.

The calibration plot (Fig. 2-3e), precision-recall curve (Fig. 2-3f), and receiver operating characteristic (ROC) curve (Fig. 2-3g) are also provided. The calibration diagram plots predicted probabilities against the true observed distribution of each class in the test dataset. The precision recall curve illustrates precision (positive predictive value) as a function of recall (sensitivity) and is complemented by the receiver operating characteristic (ROC) curve, which illustrates sensitivity and specificity. The average precision was 0.18 (SD: 0.01, chance level: 0.05) and the AUC was 0.83 (SD: 0.01, chance level: 0.5). At the selected thresholds, we obtained a sensitivity of 0.79 with specificity of 0.75 and a positive predictive value (PPV) of 0.14 with a negative predictive value (NPV) of 0.99. Feature importance is illustrated in Fig. 2-3b. Tumour size and age at diagnosis were the two most important features in the malignancy model and were the only features retained in the final model. Fig. 2-3d shows the distribution of tumour behaviour categories relative to tumour size and age at diagnosis.

Finally, figure 3c shows the learning curves (scored for AP and AUC), which illustrate the gain in classification performance attained by increasing the training sample. As a performance baseline, we also plot the classification performance of a "dummy" classifier that randomly generates predictions on the basis of the class distribution in the training set. For both AUC and AP, improvement in model performance plateaus around ~5,000-10,000 training examples (i.e. individual patients), after which additional training examples did not improve performance.

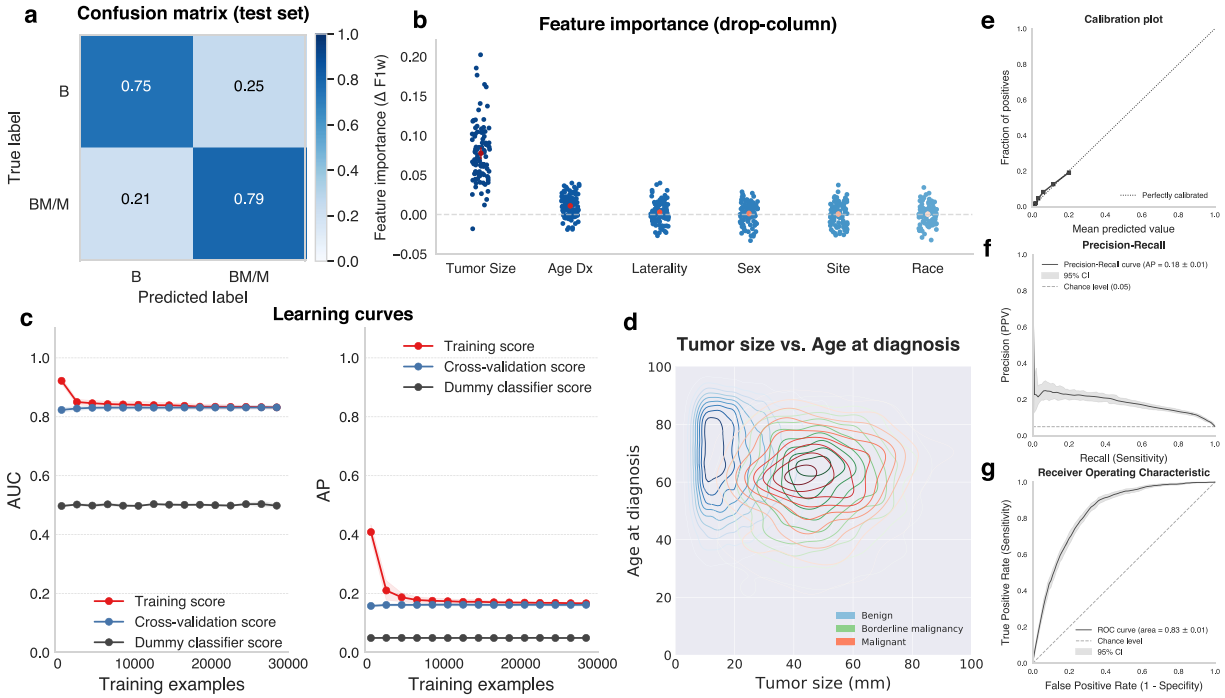

Fig. 2-3 Performance of the malignancy classifier. a, Confusion matrix illustrating predicted vs. true labels for the malignancy classifier, as evaluated on the test set. Values are normalized across each row. B: Benign, BM/M: Borderline malignancy/Malignant. **b**, Drop-column feature importance showing decrease in classifier performance resulting from dropping a given feature, in decreasing order of importance. The red dot indicates the mean and error bars 95% confidence intervals. **c**, Learning curves illustrating training (red line) and cross-validation (blue line) model performance (measured by Area under the Receiver Operating Characteristic curve and Average Precision) as a function of the number of patients used in training the classifier. The point of convergence between the training and cross-validation curves indicates when adding more cases to the training no longer results in an improvement in performance. Shaded outlines represent 1 standard deviation. The grey line represents the performance of a dummy classifier, which randomly generates predictions on the basis of the class distribution in the training set. **d**, Bivariate kernel density plot (can be understood as a "2-dimensional histogram") of tumour size vs. age at diagnosis. **e**, Calibration plot, as evaluated on the test set. **f**, Precision-Recall curve and Receiver Operating Characteristic curve (**g**) for Benign vs. Borderline Malignant/Malignant meningioma classification. For **f** and **g**, the grey dashed line indicates chance level performance and the shaded outline represents the 95% confidence intervals.

Calibration and performance scoring results for the survival model are shown in Fig. 2-4. A calibration plot for the survival model, as evaluated on the test set, is shown

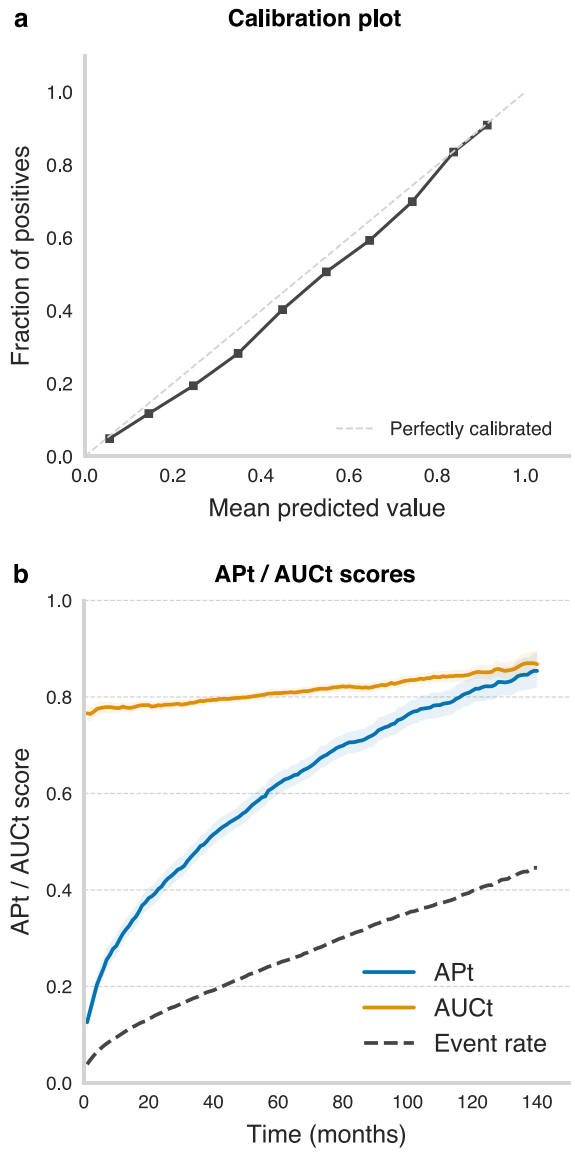

Fig. 2-4 Calibration and performance of the survival model. a, Survival model calibration plot, as evaluated on the test set. b, Time-dependent area under the curve (AUCt, yellow line) and average-precision (APt, blue line) for the survival model, as evaluated on the test set. The event rate/chance level is represented by the dashed grey line. Shaded outlines represent 95% confidence intervals.

in Fig. 2-4a. Figure 2-4b shows time-dependent average precision (APt) and area under the receiver operating characteristic curve (AUCt) [136,137] values for the survival model. For 5-year survival, overall APt was 0.62 (95% CI: 0.60-0.64, event rate: 0.25) and AUCt was 0.81 (95% CI: 0.80-0.82). We also obtained a Uno's C-statistic [138] of 0.79. Uno's C in an improvement of Harrel's concordance index [139], which has the added benefit of being independent of the study-specific censoring distribution [138]. A concordance index of 0.5 represents chance-level performance whereas a concordance index of 1 indicates perfect performance. In order to assess the generalizability of our classifiers we also subdivided the test set by SEER registry and computed the above reported scores for each registry independently (Table 2-1).

Table 2-1. Summary of performance metrics for the malignancy and survival models per SEER registry (for all registries with at least 100 cases) as evaluated on the test

	Malignancy model				Survival model			
SEER Registry	F1(w)	AP	Chance level	AUC	Uno's C	AP(5y)	Event rate	AUC(5y)
California excluding SF/SJM/LA	0.80	0.18	0.06	0.82	0.81	0.66	0.26	0.81
Seattle (Puget Sound)	0.88	0.19	0.03	0.88	0.76	0.56	0.22	0.80
Los Angeles	0.78	0.20	0.05	0.83	0.78	0.54	0.22	0.81
New Jersey	0.81	0.18	0.05	0.83	0.79	0.71	0.27	0.83
Kentucky	0.86	0.18	0.04	0.87	0.76	0.54	0.26	0.76
Greater Georgia	0.82	0.15	0.05	0.84	0.72	0.64	0.26	0.80
Detroit (Metropolitan)	0.82	0.15	0.05	0.79	0.76	0.69	0.31	0.81
San Francisco	0.81	0.22	0.06	0.82	0.8	0.60	0.23	0.84
Louisiana	0.82	0.10	0.04	0.80	0.85	0.71	0.30	0.78
Iowa	0.86	0.42	0.07	0.87	0.76	0.64	0.23	0.80
Utah	0.86	0.09	0.02	0.79	0.84	0.67	0.2	0.81
Connecticut	0.80	0.19	0.05	0.84	0.81	0.59	0.21	0.83
Atlanta (Metropolitan)	0.82	0.22	0.05	0.87	0.82	0.58	0.20	0.85
San Jose	0.81	0.21	0.06	0.83	0.77	0.45	0.20	0.79
New Mexico	0.77	0.14	0.05	0.74	0.79	0.61	0.23	0.86
Hawaii	0.78	0.21	0.04	0.88	0.77	0.59	0.27	0.81
Mean	0.82	0.19	0.05	0.83	0.79	0.61	0.24	0.81
SD	0.03	0.07	0.01	0.04	0.04	0.07	0.03	0.03

F1(w): weighted F1 score, AP: Average precision, Chance level/Event rate: baseline performance level for AP, AUC: Area under the receiver operating characteristic curve, Uno's C: Uno's concordance index, AP(5y): 5-years time-dependent average AP, AUC(5y): 5-years time-dependent AUC, SD: standard deviation

Discussion

We present the development and validation of two classifiers for the prediction of meningioma malignancy and survival. Using only a very limited set of clinical variables, we demonstrate that our models are capable of predicting meaningful clinical outcomes. Previous studies using the SEER database have used various machine learning methods for diagnosis and prognosis purposes in breast [140–144] and lung cancers [145,146], but

have not applied these techniques to the SEER data on meningiomas. As compared to classical statistical approaches, the value of predictive modelling is the ability to obtain predictions for individual patients rather than group means. In the framework of levels of evidence for predictive biomarkers proposed by Woo et al. [147], the models introduced here fall under the "development" stage and we emphasize the need for future prospective studies and model refinement using imaging and molecular data. The present models represent a valuable performance baseline and proof of concept for future studies to surpass and could, for instance, be used in a Bayesian framework as priors to improve the performance of models developed solely on the basis of imaging or molecular features. We nonetheless believe that meningioma.app provides a unique entry point for furthering the translatability and transparency of machine learning models, which too often remain impossible for the average clinician to evaluate because of the time and programming knowledge this would require. Our intention here is to allow for clinicians to easily test out the models to provide feedback for improvement and generate interest in the possibilities of such tools. We also hope that this will inspire others to replicate our approach and have therefore made the source code of meningioma.app available under a free open-source license.

We report on the meningioma data up to the November 2017 SEER release, but our observational results are broadly consistent with what has been reported in previous epidemiological literature on meningiomas. From 2004 to 2010, Kshettry et al. reported that WHO grade II and III meningiomas accounted for 4.2% and 1.2% of newly

diagnosed meningiomas, respectively [148]. Likewise, after exclusions, we identified a total of 62,844 meningiomas for the period between 2004 and 2015, of which 4.0% were coded as borderline malignant and 0.9% as malignant. As in our previous work, we found that while paediatric meningiomas may include relatively more aggressive subtypes, young age is overall associated with reduced all-cause mortality [133]. In regard to sex, across all ages overall, meningiomas were more frequent in females than in males, but malignancy [148] and mortality [132,149,150] were greater in males than females. Also concordant with previous reports, black race and larger tumour size were found to be adverse prognostic factors [132,151,152]. Regarding lateralisation, we found that the proportion of malignant/borderline malignant tumours was greater for bilateral meningiomas. This effect is presumably explained by size as bilateral tumours were on average larger (41.5 mm) than midline (30.0 mm) or unilateral (27.2 mm) tumours. Gross total resection was also found to be a strong predictor of longer survival [132,150,152]. Additionally, in patients who did not undergo surgery, we found differences in survival based on the reason why no cancer-directed surgery was performed, with relatively worse survival in patients who refused surgery or for whom surgery was contraindicated due to another condition as compared to patients for whom surgery was not recommended. We also found, as expected, that uninsured patients had worse survival than insured patients.

As compared to previous studies of meningiomas in SEER, our present study is chiefly differentiated by the application of statistical learning methods. Specifically, we trained an ensemble voting classifier using a random undersampling procedure inspired by the Balanced Random Forest algorithm [153] and proportional hazards models

[154,155] to predict malignancy and survival. Ensemble classifiers often outperform any classifier used independently and also can help reduce the risk of overfitting the training data [156]. In this study, we found that the method indeed did help produce a better calibrated model while also marginally improving classification performance over either balanced random forest or balanced logistic regression used alone (Supplementary Figures 2-1 & 2-2). The results in Fig. 2-3e indicate that the model is well-calibrated (e.g. a predicted probability of 20% that a meningioma is non-benign suggests a true 20% chance that the meningioma is indeed non-benign), but does not make predictions with high probability values. This is consistent with the classification accuracy of the model, but is also in part due to very imbalanced base class distribution in this dataset; any randomly selected meningioma has about a 95% chance of being benign and, conversely, only a 5% chance of being non-benign.

An intrinsic advantage of ensemble classifiers is the ability not only to provide a binary prediction of the predicted outcome, but also to provide probability estimates by calculating the proportion of votes in the ensemble (e.g. if 50 of 100 base classifiers in the ensemble predict one outcome, the predicted probability estimate is 50%). This is illustrated together with individualized survival curves for an example 56-year-old man in the screenshots of our app shown in Fig. 2-5. A second calibration step was however necessary to provide well-calibrated probability estimates for the malignancy classifier, as discussed in the Methods below. One important consideration is that the provided individualized survival curves should only be used to estimate survival of a

patient for whom a specific treatment course has been decided and not to guide treatment decisions for that specific patient. While perhaps a seemingly subtle interpretation difference, the second use would likely be invalid due to probable patient selection effects in SEER (e.g. the patients who did not undergo surgery are not the same patients who received a gross total resection). Our smartphone optimized web app (www.meningioma.app), allows inputting basic clinical details for any new patient to obtain straightforward predictions of malignancy and survival. The details entered into the app are run through exactly the same models described in this paper, but without the need for any advanced technical or programming knowledge.

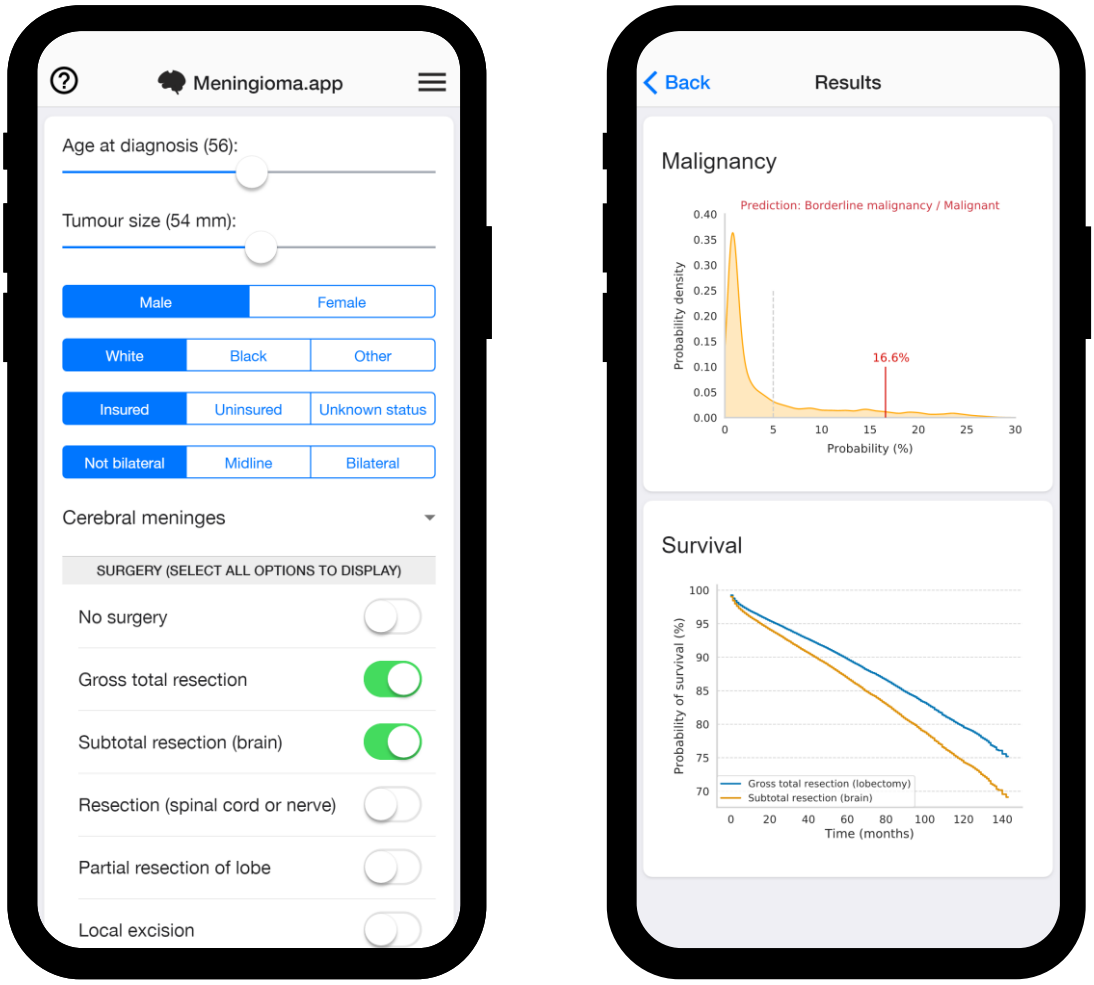

Fig. 2-5 Example predicted malignancy and survival curves for an insured 56-year-old white man with a unilateral 54 mm wide meningioma localizing to the cerebral meninges. Try the app at www.meningioma.app

Previous studies have used classifiers for the detection and grading of meningiomas and other CNS tumours, but these have almost exclusively focused on MRI [24,157] or histopathological [158] imaging characteristics to drive their predictions. We also extend classical survival analysis methods to the machine learning framework and demonstrate how proportional hazard ratios can be used to create individualized patient-specific survival curves (also illustrated in Fig. 2-5). While predictive modelling of

imaging and molecular-genetic profiles should undoubtedly form part of the effort for more accurate diagnostic and prognostic tools [159], we demonstrate here that the informational value to be gained from even the simplest of clinical variables is not to be ignored. Moreover, we position the value of such a tool as being of particular relevance at the pre-biopsy/surgery stage, which is of particular interest in the case of meningiomas where only roughly half of tumours are microscopically confirmed [151]. It is also worth noting that the sample size of these previous studies was on an entirely different scale, ranging from dozens to a few hundred patients at most. Rather than competing with these prior models, what we hope to highlight here is the potential value of combining models trained on large epidemiological datasets with classifiers trained on smaller but richer datasets. Further improvements to model performance will be needed before clinical translatability can be achieved. While marginal improvements might still be achievable with the current dataset by refining the models themselves, a larger challenge for translatability lies in collecting and curating large multimodal datasets for training and validation against clinical outcomes.

With ever decreasing storage costs and the advent of open databasing solutions for genetic [160] and neuroimaging data [45,161], the possibility of expanding the scope of national cancer registries for large-scale inclusion of de-identified source data will lead the way for the next generation of predictive models. Recent large-scale projects for population genotyping and brain imaging such as the UK biobank represent a significant opportunity in this regard [162,163]. Additionally, efforts to provide curation as well as

streamlined consent [164] and de-identification [46,47] of data from electronic medical records and picture archiving communication systems are another important step in this direction [44,165–167]. Allowing for the wealth of patient data already being recorded for routine care to be used to advance predictive disease modelling has the potential to simplify specific aspects of clinical decision making as well as improve diagnostic and prognostic accuracy for future patients. We also highlight the need to expand outcome variable reporting beyond survival. Indeed, functional outcomes and quality of life are also key to informed clinical decision making and patient counselling. In the case of meningiomas, surgery for benign tumours is frequently undertaken to treat comorbid seizures or other neurological symptoms. We could therefore imagine predictive models being developed to determine which patients are more likely to benefit from such interventions. Likewise, we could foresee training models to learn patterns of association between certain tumour features (e.g. size and location) and treatment variables (surgery type, adjunctive therapy), and the probability of specific neurological complications.

There are inherent limitations to any study of retrospective registry-based data, such as selection and reporting biases. We have described these in detail in previous work [168–171]. Nonetheless, one of the benefits of the present study in this regard was the random assignment of 30% of patients to a "test" dataset, which was sequestered until the final models were developed. This allowed for pseudo-prospective evaluation of our models and therefore reduced bias in the scoring of model performance. While we demonstrated good generalizability of the model across SEER registries, the true

test of these models will have to come from replication with prospective, multi-registry, and international patient cohorts. Also, given the poor discrimination between borderline malignant and malignant meningiomas (Fig. 2-3d) based on the limited set of clinical variables available in SEER, we opted to focus current analyses on binary classification between benign and non-benign tumours. We consider the ability to differentiate these two categories to be the more important question from a clinical perspective since, as previously reported by Dolecek et al. [151], only 29% of borderline malignant and 31% of malignant meningiomas received no initial treatment, as compared to 60% of benign meningiomas. Future work with richer datasets should, however, attempt to distinguish between these categories.

Regarding treatment variables, only surgery was investigated and we did not include radiotherapy or chemotherapy as features of interest in the survival classifier because there are substantive concerns with these data in SEER [172]. Starting with the November 2016 data submission, these data have been removed from the main SEER research databases. We do, however, emphasize the need for radiotherapy in particular to be investigated with another dataset. Also, Simpson grading is not available in SEER and some heterogeneity is therefore expected in the gross total resection group [173]. We also excluded the small percentage of patients who had a second meningioma recorded in SEER so as not to bias scoring of the model (i.e. each training or testing example was one patient). It would, however, be valuable to predict outcomes in these patients with subsequent meningiomas—or any second cancer, whether occurring prior

to or after the meningioma. Finally, this study remains, at least in part, a proof of concept of what can be achieved with predictive modelling of cancer registry data. We fully realize that more powerful models will need to integrate radiographic and molecular features in their predictions, and hope to update meningioma.app with such models in future work.

We report the development and validation of predictive models of meningioma malignancy and associated survival. On the basis of a very limited set of clinical variables such as age, sex, and tumour size, our models are shown to be capable of predicting individual-patient outcomes. Our modelling approach provides complementary information to previous epidemiological reports and could lead to the development of new practical diagnostic and prognostic tools in oncology. Beyond the traditional paper-and-pencil nomograms, we provide an original open-source smartphone and web application to illustrate the translation of complex nonlinear predictive models to real-world practice. In particular, the ability of our statistical learning models and app to provide individual-specific predicted survival curves could be valuable for patient counselling.

Methods

Participants

The latest SEER data release (November 2017) was queried using SEER*Stat v8.3.5 for all cases of meningioma (WHO ICD-O-3 histology codes 9530-9539) recorded in the

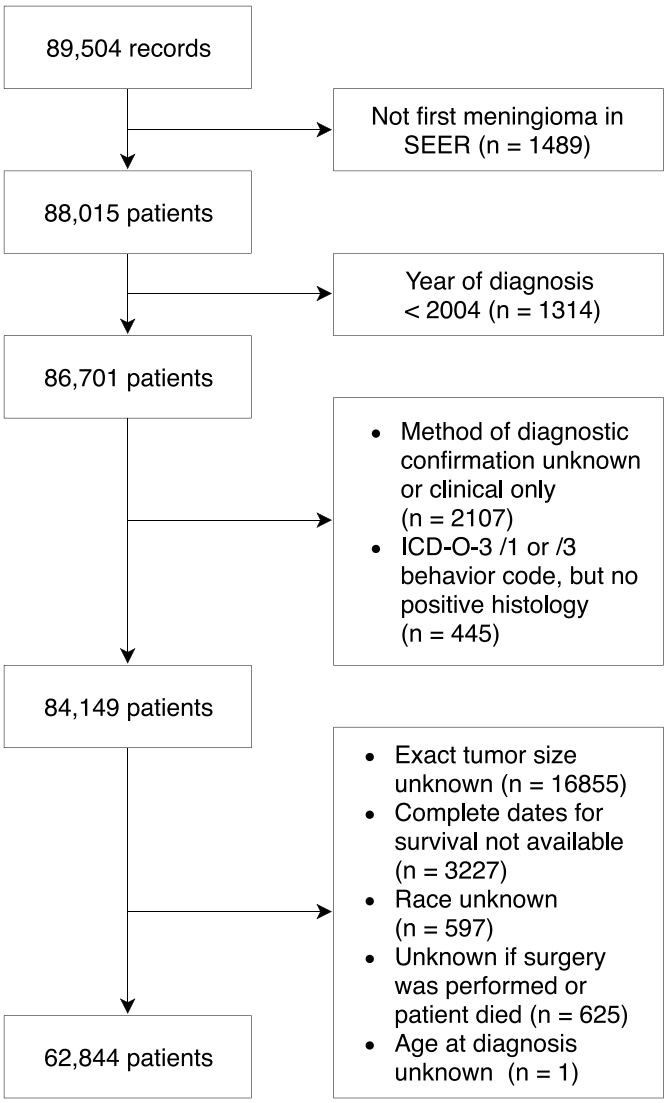

Fig. 2-6 Flow diagram illustrating criteria for patient inclusion.

brain and spinal cord. A complete description of the SEER*Stat search query is provided in the supplementary information (Supplementary Note 1). The data included patients diagnosed between 2004 and 2015 across 18 registries in 13 states. Only the first meningioma recorded in SEER for each patient was included in analyses. In total, 88,015 patients were initially identified. Patients diagnosed prior to 2004 were excluded because their diagnosis predates the passage of Public Law 107-260, which mandated the collection of non-malignant tumours [151]. Patients for whom the method of diagnostic confirmation was unknown or clinical only were also excluded. Moreover, all ICD-O-3 /1 (borderline malignant) and /3 (malignant) meningiomas without positive histological diagnosis were excluded. We also excluded meningiomas recorded as being larger than 150mm as such cases are extremely rare and more likely represent coding errors in SEER (e.g. an "803 mm" meningioma). In addition to these exclusion criteria, we excluded case listings for which features (age, tumour size, race, tumour site,

surgery) or outcome variables (malignancy, survival) of interest were not available. Exclusion criteria are illustrated in Fig. 2-6. After exclusions, the final number of patients included in analyses was 62,844. As SEER contains no personally identifiable information and this study relied exclusively on secondary use of observational epidemiological data from a public national database, our institutional research ethics board deemed this study to be exempt from review. Transparent Reporting of a multivariable prediction model for Individual Prognosis Or Diagnosis (TRIPOD) reporting guidelines were implemented in this manuscript [174].

Feature selection

Descriptive statistics were computed and exploratory data analysis was performed to identify potential features (i.e. predictor variables) for inclusion in the machine learning models. Selection criteria for features included data availability (variables with large numbers of missing points were excluded) and discriminatory capability in relation to the two outcomes of interest—malignancy and survival. Malignancy was defined as per WHO ICD-O-3 histology and behaviour codes. ICD-O-3 behaviour codes were used as WHO grade is not consistently available for meningiomas in SEER [148,152]. Previous studies have used the following correspondence from WHO grade to ICD-O-3 histology and behaviour codes: WHO I: 9530/0, 9531/0, 9532/0, 9533/0, 9534/0, 9537/0; WHO II: 9530/1, 9531/1, 9532/1, 9533/1, 9534/1, 9537/1, 9538/1, 9539/1; WHO III: 9530/3, 9531/3, 9532/3, 9533/3, 9534/3, 9535/3, 9537/3, 9538/3, 9539/3 [148,152]. We have opted

here to display the original ICD-O-3 labels as they are reported in SEER (i.e. /0: benign, /1: borderline malignancy, /3: malignant).

All-cause mortality was used in survival analyses because cause-specific mortality is not reliably available across all meningioma cases in SEER [133]. Moreover, as demonstrated in Fig. 2-2, treatment and clinical variables other than age clearly impact all-cause survival. We also obtained a Uno's C of 0.70 for a model excluding malignancy and age at diagnosis, as compared to a Uno's C of 0.79 for the model including all features. Supplementary Fig. 2-3 additionally illustrates AUCt and APt when age and malignancy are excluded from the survival model. Survival was defined on the basis of the "Survival months" variable in SEER, which is calculated on the basis of the date at diagnosis and date at last contact [134]. Censoring was based on the "Vital status recode" variable in SEER. Features with low-frequency classes were recoded into more general classes where appropriate in order to have sufficient examples for training and cross-validation. Features were also recoded when it was found that two or more classes did not provide additional information in respect to the outcome variable (e.g. patients with left vs right sided meningiomas had equivalent survival). Primary tumour site was recoded by ICD-O-3 topography codes as either "cerebral meninges" (C70.0), "spinal meninges" (C70.1), "meninges not otherwise specified" (C70.9), and "other". Race, as defined in the SEER database, was recoded into "white", "black", and "other" groups. Tumour laterality was recoded as "bilateral" (e.g. large meningiomas extending over both hemispheres), "midline" (e.g. falcine meningiomas), or "not bilateral". The original SEER coding for surgical procedures was preserved except for "10: Tumor destruction

NOS", "50: Surgery stated to be "debulking", and "90: Surgery, NOS" codes, which were recoded as "other surgery" because they accounted in total for only 0.7% of all surgically-treated cases.

Classifier design and validation

Of the 62,844 included patients, 30% (18,854) were randomly selected and set aside for use as a test (validation) dataset whereas the data of the remaining 43,990 patients were used for training (development) and cross-validation. 13,197 of these 43,990 cases were used for cross-validation and initial model exploration (Supplementary Fig. 2-1). The use of a true "test" set allows for unbiased estimation of model performance, which cannot be achieved through cross-validation alone since human or automated optimization of models and model parameters inherently biases scoring towards artificially inflated classification accuracy [175]. Two separate classifiers were trained and tested, one for each of the outcome variables of interest. Preprocessing, hyperparameter optimization, cross-validation, and scoring were performed using the scikit-learn Python module [176].

For the malignancy model, a voting ensemble classifier (BLR-RF) combining balanced logistic regression and balanced random forest base models was implemented. This BLR-RF classifier implements a random undersampling procedure akin to that of the Balanced Random Forest (BRF) [153] algorithm whereby each base classifier in the ensemble is trained on a randomly selected class-balanced subsample of the training dataset. The imbalanced-learn Python package [177] was used to perform the random undersampling and the MLxtend package to build the ensemble voting classifier [178].

As compared to BRF, we found that, in this dataset, our BLR-RF classifier provided better probability calibration and was less prone to overfitting (Supplementary Fig. 2-1). The BRF algorithm is an extension of the popular random forest algorithm [179], which builds ensembles of decision trees and uses a voting procedure to output the overall classification decision. Both our BLR-RF classifier and BRF are distinguished from standard random forests by additionally resampling data within random bootstrap samples (smaller samples randomly drawn from the training data) to address the problem of class imbalance [153]. We found this procedure to be effective in this highly imbalanced dataset (i.e. ~95% of meningiomas were benign), as compared to regular logistic regression or random forests (Supplementary Fig. 2-1). In the implementation used in the present study, we resampled the non-minority classes (i.e. all non-malignant tumours) so that each bootstrap sample contained roughly equal numbers of benign and non-benign tumours. In order to improve model calibration, we applied a second probability calibration step using Platt scaling [180] with a subset of data not used in the initial training (Supplementary Fig. 2-1) .

Hyperparameter optimization was performed using 1000 iterations of randomized [181] 5-fold stratified K-fold cross-validation using the weighted F1 score, as implemented in scikit-learn [176], as the primary scoring metric. We selected this weighted F1 score as the scoring metric for training the model as it penalises misclassifications of the minority class (i.e. non-benign meningiomas) to a greater extent, which is critical in this very imbalanced dataset (e.g. we could obtain 95% accuracy simply by classifying

all meningiomas as benign). The F1 score ranges from 0 (worst) to 1 (best) and is defined as the harmonic mean of precision (PPV) and recall (sensitivity). It is better suited than accuracy or area under the receiver operating characteristic curve (AUC) for measuring classifier performance in imbalanced datasets [182]. Candidate models were also evaluated using confusion matrices obtained from the cross-validation set. Confusion matrices are a simple way to represent true vs. predicted classes and calculate rates of true and false positives and negatives. For the survival model, we used the implementation of Cox's proportional hazards model in the lifelines Python package [155]. This model is suited for working with censored survival data and has the benefit of providing easily interpretable prediction probabilities.

Model scoring for the malignancy model was performed using a series of metrics including the F1 score and confusion matrices, as described above, but also precision-recall and receiver operating characteristic (ROC) curves, which can also be summarised by the average precision (AP) and area under the curve (AUC) metrics. AUC tends to provide overly optimistic estimates of performance in imbalanced datasets and it is therefore also useful to evaluate the precision-recall curve in these cases [183]. Average precision is prevalence-dependent and should therefore be evaluated in the context of the baseline population prevalence. We report chance-level values to illustrate this baseline. For the survival model, we report time-dependent average precision (APt) [136] and area under the curve (AUCt) [184] values, using the R implementation in the APtools package [137], as well as Uno's C-statistic [138]. We used the implementation of Uno's C provided in the scikit-survival Python package [185]. In addition to Uno's C, time-

dependent AP and AUC values provide a useful complement for model evaluation. APt has been suggested to be of particular value for assessing low probability events [137], but is also dependent on prevalence and should therefore be evaluated against the baseline event rate at each time point. In addition to the above metrics, we also provide calibration plots of predicted vs. observed risk. Confidence intervals were computed using bootstrap resampling of the test set with 1000 iterations for precision-recall, ROC, APt, and AUCt values.

Data availability

All data used in this study are available for download through the SEER program: https://seer.cancer.gov/data-software

Code availability

The source code for meningioma.app is available for download at https://github.com/jeremymoreau/meningioma

Acknowledgments

We thank the Department of Neurosurgery of the Montreal Neurological Institute for providing the funding for the computational resources used in this project. J.T.M. was supported by the *Fonds de Recherche du Québec - Santé* and the Foundation of Stars. S.B. was supported by a Discovery Grant from the Natural Science and Engineering Research Council of Canada (436355-13), the NIH (1R01EB026299-01), and a Tier-1

Canada Research Chair in Neural Dynamics of Brain Systems. This research was undertaken thanks in part to funding from the Canada First Research Excellence Fund, awarded to McGill University for the Healthy Brains, Healthy Lives initiative.

Competing interests: The authors declare no competing interests.

Supplementary information

Supplementary Figures

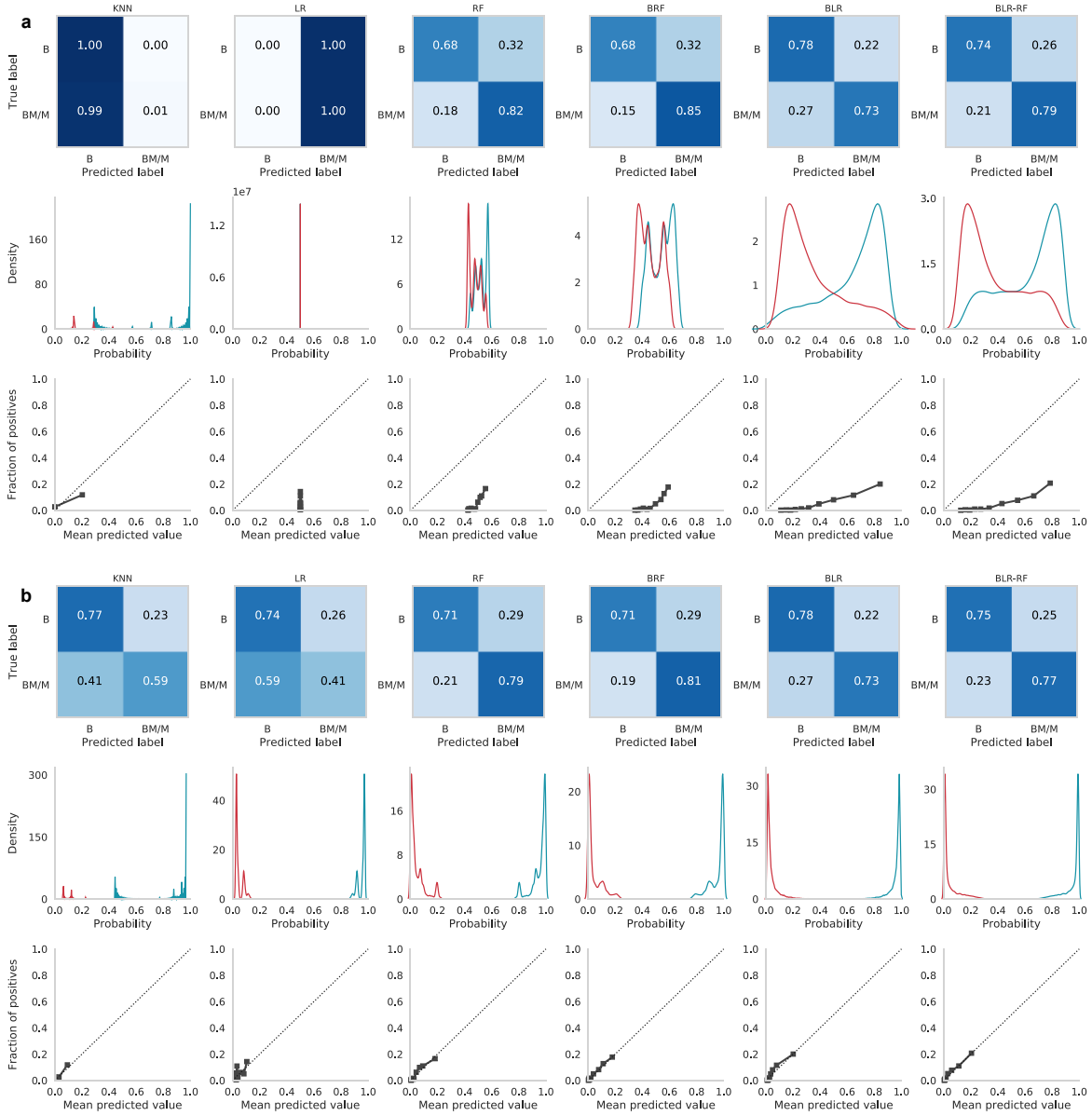

Supplementary Fig. 2-1 Exploratory model comparison for initial models after hyperparameter optimization but prior to probability calibration **(a)**, and after calibration **(b)**. KNN: K-Nearest Neighbours, LR: Logistic regression, RF: Random Forests, BRF: Balanced Random Forest, BLR: Balanced Logistic Regression, BLR-RF: Balanced Logistic Regression-Random Forests. For (a) and (b), the first row contains confusion matrices illustrating predicted vs. true labels, as evaluated on the test set. Values are normalized across each row. B: Benign, BM/M: Borderline malignancy/Malignant. The second row consists of kernel density plots illustrating the distribution of predicted probabilities for the benign (blue) and non-benign

(red) meningioma classes. The third row consists of calibration diagrams plotting predicted probabilities against the true observed distribution of each class in the test dataset.

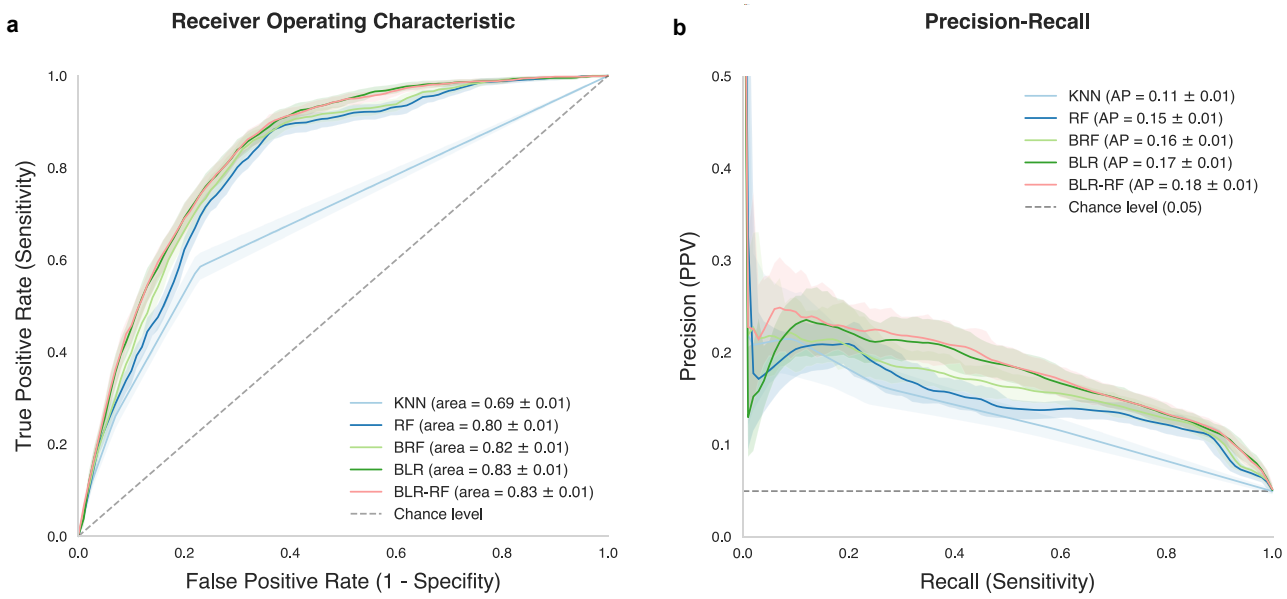

Supplementary Fig. 2-2 Receiver Operating Characteristic curve **(a)** and Precision-Recall curve **(b)** for Benign vs. Borderline Malignant/Malignant meningioma classification. The grey dashed line indicates chance level performance and the shaded outlines represents 95% confidence intervals. KNN: K-Nearest Neighbours, LR: Logistic regression, RF: Random Forests, BRF: Balanced Random Forest, BLR: Balanced Logistic Regression, BLR-RF: Balanced Logistic Regression-Random Forests

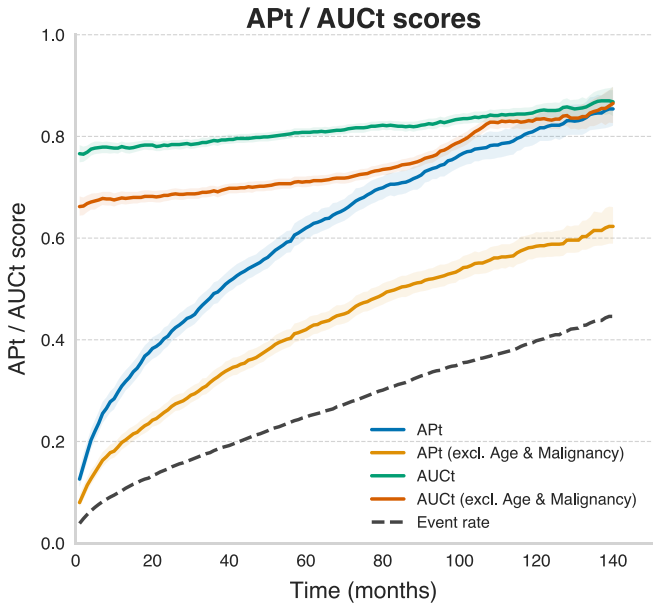

Supplementary Fig. 2-3 Time-dependent area under the curve (AUCt) and average-precision (APt) for the survival model including or excluding age and malignancy as features of interest, as evaluated on the test set. The event rate/chance level is represented by the dashed grey line. Shaded outlines represent 95% confidence intervals.

Supplementary Notes

Supplementary Note 1. SEER*Stat search query.

Database Name:

Incidence - SEER 18 Regs Research Data + Hurricane Katrina Impacted Louisiana Cases, Nov 2017 Sub (1973-2015 varying)

Selection:

{Site and Morphology.Primary Site - labeled} = 'C70.0-Cerebral meninges','C70.1-Spinal meninges','C70.9-Meninges, NOS','C71.0-Cerebrum','C71.1-Frontal lobe','C71.2-Temporal lobe','C71.3-Parietal lobe','C71.4-Occipital lobe','C71.5-Ventricle, NOS','C71.6-Cerebellum, NOS','C71.7-Brain stem','C71.8-Overlapping lesion of brain','C71.9-Brain, NOS','C72.0-Spinal cord','C72.1-Cauda equina','C72.2-Olfactory nerve','C72.3-Optic nerve','C72.4-Acoustic nerve','C72.5-Cranial nerve, NOS','C72.8-Overlapping lesion of brain & CNS','C72.9-Nervous system, NOS','C75.1-Pituitary gland','C75.2-Craniopharyngeal duct','C75.3-Pineal gland'

AND {Site and Morphology.ICD-O-3 Hist/behav} = '9530/0: Meningioma, NOS','9530/1: Meningiomatosis, NOS','9530/3: Meningioma, malignant','9531/0: Meningothelial meningioma','9531/1: Meningiothelial meningioma, borderline','9531/3: Meningiothelial meningioma, malignant','9532/0: Fibrous meningioma','9532/3: Fibrous meningioma, malignant','9533/0: Psammomatous meningioma','9533/3: Psammomatous meningioma, malignant','9534/0: Angiomatous meningioma','9534/3: Angiomatous meningioma, malignant','9537/0: Transitional meningioma','9537/3: Transitional meningioma, malignant','9538/0: Clear cell meningioma, benign','9538/1: Clear cell meningioma','9538/3: Papillary meningioma',

Select Only: Cases in Research Database

3

Chapter 3 – Biased intelligence: on the subjectivity of digital objectivity

I assure you, Watson, without affectation, that the status of my client is a matter of less moment to me than the interest of his case.

– Sir Arthur Conan Doyle, The Adventure of the Noble Bachelor

Preface

The manuscript in this chapter offers a timely discussion of some less discussed ethical issues relating to the application of AI and machine learning to medical diagnostics. While developing AI systems applied to neurosurgery was one of the objectives of this thesis, I felt it was also important to consider the potential sources and consequences of systemic biases that can unintentionally affect the predictions of AI systems. This chapter includes a discussion of our own work described in the previous chapter as well as theoretical cases and notable recent examples from the published literature. The manuscript was submitted and is currently under review as:

Moreau JT, Baillet S, Dudley RWR. Biased intelligence: on the subjectivity of digital objectivity.

Whether IBM's Watson, Google's DeepMind, or Tencent's WeDoctor, the last few years have been characterised by unprecedented levels of research interest and new investments in artificial intelligence (AI) and digital healthcare technology. The number of publications on applications of AI and machine learning to medical diagnosis has dramatically increased since around 2015 (Fig. 3-1). Correspondingly, venture capital-backed digital health and AI startups worth over $1 billion now number in the dozens (Fig. 3-1) [186]. Yet, this influx of new investment has not been without controversy. Google's recent partnership with national health group Ascension, which gave the company access to the clinical data of around 50 million patients, has been the target of significant mediatic and congressional scrutiny [187]. Likewise, pharmaceutical giant GlaxoSmithKline's (GSK) $300 million investment in direct-to-consumer genetic testing provider 23andMe has aroused similar concerns [188]. Under the terms of their 4-5 years agreement, GSK gained access to 23andMe's genetic data and became its exclusive collaborator for drug target discovery programmes [189]. While much of the coverage of these partnerships has focussed on issues of privacy and consent, we argue that another key consideration lies in the risks associated with exclusive or privileged access to databases of patient data and the development of proprietary diagnostic algorithms.

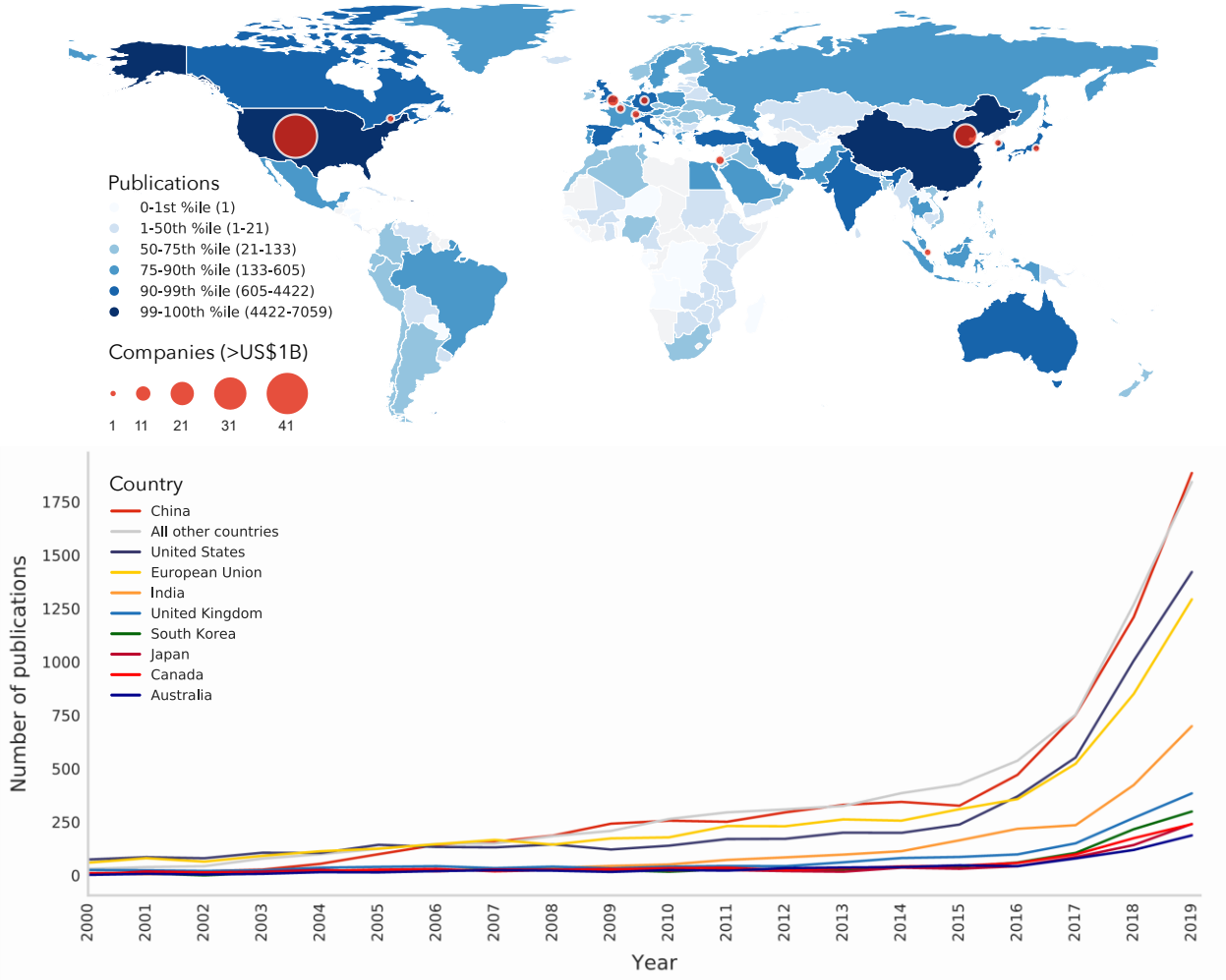

Fig. 3-1Publications on AI/machine learning applied to medical diagnosis and number of private AI or healthcare startup companies valued at >US$1B. Map shows the total number of publications on AI/machine learning applied to medical diagnosis by country from 2000 to 2019. In the legend, numbers in brackets represent number of publications while the colour gradient illustrates percentile categories. The bottom line diagram plots the same data by year and country. Data were extracted from Scopus using the search strategy reported by Liu et al. [190] Red dots on the map illustrate the number of venture capital-backed private AI or healthcare startup companies with a valuation of over >US$1B [186].

Why should we care about openness and transparency in AI development? Take the hypothetical case of a tech company developing a new proprietary AI to make prescription recommendations using electronic health record data from a large academic

medical centre. Aware of this ongoing programme, a pharmaceutical company decides to make its drugs available at a discounted price to the hospital, resulting in increased prescription of its drugs relative to competitors. Now, without any overt collusion, the tech company's AI may learn that these drugs are more often prescribed by the hospital's physicians and therefore have increased probability of recommending them in the future. Clearly these recommendations are inappropriate and not based on any medical evidence, yet without the ability to inspect the proprietary AI or the data it was trained on, the possibilities for peer review and scrutiny would be severely limited. Should AIs have their own disclosures? How would such disclosures be regulated and enforced? Would it be desirable to avert healthcare "data monopolies" with new antitrust legislation? These are questions regulators will need to answer sooner rather than later. While not AI-driven, the recent revelation that popular electronic health record vendor Practice Fusion received kickbacks in exchange for displaying alerts in its software designed to increase prescriptions of opioid analgesics [191] is a chilling reminder of the ability of software vendors to influence treatment decisions. The unmonitored allowance of proprietary healthcare AIs trained on privately held datasets risks providing an avenue for plausible deniability in addition to further hindering the detectability of such complicit partnerships between drug manufacturers and software vendors.

Beyond theoretical scenarios, take also for example a recent study by a group of Google researchers who designed an AI system to read mammograms that outperformed radiologists on a breast cancer identification task [192]. While unintentional and

acknowledged by the authors, 95% of the over 90,000 mammograms used in the study were acquired on devices made by a single manufacturer. Would the AI perform as well on images from another manufacturer's systems? What about the 10-year-old mammography system still operating in an under-resourced community? Further studies and clinical trials will be needed to obtain these answers, but this case highlights just how easy it is for systemic biases to be introduced even when no foul play is involved. Nonetheless, AI presents a tremendous opportunity to reduce barriers to care in low-resource settings around the world [193]. Unfortunately, current trends in AI research and private funding (Fig. 3-1) suggest the existence of strong geographical bias. A select group of countries, including notably China and the US, are responsible for most of the research and investment in AI-assisted medical diagnostics. Unless representative samples of patients are included, the likelihood of these tools providing equal benefits outside of their countries of origin is limited. Collaboration and exchange of data and experience between healthcare systems on a global scale is needed if we are to benefit from truly generalisable and equitable AI systems.

AI systems often—even to the ignorance of their creators—replicate the societal biases extant within the data they are trained on. In our own study [194], we found that the models we had trained to predict meningioma malignancy and survival predicted worse survival for black and uninsured patients. While these predictions are factually representative of the data in the large population-based national cancer registry on which we trained our models, the predicted outcomes are much more reflective of so-

cial and economic realities than they are of any biology. Other previously reported examples of bias include a melanoma diagnosis algorithm that did not factor skin colour or the use of genomic databases in which minorities are underrepresented [8]. These cases underscore the importance for healthcare practitioners to critically assess the predictions of putatively "objective" machine learning systems. They are also a reminder that while technological solutions will undoubtedly form part of our efforts for better care delivery, other systemic issues remain just as, if not more, critical to address.

Sensitivity, specificity, and other metrics tell only part of the story. While we can and should attempt to build performant AI systems that emulate ethical decision making, we must remember that human-designed AI remains biased by the same social, cultural, and political biases that shaped the data these systems were trained on. The physician's role as an advocate for patients' interests is as important today as it has ever been. We will increasingly come to rely on AI-assisted diagnosis and prognosis in the years to come, but treatment recommendations must remain conscious of societal context and continue to represent a shared decision-making process between physician and patient.

Competing interests

The authors declare no competing interests.

Role of the funding source

No funding was received specifically for this work. J.T.M. has received training awards from the Canada First Research Excellence Fund awarded to McGill University for the Healthy Brains, Healthy Lives initiative, the Fonds de Recherche du Québec-Santé, and the Foundation of Stars. S.B. was supported by a Discovery Grant from the Natural Science and Engineering Research Council of Canada (436355-13), the NIH (1R01EB026299-01), and a Tier-1 Canada Research Chair in Neural Dynamics of Brain Systems.

4

Chapter 4 – MNI SISCOM: An open-source tool for computing subtraction ictal single-photon emission CT coregistered to MRI

The Analytical Engine has no pretensions whatever to originate anything. It can do whatever we know how to order it to perform... But it is likely to exert an indirect and reciprocal influence on science itself.

– Ada Lovelace, Notes

Preface

This chapter describes a software tool I wrote for computing subtraction ictal single-photon emission CT coregistered to MRI (SISCOM). In line with the objectives of the thesis, the goal of this program is to develop imaging tools to aid with the presurgical evaluation for epilepsy surgery. The program was also used for parts of the analyses in chapter 6. This chapter provides a concise overview of the rationale for the tool, its uses, and a description of the available features. The program and source code are made freely available. The manuscript was submitted and is currently under review as:

Moreau JT, Saint-Martin C, Baillet S, Dudley RWR. MNI SISCOM: An open-source tool for computing subtraction ictal single-photon emission CT coregistered to MRI.

Abstract

Objective. We aimed to develop a simple user-friendly desktop application for computing subtraction ictal single-photon emission CT coregistered to MRI (SISCOM).

Conclusion. MNI SISCOM is a new free and open-source software application for computing SISCOM and producing practical MRI/SPECT/SISCOM image panels for review and reporting. It minimises manual user interaction and helps save time as compared to more general-purpose neuroimaging data analysis tools.

Introduction

Subtraction ictal single-photon emission CT coregistered to MRI (SISCOM) [1] is a widely used and well-established technique for quantitative analysis of ictal vs interictal SPECT images. The technique consists of computing difference images between coregistered and standardised ("z-scored") SPECT scans captured in the interictal and ictal phases. The technique highlights areas of hyperperfusion in the ictal as compared to the interictal scan, which has been demonstrated to be valuable in helping localise the seizure onset zone [107]. In a prospective study evaluating SISCOM in patients with either non-lesional MRIs or discordant data in the presurgical evaluation (e.g. discordant EEG and MRI), SISCOM was found to be concordant with the surgical resection in 82% of patients and 22/26 patients with post-surgical follow-up achieved Engel class I (15) or class II (7) outcomes [108]. In one recent meta-analysis [107], concordance between SISCOM and the surgical resection as compared to non-concordant SISCOM was associated

with a 3.28 times higher seizure-free odds ratio for temporal cases (2.44 for extra-temporal cases). Timing of the tracer injection however remains a critical determinant of the localisation sensitivity of SISCOM [107,108].

The conceptual basis of SISCOM is relatively simple, but there is presently a lack of user-friendly free and open-source software to compute SISCOM results from raw SPECT and MRI images. general-purpose neuroimaging data analysis packages such as SPM [195] already provide tools (e.g. coregistration and image calculators) that allow for the computation of SISCOM results, but obtaining these results typically requires several time consuming manual steps and necessitate a certain level of technical expertise. There have been previous efforts to design purpose-built software for computing SISCOM [196], but we could not find any open source software program that is actively maintained and runs on current versions of Mac/Windows/Linux operating systems. Here we present a newly developed cross-platform and open-source application to facilitate the process of computing SISCOM images. The goal of this project is to provide a freely available single-purpose and user-friendly tool to implement SISCOM.

Materials and Methods

The MNI SISCOM desktop application (Fig. 4-1) runs on Windows, Mac, and Linux computers and can be downloaded here: https://github.com/jeremymoreau/mnisiscom. Detailed installation instructions are provided on the download page linked above. In addition to MNI SISCOM, the SPM software package [195] must also be installed. SPM is a popular general-purpose brain imaging data analysis program and is used by MNI

SISCOM for SPECT and MRI image coregistration (i.e. aligning the SPECT images to the T1 MRI) and normalisation (warping MRI and SPECT images into standard MNI co-ordinate space).

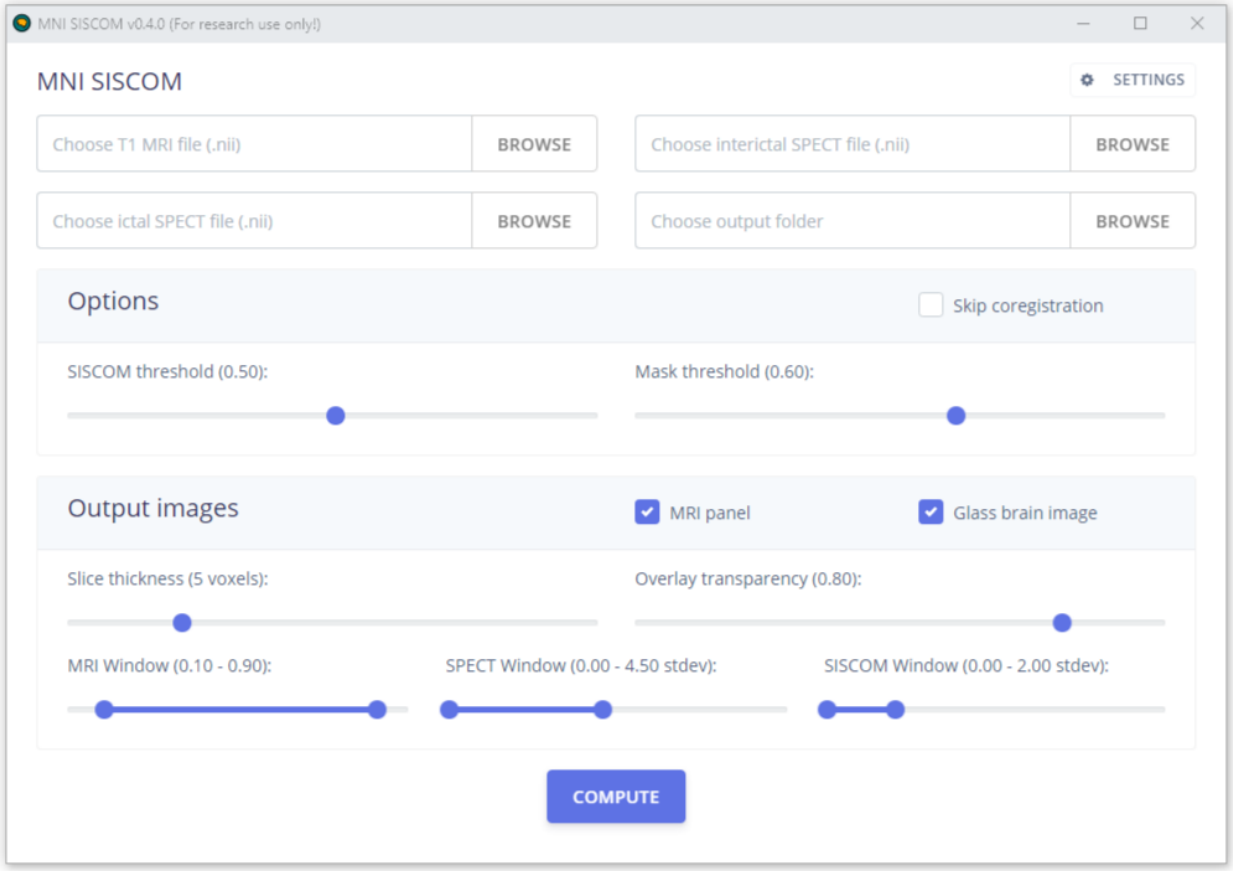

Fig. 4-1 Screenshot of main graphical user interface window of MNI SISCOM.

Usage of the desktop application is very straightforward. Simply launch the app and, after setting the SPM installation path in the "Settings" menu, select the T1 MRI, interictal SPECT, ictal SPECT, and folder where results will be saved. The other options do not generally require tweaking, but detailed explanations of each option can be viewed by hovering over the option label in the app. Once the "Compute" button is

clicked, MNI SISCOM will take ~2-5 minutes to compute the SISCOM results, depending on the speed of the computer. Of note, currently only MRI and SPECT images in NIfTI format (https://nifti.nimh.nih.gov) are supported. If exporting original DICOM images from PACS, we recommend using MRIcron [197] to convert DICOM images to NIfTI. MRIcron can be downloaded here: https://www.nitrc.org/projects/mricron. In MRIcron click on the "Import" menu and select "Convert DICOM to NIfTI".

In addition to the desktop application, a command line interface and user scriptable library written in the Python programming language is also made available for more technically inclined users. These interfaces allow for the integration of MNI SISCOM into other software pipelines or tools developed by others. An example Python script is provided (https://github.com/jeremymoreau/mnisiscom/tree/master/examples) to illustrate how these tools can be used to run MNI SISCOM on a group of patient MRI and interictal/ictal SPECT images without any user intervention. The command line tool and Python library can easily be installed via the standard Python Package Index: https://pypi.org/project/mnisiscom/

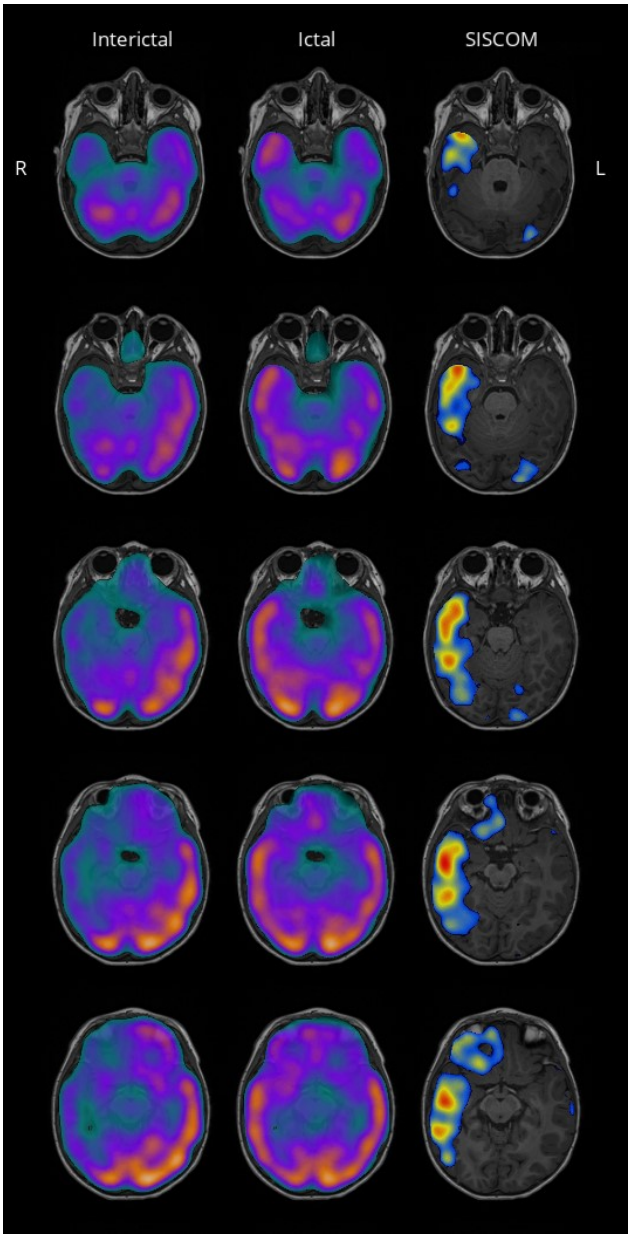

Fig. 4-2 Example MRI panel result file generated by MNI SISCOM showing interictal/ictal SPECT and SISCOM results side-by-side. This figure shows only 5 consecutive slices out of 23 axial slices with 5mm thickness. Coronal and sagittal panels are also generated, but not shown here.

Results

MNI SISCOM outputs scrollable 3D volumes of SISCOM results in NIfTI format, but also produces convenient image panel slides for rapid review and inclusion in presentations/reports. These panel slides include large panels showing interictal/ictal SPECT and SISCOM results side-by-side (Fig. 4-2) as well as a series of compact panels in axial, coronal, and sagittal orientation showing only interictal/ictal SPECT or SISCOM results (Fig. 4-3a). Moreover, MNI SISCOM can optionally output, using the bundled Nilearn module [198], schematic maximum intensity projection ("glass brain") images showing thresholded SISCOM maps superimposed over an anatomical reference drawing (Fig. 4-3b). For group studies, MNI SISCOM also provides the option to produce 3D NIfTI volumes in the standard MNI coordinate space, which can then be used in SPM [195] or other neuroimaging software packages to perform statistical comparisons between groups of patients.

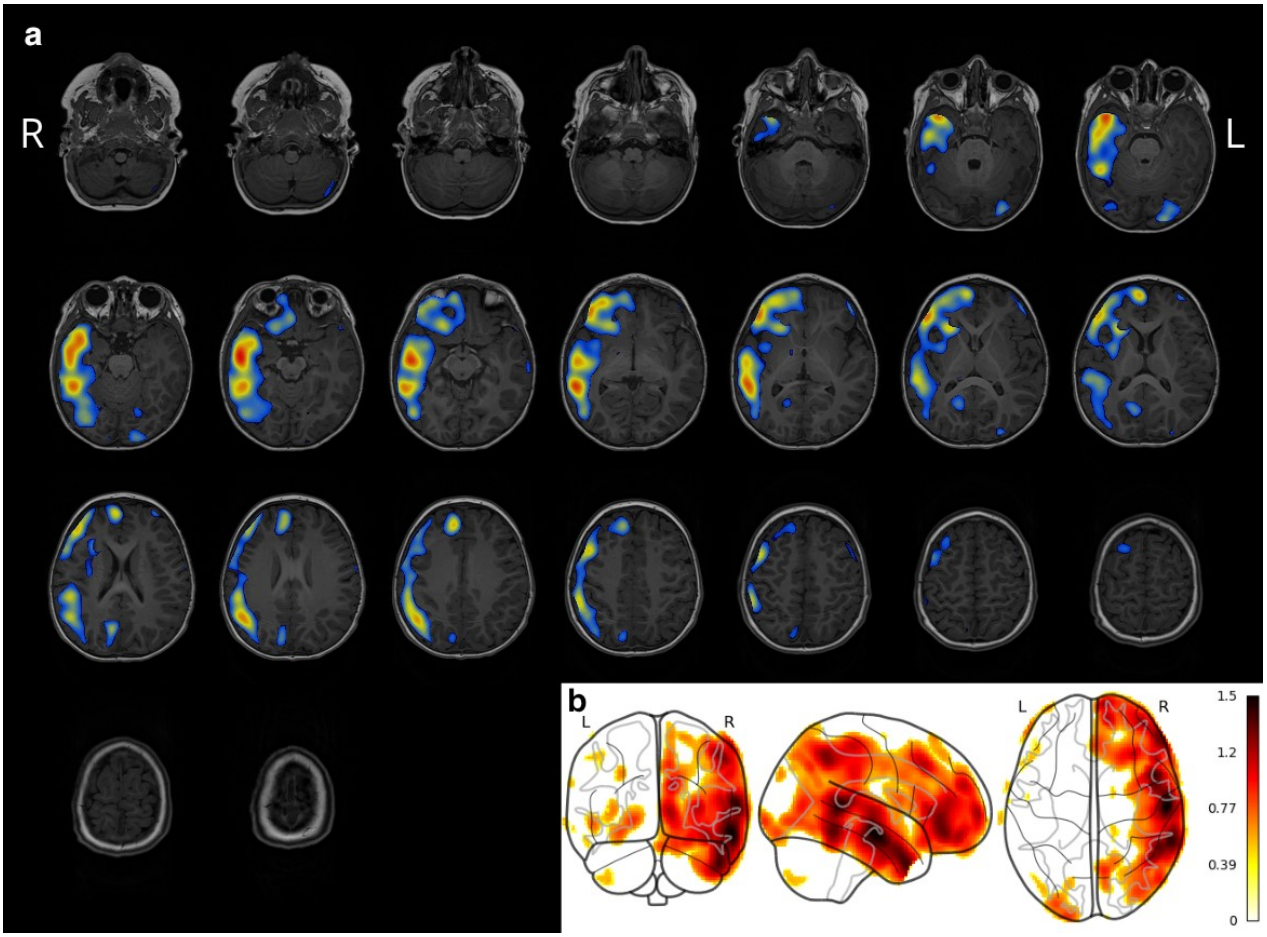

Fig. 4-3 Other types of result files generated by MNI SISCOM include compact axial/coronal/sagittal slides showing only interictal/ictal SPECT or SISCOM results (**a**) and schematic maximum intensity projection ("glass brain") images showing thresholded SISCOM maps superimposed over an anatomical reference drawing (**b**).

Discussion

Computation of SISCOM results is possible using existing general-purpose brain imaging data analysis programs, but obtaining such results is often time consuming and labour intensive. Our aim was to eliminate all the steps usually involved in obtaining SISCOM with a simple and modern desktop application. MNI SISCOM greatly simplifies the process by providing nearly entirely automatic processing of SPECT and MRI

images in order to generate SISCOM results with minimal user interaction. The application is also completely free and open-source, and we will continue contributing new features and usability improvements. We are also happy to receive suggested feature requests and help tailor the functionality of the application to the community's needs. Limitations include currently only supporting the NIfTI file format and requiring another program to convert DICOMs to NIfTI as well as only supporting the classical SISCOM algorithm. Additionally, MNI SISCOM currently depends on SPM for image coregistration, which requires another program to be installed. Future steps will include implementation of additional algorithms such as STATISCOM, which has been demonstrated to be superior to the more commonly used classical SISCOM algorithm in many cases [199]. We are also planning on building and bundling a database of interictal SPECT images in standard MNI space to allow for statistical comparison of individual patient ictal SPECT scans against the norm without the need for an interictal SPECT.

Conclusion

MNI SISCOM is a user-friendly free and open-source application for computing SISCOM. It provides a straightforward graphical desktop interface and helps minimise manual image manipulation tasks as compared to more multi-purpose brain imaging processing tools. Finally, the MRI/SPECT/SISCOM image panels generated by MNI SISCOM are a useful addition to help increase the efficiency of review and reporting of SISCOM results.

Disclosure

All authors report no conflicts of interest relevant to this article.

Acknowledgments

J.T.M. was supported by the Fonds de Recherche du Québec - Santé and the Foundation of Stars. S.B. was supported by a Discovery Grant from the Natural Science and Engineering Research Council of Canada (436355-13), the NIH (1R01EB026299-01), and a Tier-1 Canada Research Chair in Neural Dynamics of Brain Systems. This research was undertaken thanks in part to funding from the Canada First Research Excellence Fund, awarded to McGill University for the Healthy Brains, Healthy Lives initiative.

5

Chapter 5 – Overnight Ictal Magnetoencephalography

I have known many persons in sleep groaning and crying out, some in a state of suffocation, some jumping up and fleeing out of doors, and deprived of their reason until they awaken, and afterward becoming well and rational as before, although they be pale and weak.

– Hippocrates, On the Sacred Disease

Preface

This chapter presents two case reports of the first patients we recorded sleeping overnight while undergoing magnetoencephalography (MEG). While big datasets give us the ability to utilise new developments in machine learning and AI, in the next two chapters I explore how new ideas in multimodal imaging can also contribute to the presurgical evaluation. This is to our knowledge, the first published report of overnight ictal MEG. In this chapter, we discuss the analysis and outcomes, but also some of the practical considerations of performing such recordings in children. The manuscript was submitted and is currently under review as:

Moreau JT, Simard-Tremblay E, Albrecht S, Rosenblatt B, Baillet S, Dudley RWR. Overnight Ictal Magnetoencephalography.

Practical Implications

In patients with drug-resistant epilepsy for whom nocturnal seizures are recorded during an admission for EEG telemetry, overnight ictal magnetoencephalography is a viable methodology that can help localise the seizure onset zone.

The added value of magnetoencephalography (MEG) in the presurgical evaluation for drug-resistant epilepsy is well-recognised [113,119,200,201]. However, MEG remains for the most part limited to analysis of interictal epileptic activity [69,113]. Seizures are uncommonly captured due to logistical considerations despite mounting evidence of the value of ictal MEG in localising the seizure onset zone [69,202]. Here we report the recording and analysis of ictal MEG recordings in two drug-resistant epilepsy presurgical candidates that spent a night sleeping in the MEG at our institute.

Case 1

An 8-year-old girl with drug-resistant epilepsy of suspected right fronto-temporal origin was admitted for presurgical workup. Up to 4 months prior to this admission the patient only had nocturnal seizures. Frequency increased up to ~10 seizures/day and she began having daytime events that were described by the mother as consisting of a blank stare and non-responsiveness. Her first MRI revealed only asymmetry between bilateral temporal sulci. Following routine admission for EEG telemetry during which frequent nighttime seizures were recorded, a 4h overnight MEG recording was performed during sleep. One brief seizure lasting ~45s was captured at 2:13am (Fig. 1A),

which consisted of arousal followed by forced head version to the left. Electrographic onset preceded the head turn by ~6s and was characterised by rhythmic alpha activity beginning at T4 on EEG and over right temporal sensors on MEG. MEG source imaging of alpha frequencies at seizure onset suggested a right anterior temporal generator (Fig. 1B). A second 3T MRI including 3D T1 and FLAIR sequences showed anterior temporal blurring of the grey-white matter junction (Fig. 2C). FDG PET and SPECT scans showed right temporal hypometabolism and hypoperfusion, respectively. She underwent a tailored resection including the anterior temporal cortex all the way to mid-posterior temporal cortex. Surgical pathology (Fig. 1D-G) from the anterior temporal cortex, which included the MEG seizure onset zone, showed focal cortical dysplasia (FCD) type IIa, while the posterior aspect of the superior temporal gyrus contained rare dysmorphic neurons in cortex, but no frank FCD. The patient is currently seizure-free at 11 months follow-up.

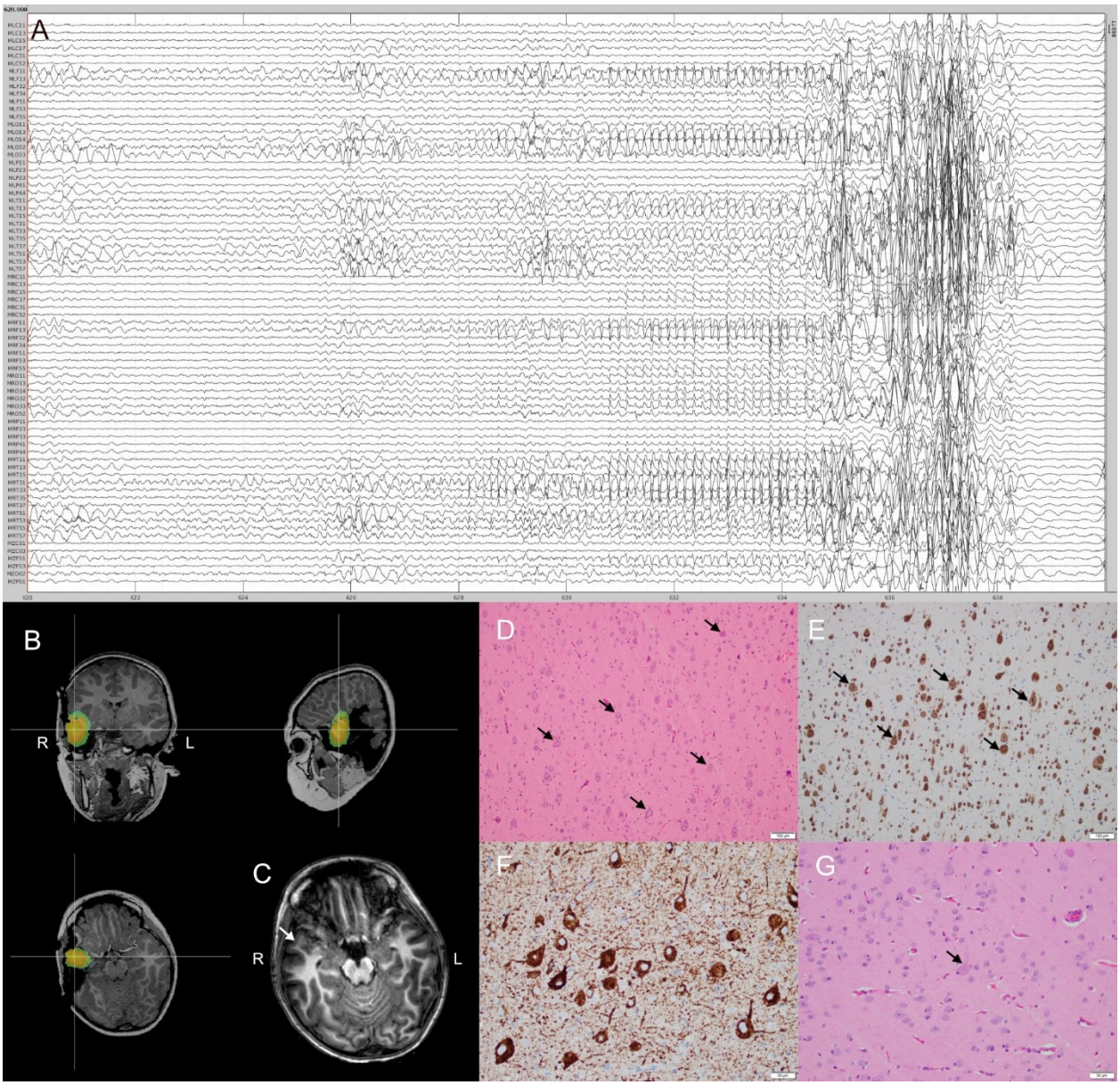

Fig. 5-1 Case 1 ictal MEG and pathology. (A) Reduced montage (76 of 275 MEG channels displayed) showing the seizure onset followed by movement artefact. (B) Magnetic source imaging of preop ictal MEG overlaid on postop MRI. (C) Preop T1 MRI showing blurring of the grey-white matter junction in an area colocalising with the MEG seizure onset zone. (D, E, F) Surgical pathology consisting of cortex and subcortical white matter from the resected anterior aspect of the superior temporal gyrus, showing focal cortical dysplasia (FCD) type IIa. (G) Surgical pathology consisting of cortex and subcortical white matter from the resected posterior aspect of the superior temporal gyrus, showing rare dysmorphic neurons in cortex, but no frank FCD. (D) H&E 10x. (E) NeuN 10x. (F) SMI-32 20x. (G) H&E 20x.

Case 2

A 13-year-old boy with drug-resistant epilepsy who underwent a previous SEEG study that failed to localise the seizure onset zone was readmitted for presurgical evaluation. Since 2.5 years of age, multiple EEGs recorded nocturnal electrographic seizures localising to the left posterior temporal-occipital region. In later EEGs, clinical seizures were additionally recorded in left frontal and frontopolar regions. Interictally, abundant spikes and continuous slow waves were recorded in the left temporal region. Prior to the present admission, the patient was having up to 20 seizures per night. Semiology was characterised by sudden arousal from sleep, confusion, agitation, some pelvic twisting and thrusting, and dystonic posturing of the right hand. A 5h overnight MEG recording was performed and 14 clinical seizures were recorded. One representative seizure is shown in Fig. 2B (onset for all seizures in Fig. 2C) together with MEG source imaging of the low-voltage fast activity in Fig. 2A. FDG PET also showed diffuse left hemispheric hypometabolism (Fig. 2E). Given that a majority of seizures on EEG and MEG localised to an area of left inferior parietal/posterior temporal cortex not covered by the previous SEEG study (Fig. 2D) and suspected signal abnormalities in left temporal opercular/posterior insular cortex on 3T MRI, a second SEEG implantation with broader coverage was undertaken. While abundant seizures were recorded, the study failed to localise a focal generator. Ictal spread to the same posterior perisylvian region that we had localised with ictal MEG preceded the stereotyped clinical onset, but this occurred late in the seizure. No surgery could be offered.

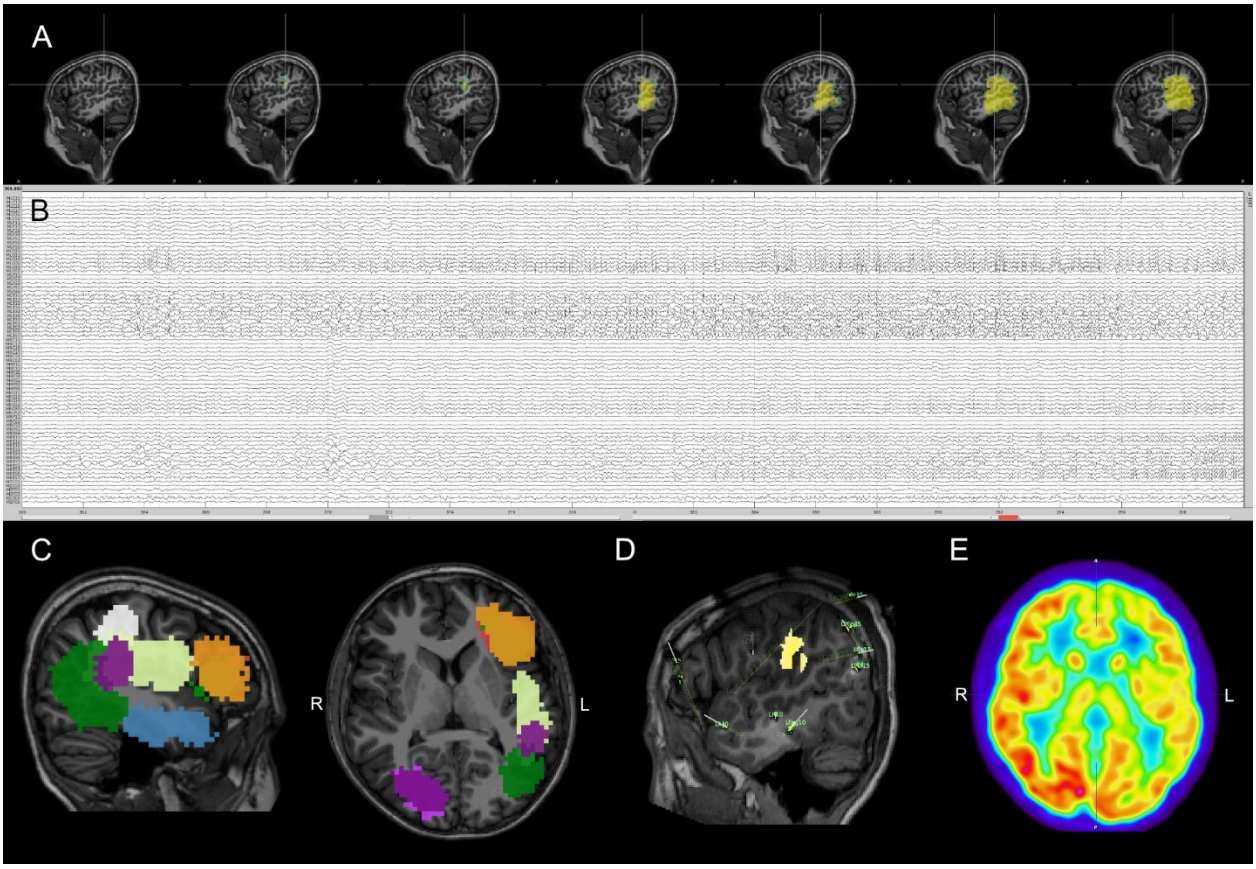

Fig. 5-2 Case 2 ictal MEG, FDG PET, and SEEG. (A) MEG source imaging over 5s windows of the seizure in (B) showing ictal spread beginning in the left supramarginal gyrus. (B) Reduced montage (76 of 275 MEG channels displayed) showing seizure onset and spread. (C) MEG source imaging of seizure onset in 9 independent seizures (4 L parietal, 3 L frontal, 1 L inferior temporal, 1 R occipital) captured during the overnight ictal MEG. 5 seizures were excluded because of artefact or missed onset. Each colour represents a different seizure. (D) ictal MEG source imaging plotted over first SEEG postimplantation MRI. SEEG electrodes are shown in grey, with green channel labels. (E) ^{18}F-FDG PET showing diffuse left hemispheric hypometabolism.

Discussion

In many tertiary epilepsy centres, including our own, MEG is presently rarely utilised during nighttime off-hours. We argue that overcoming the logistical challenges of such recordings presents a significant opportunity for the acquisition of routine ictal MEG.

In the two cases presented here, we demonstrate that recording natural sleep in unsedated children overnight is both achievable and can allow for routine ictal MEG recordings in well-selected patients, such as those with sleep-related seizures.

Practically, some suggestions from our experience include adding a comfortable mattress above the standard patient support and a thin pillow in the MEG helmet to prevent discomfort from the EEG electrodes, and placing a second bed in the magnetically shielded MEG room for a parent to sleep next to the child. In conclusion, overnight MEG recordings in well-selected candidates are proposed as a viable methodology to obtain routine ictal MEG in the presurgical evaluation for drug-resistant epilepsy.

Study funding

Funding for the overnight MEG scans and ancillary expenses was provided by the Foundation of the Department of Neurosurgery, Faculty of Medicine, McGill University as well as a "New Directions in Research" award from the Montreal Children's Hospital Foundation. J.T.M. was supported by the *Fonds de Recherche du Québec - Santé* and the Foundation of Stars. S.B. was supported by a Discovery Grant from the Natural Science and Engineering Research Council of Canada (436355-13), the NIH (R01 EB026299), and a Tier-1 Canada Research Chair in Neural Dynamics of Brain Systems. This research was undertaken thanks in part to funding from the Canada First Research Excellence Fund, awarded to McGill University for the Healthy Brains, Healthy Lives initiative.

Disclosure

The authors report no disclosures relevant to the manuscript.

6

Chapter 6 – Localisation of oligodendroglial hyperplasia and differentiation from focal cortical dysplasia type II with multimodal imaging

Medicine is a science of uncertainty and an art of probability.

– Sir William Osler

Preface

In this chapter we describe the application of multimodal imaging to a newly characterised histopathological entity in children with drug-resistant epilepsy. We demonstrate that some imaging modalities not previously investigated in these patients can help localise and differentiate this pathology from more common malformations of cortical development. This chapter again highlights how novel applications of imaging techniques can aid in the presurgical evaluation for paediatric epilepsy. The manuscript was submitted and is currently under review as:

Moreau JT, Vinaik R, Simard-Tremblay E, Albrecht S, Saint-Martin C, Rosenblatt B, Baillet S, Dudley RWR. Localisation of oligodendroglial hyperplasia and differentiation from focal cortical dysplasia type II with multimodal imaging.

Abstract

Newly defined histopathological entities such as oligodendrocyte hyperplasia (OH) might account for some cases of previously described negative pathology focal epilepsy. The imaging characteristics of OH are however poorly characterised. In this study, we obtained 3T T1, T2, and diffusion-weighted MRI (DWI) as well as MEG, FDG PET, and interictal/ictal SPECT in 4 patients with OH and 7 control patients with FCD. Surgical specimens were stained with OLIG2 and cell density measurements were performed. Patients with OH showed significantly greater OLIG2-positive cell densities (3046 ± 839 cells/mm^2) than FCD patients (1506 ± 265 cells/mm^2). Normalised apparent diffusion coefficient (ADC) values within the resection volume were significantly higher in OH as compared to FCD. ADC, PET, and MEG had the highest localisation value and high interrater agreement in patients with OH. Mean resection volume was significantly greater for OH (43.2 cm^3) than FCD (5.3 cm^3). 7/7 FCD patients and 2/4 OH patients were seizure free at >18 months follow-up. We conclude that quantitative analysis of DWI could allow for non-invasive differentiation between OH and FCD. PET, ADC, and MEG imaging of focal slowing could be particularly valuable in localising poorly defined lesions in patients with OH.

Keywords: epilepsy surgery, oligodendroglial hyperplasia, PET, SPECT, magnetoencephalography, diffusion-weighted MRI

Introduction

Malformations of cortical development are the most frequent cause of focal drug-resistant childhood epilepsy [203]. While focal cortical dysplasia (FCD) accounts for the majority of these cases [203], newly defined histopathological entities such as oligodendroglial hyperplasia (OH)—which is characterised by increased densities of oligodendroglial-like cells (OLCs) in subcortical white matter [204]—may explain some of the previously described negative pathology cases [203]. Here, we specifically use the term OH to refer to a focal increase in OLIG2-immunoreactive cells in patients with drug-resistant epilepsy, though terms including "oligodendrocytosis" [205] and "mild malformation of cortical development with oligodendroglial hyperplasia" [204] have also been used.

In a study of histopathological findings in 2623 children, Blümcke et al. reported 1-year seizure-free rates of 79.9% for tumours, 59.9% for malformations of cortical development, and 55.2% for children in whom no specific lesion could be identified [203]. Reports of seizure freedom rates in OH vary, with one study reporting seizure freedom in only 6/18 (33%) patients (mean 11.8 years follow-up) [204], while another group reported 1-year seizure-freedom in 13/18 (72%) of their patients, which they attributed to more extensive surgical resections [205]. As with this later study, there is mounting evidence suggesting that observed increases in OLCs could be associated with more extensive epileptic networks in children, which might require more extensive multilobar resections to achieve seizure freedom [205–207]. While the exact mechanisms have not been fully explored, Sakuma et al. [207] have proposed that interactions between cortical

epileptic neurons and subcortical OLCs in OH could contribute to these extensive epileptogenic networks.

Given possible differences in surgical treatment and outcomes, the ability to localise and differentiate OH from other malformations of cortical development would be valuable. Previous case series of patients with OH have noted blurring of the grey-white matter junction, increased cortical thickness, and subcortical T2/FLAIR signal hyperintensities [204,205,208–210]. However, in one study that compared MRI and MEG imaging characteristics between OH and FCD I, imaging features were similar between the two pathologies [205]. We aimed to assess the value of additional imaging modalities, beyond conventional MRI, in either helping localise or differentiate tissue with OH from controls with FCD alone. Specifically, we qualitatively and quantitatively evaluated contributions from diffusion-weighted MRI, ^{18}F-FDG PET, interictal/ictal SPECT, interictal magnetoencephalography (MEG), MEG power spectral density, and T1/T2 ratio MRI, in a series of patients with OH and a group of control patients with FCD.

Materials and Methods

Patients

The study received full approval from the McGill University Health Centre's Research Institute Ethics Board, and all involved patients and/or parents/guardians signed an informed consent form to be enrolled in the study. Pathology reports for all patients who underwent epilepsy surgery at the Montreal Children's Hospital between 2015

and 2019 were reviewed. These dates were selected as they correspond to the introduction of a new imaging protocol at our centre that included all the imaging modalities discussed in this study. All 4 patients with a pathological diagnosis of oligodendroglial hyperplasia and a consecutive series of 7 control patients with focal cortical dysplasia were included.

MRI, PET, SPECT, and MEG image acquisition

We obtained 3T T1, T2, and diffusion MRI pre-operatively (preop) and post-operatively (postop) in all patients. ^{18}F-FDG PET, ictal and interictal SPECT, and MEG were acquired only preop. Preop MRIs were acquired on a Siemens Skyra 3.0T while postop MRIs were acquired on either this same scanner (n = 5) or a Philips Achieva 3.0T intraoperative MRI (n = 6). Preop and postop T1 MRIs were acquired with a 1-mm isotropic resolution. T2 MRIs were acquired with either 3.5-mm slice thickness and 0.5-mm in-plane resolution or 1-mm slice thickness and 0.5-mm in-plane resolution. Apparent diffusion coefficient (ADC) images with 5-mm slice thickness and 1-mm in-plane resolution were obtained from diffusion-weighted images with b-values of 0, 500, and 1000 s/mm^2. PET was acquired on a Philips Gemini TF scanner with a 2-mm isotropic resolution. SPECT was acquired on a GE Tandem Discovery 670 with a 4.4-mm isotropic resolution. MEG was acquired on a 275-channel CTF system with a sampling rate of 2.4KHz.

Pathology and image processing

Surgical specimens were stained with OLIG2, an immunohistochemical marker of oligodendroglial-like cells [207]. Quantitative cell density measurements of OLIG2-positive

cells were performed using QuPath [211]. For each patient, all MRI, PET, and SPECT imaging was first coregistered to the preop T1 MRI using SPM [195]. MRIs were resliced into 1-mm isotropic voxel dimensions and skull-stripped using pstrip [212]. Surgical cavity margins were manually outlined using Freesurfer's [213] FreeView. T1/T2 ratio images were computed using the MRTool SPM12 toolbox [214]. ADC images were masked using a white matter mask generated using Freesurfer and intensities were normalised within image volumes. PET and SPECT values were normalised to the cerebellum. MEG analyses were performed using Brainstorm [215]. An overlapping spheres volume head model was computed from Freesurfer surfaces generated from the preop T1 MRI. Source imaging was performed using dSPM and power spectral densities were computed in source space using Welch's method (as implemented in Brainstorm). Mean volumes and normalised mean imaging values within the margins of the surgical cavity were extracted using FSL [216].

Interrater agreement and statistical analyses

For all qualitative analyses, 3 independent raters (C.S.M, J.T.M, R.W.R.D.) reviewed the imaging with an outline representing the margins of the surgical cavity overlaid above the volume. They were asked to rate whether there was no signal abnormality, a subtle abnormality, or a clear abnormality within the outline. For calculations of interrater agreement, the "yes" and "yes (subtle)" choices were combined. After reviewing the imaging independently, the three raters re-examined all images together and made a consensus decision. All statistical analyses were performed in R. Mean differences in imaging values, resection volumes, and cell densities between the OH and FCD groups

were compared using Welch's 2-sample t-tests and corrected for multiple comparisons using the Bonferroni method. Robust regressions between cell densities and imaging values were performed using the *robustbase* R package (MM-estimator) to minimise the impact of potential outliers. Interrater reliability was assessed using percentage agreement. Means ± one standard deviation are reported unless otherwise specified.

Results

Example OLIG2-pathology slides as well as PET, ADC, T1/T2 MRI, and MEG imaging results for two FCD and two OH patients are presented in Fig. 6-1. Qualitative localisation value consensus results are shown in Fig. 6-2A and interrater agreement in Fig. 6-2B. ADC, PET, and MEG had the highest localisation value for OH (concordant in 4/4 patients) with high inter-rater agreement (ADC: 82%, PET: 91%, MEG delta power: 100%). There were no significant differences in preop mean imaging values within the volume of the surgical resection between the OH and FCD II groups (adj. $p > 0.05$) except for ADC (adj. $p = 0.02$, Fig. 6-2C). There was also a significant positive relationship between OLIG2-positive cell densities and ADC intensities (adj. $R^2 = 0.49$, adj. $p = 0.01$, Fig. 6-2C). Mean resection volumes were significantly greater for OH (42.2 ± 16.1 cm^3) than FCD II (5.3 ± 2.5 cm^3), $p = 0.006$ (Fig. 6-2D). Patients with OH showed significantly greater OLIG2-positive cell densities (3046 ± 839 cells/mm^2) than FCD II patients (1506 ± 265 cells/mm^2), $p = 0.01$, or literature-reported autopsy values (~950 ± 200 cells/mm^2) [204] (Fig. 6-2E). 7/7 FCD patients and 2/4 OH patients were seizure free at an average 31 months postop (range 18-55 months, Supplementary Table 6-1).

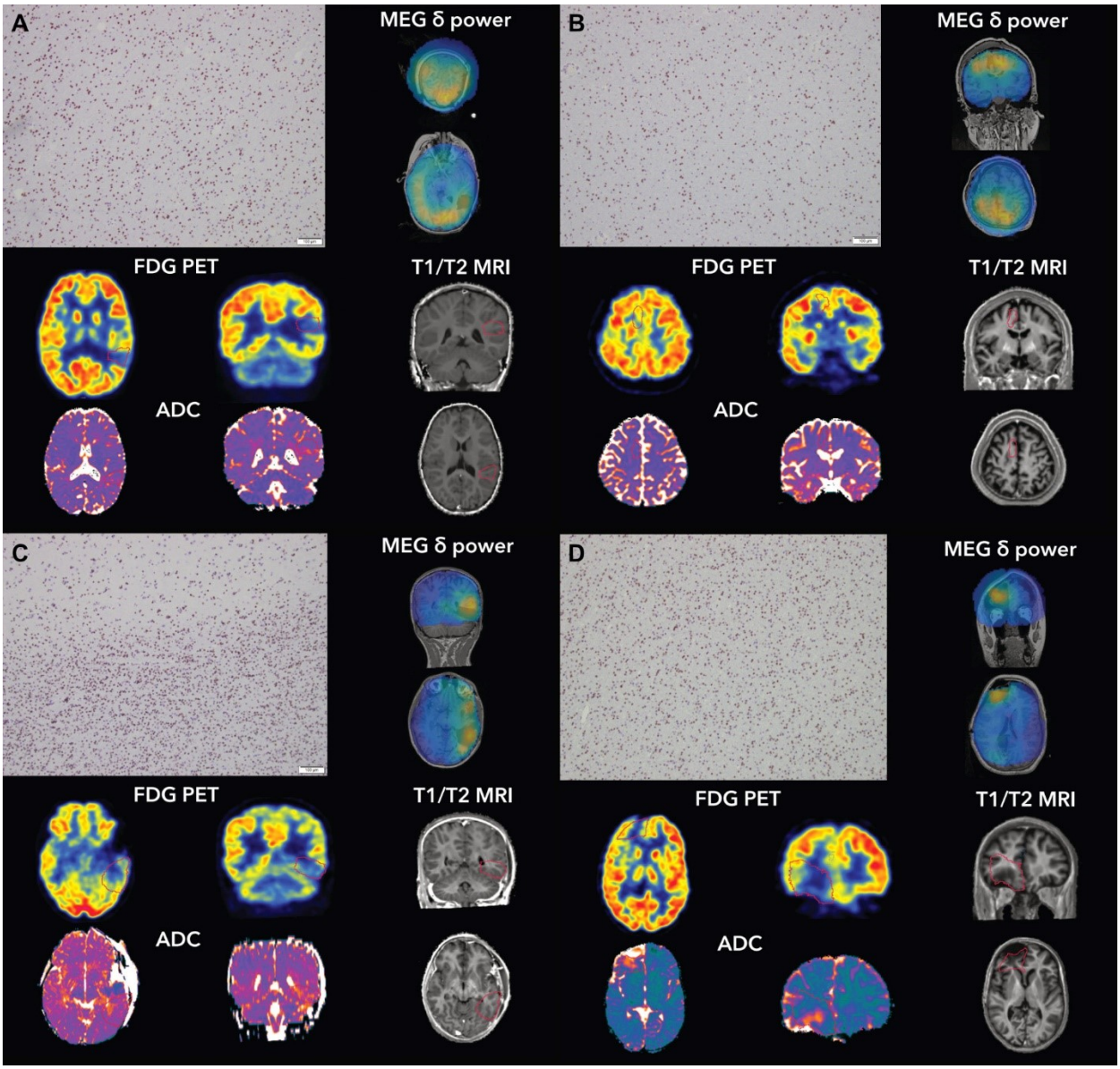

Fig. 6-1 Example pathology, PET, ADC, T1/T2 MRI, and MEG results in 2 OH and 2 FCD patients. OLIG2-stained surgical pathology slides, MEG delta power overlaid on postop MRI, ^{18}F-FDG PET, apparent diffusion coefficient (ADC), and T1/T2 ratio MRI for two example focal cortical dysplasia type II patients (A, B) and two patients with oligodendroglial hyperplasia (C, D). Red outline indicates the margins of the surgical resection. *δ*: delta (2-4Hz)

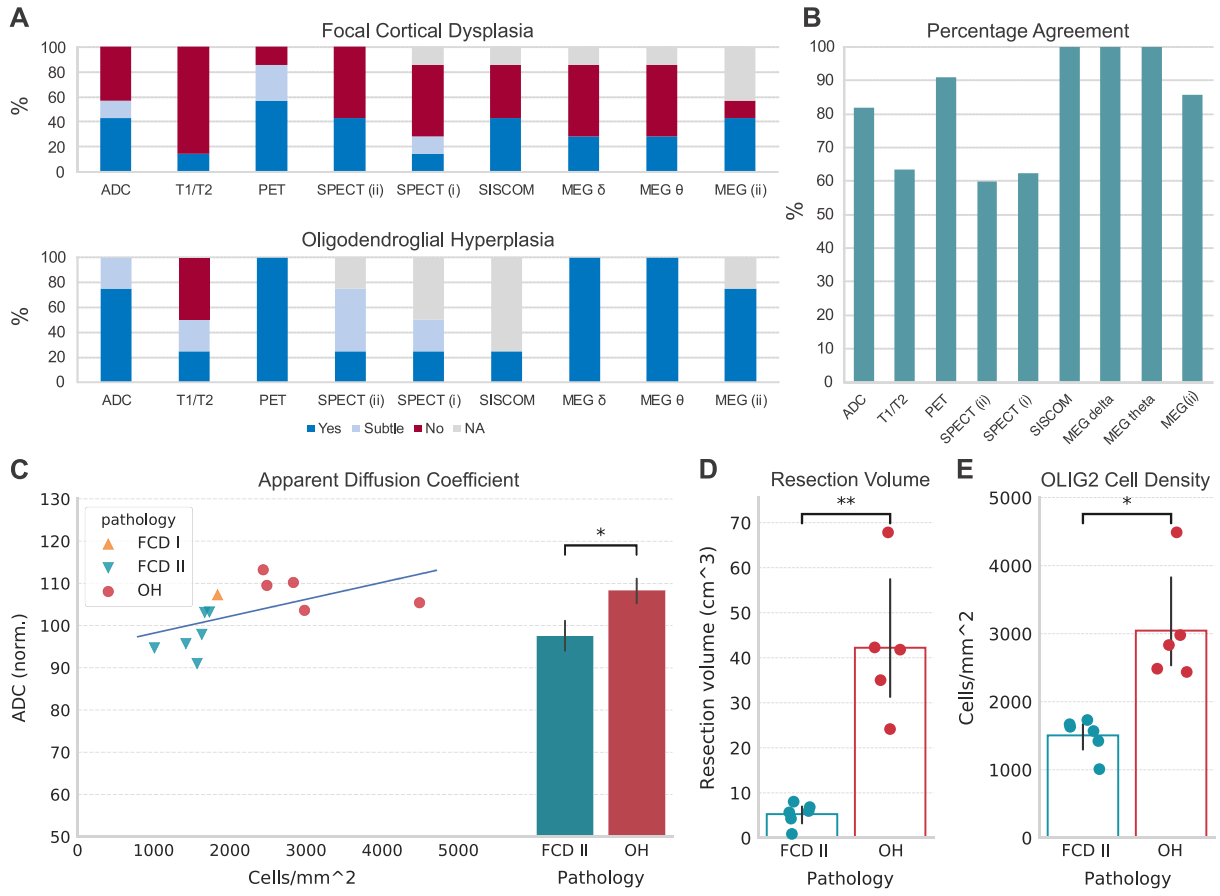

Fig. 6-2 Qualitative (A, B) and quantitative (C, D, E) evaluation of imaging and pathology for focal cortical dysplasia (FCD) and oligodendroglial hyperplasia (OH). A, Percentage of patients for whom a signal abnormality was observed within the margins of the surgical resection. Results show the consensus decision of the 3 raters. B, Percentage interrater agreement for each of the modalities. C, Scatter plot shows normalised apparent diffusion coefficient (ADC) as a function of OLIG2-positive cell density within resected tissue. Bar plots show mean ADC values and 95% confidence intervals for FCD II and OH. D, Mean resection volume and 95% confidence intervals for FCD II and OH. E, Mean OLIG2-positive cell density for FCD II and OH.

Discussion

The objectives of the present study were to identify imaging modalities that could help localise OH and, if possible, differentiate OH from FCD radiologically. We found that FDG PET, ADC, and MEG imaging of focal slowing were particularly useful in localising pathological tissue in patients with OH (Fig. 6-2A). Several previous case reports and

small case series have identified imaging characteristics of OH on T1, T2, and FLAIR MRI [204,205,208–210,217]. Beyond MRI, one study additionally reported that MEG spike source clusters were identified in 67% of patients with olidodendrocytosis and were concordant with the surgical resection in all cases [205]. In addition to MEG source imaging of interictal spikes, MEG localisation of focal slowing localised the epileptic generator in the present sample of patients with OH. As with the previous study [205], however, we found no significant differences in MEG features between the OH and FCD groups. In fact, of the 5 imaging modalities investigated, only ADC showed significant differences between OH and FCD. Given the value of diffusion-weighted MRI for white matter imaging, it seems reasonable to expect that ADC may be particularly relevant in patients with OH.

ADC is one of the methods frequently utilised in the radiological diagnosis of oligodendrogliomas [218]. As with oligodendroglioma, our results suggest that ADC can help localise abnormal tissue in patients with OH. The noted increase in ADC values we report with OH is akin to the higher ADC values typically observed in low-grade tumours [218]. However, it has also been reported that the high nucleus-to-cytoplasm ratios observed in high-grade tumours are associated with lower ADC values due to restriction of water diffusion [219]. While associated with increased cellularity, cell densities in OH remain on average lower than even low-grade oligodendroglioma [204], which may explain why increased, rather than decreased, ADC was observed in our sample of patients with OH.

Regarding surgical outcomes, previous studies have suggested that OH may be associated with relatively poorer seizure freedom outcomes. Likewise, while the present sample is small, 2/4 patients with OH were not seizure free (Engel IIb and Engel IIIa) as compared to 7/7 FCD patients who were seizure-free at an average of over 2 years postop. Despite the poorer outcomes, our patients with OH underwent significantly larger resections than those with FCD (Fig. 6-2D). This is consistent with previous reports suggesting that OH may require larger resections than FCD [205].

Some methodological limitations of this study include the small sample size, the use of different scanners and sequences in some patients, and the lack of more advanced diffusion-weighted MRI (e.g. HARDI, DTI, DKI). OH remains a relatively rare if perhaps underreported pathological entity [204], and multi-institutional collaboration will be needed to provide reliable assessments of seizure freedom rates and to validate the present preliminary imaging results on larger cohorts. While we relied on retrospective analysis of available imaging at our institution, future studies would benefit from prospective evaluation with standardised imaging protocols. In particular, given the promising results obtained with ADC, we feel that the inclusion of higher spatial and angular resolution diffusion-weighted MRI sequences could be a particularly interesting avenue to explore in future work.

In conclusion, the present study provides preliminary evidence that PET, ADC, and MEG source imaging of focal slowing could have value in localising epileptogenic tissue in patients with histologically-confirmed OH. Additionally, quantitative analysis of ADC could allow for differentiation of OH from FCD II alone.

Supplementary Table 6-1 Demographic and clinical information of the study sample.

ID	Age	Sex	Seizure onset zone	Pathology	Follow-up (months)	Outcome (Engel)
FCD1	5	F	L Temporal	FCD 2b	39	Ia
FCD2	14	F	R Precentral	FCD 2a	40	Ia
FCD3	2	M	L Precentral	FCD 2b	55	Ia
FCD4	5	M	R temporo-occipito-parietal	FCD 1a	20	Ia
FCD5	10	F	R SMA	FCD 2a	18	Ia
FCD6	11	F	L fronto-central	FCD 2a	18	Ia
FCD7	7	M	L Precentral	FCD 2a	19	Ia
OH1	13	M	L Temporal	OH and FCD 1b	45	IIb
OH2	14	M	R Frontal	OH and FCD 2a/2b	42	Ia
OH3	11	M	R Frontal	OH and gliosis	22	Ia
OH4	10	F	R Temporal	OH and HS	21	IIIa

Acknowledgments

Funding for the MEG scans and ancillary expenses was provided by the Foundation of the Department of Neurosurgery, Faculty of Medicine, McGill University as well as a "New Directions in Research" award from the Montreal Children's Hospital Foundation. J.T.M. was supported by the *Fonds de Recherche du Québec - Santé* and the Foundation of Stars. S.B. was supported by a Discovery Grant from the Natural Science and Engineering Research Council of Canada (436355-13), the NIH (R01 EB026299), and a Tier-1 Canada Research Chair in Neural Dynamics of Brain Systems. This research was undertaken thanks in part to funding from the Canada First Research Excellence Fund, awarded to McGill University for the Healthy Brains, Healthy Lives initiative.

Conflict of Interest

None of the authors has any conflict of interest to disclose. We confirm that we have read the Journal's position on issues involved in ethical publication and affirm that this report is consistent with those guidelines.

7

Chapter 7 – General discussion

I may not have gone where I intended to go,
but I think I have ended up where I needed to be.

– Douglas Adams, The Long Dark Tea-Time of the Soul

In this thesis, I presented a body of work demonstrating how predictive analytics and multimodal imaging can assist in some aspects of decision-making in neurosurgery. Specifically, I contributed studies demonstrating applications of machine learning techniques and novel applications of multimodal imaging in the context of neuro-oncology and paediatric epilepsy surgery. These studies represent a beginning rather than an end to the direction I would like to take in future work. Many of the tools and techniques developed in this thesis have the potential to contribute to new advancements in related areas. The meningioma malignancy and prediction app presented in chapter 2 for instance could easily be adapted for other cancers, neurological or otherwise. Likewise, it is my intention to continue updating the SISCOM app discussed in chapter 4 to add new features such as support for newer algorithms like STATISCOM [199] and add support for quantitative analysis of other imaging modalities such as PET. This reflects a general theme of this thesis, to not only build new tools, but also to share them and make them available for anyone to adapt and expand upon.

In chapter 2, I presented machine learning models, trained on data from over 60,000 patients, designed to aid in the diagnosis and prognosis of meningiomas. While the actual implementation remains foremost a proof of concept, much of the methodology remains very applicable to future endeavours. In particular, as is discussed in the body of the paper, I am keen to expand the predictive models to build in molecular and imaging data into the predictions. In future developments, I envisage it being possible to upload an MRI and lab values in the app, which would then use these additional data to provide more accurate predictions. Nonetheless, at least for survival predictions, the models and app could already be valuable in providing better estimates of survival probabilities, which could aid in patient counselling. In this regard, I would like to conduct follow-up prospective validation studies to better assess on one hand the predictive validity of the estimates, but also user experience of physicians using the app and patient feedback on the personal relevance of these kinds of predictions. In the end, I feel tools must be developed in the interest of patients and improving care, and obtaining this kind of feedback is crucial in determining where we should be investing more time and resources.

In chapter 3, I followed-up on the practical application presented in chapter 2 with a discussion of some of the ethical issues involved in the use of machine learning in medicine. I presented original statistics on geographical publication bias and spatial inequality in investments in AI applied to medical diagnostics. AI has great potential to decrease costs and improve diagnostic accuracy in lower-resource settings [193], but this

will require early attention, and perhaps legislation, ensuring that representative datasets of patient information can be collected and applied in training AI systems. In this chapter I also highlight how AI does nothing in the way of addressing the systemic biases already extant within our healthcare systems, and, if left unaddressed, even runs the risk of exacerbating some of these issues by giving healthcare providers a false sense of "objectivity" in making healthcare decisions that may, at least in part, be driven by socioeconomical rather than medical factors. From a legal perspective also, the "black box" nature of many of these algorithms could make it harder to detect foul play from ill-intentioned actors guided by commercial interest. While there are no easy answers to any of these problems, at least discussing their existence and publicising not just the potential, but also the limitations of AI applied to healthcare will hopefully lead to the development of fairer, more equitable, AI systems in real-world practice.

In chapter 4, I transitioned to discussing an open-source software application I recently developed for the computation of subtraction ictal single-photon emission CT coregistered to MRI (SISCOM). I started out this project mostly because we needed such a tool to compute SISCOM, but have developed it over the last year to make it more user-friendly and accessible to others. One benefit of open-source software is that anyone with the inclination can modify the program to suit their own needs. Beyond the future directions discussed in the chapter itself, one additional aspect I would like to develop is the use of deep learning to combine predictions from multiple imaging modalities (e.g. SISCOM, PET, and MRI). This would likely require larger datasets of

MRI and nuclear imaging scans than I currently have available, but could further contribute to better outlining the lesional and functional deficit zones. It would also be interesting to include an aspect of seizure-freedom prognostication, by training not only on surgical patients who achieved seizure freedom, but also on seizure frequency in those who did not. For instance, we could imagine the software predicting a percentage probability of seizure-freedom if the highlighted region were to be resected.

In chapter 5, I begin my discussion of applications of multimodal imaging to the presurgical evaluation in patients with drug-resistant epilepsy. In this chapter, I begin with two case presentations of the first two children we recorded sleeping overnight in the MEG at the MNI. I discussed the analysis and implications for one "positive" and one "negative" case to illustrate both the benefits and challenges involved in the application of ictal MEG. I additionally offered some practical recommendations on certain changes we have made that have facilitated and improved the comfort of these overnight recordings. While logistically challenging, these scans have the potential to provide valuable information in well-selected patients with nocturnal seizures. They also represent a better utilisation of expensive equipment that is presently underutilised outside of regular working hours. Future directions will include amassing a larger case-series of overnight ictal MEG recordings and prospectively evaluating localisation accuracy against invasive EEG and surgical outcomes.

Finally, in chapter 6 I present the results of a study investigating the potential of a series of imaging modalities in helping localise and differentiate a recently characterised histopathological entity, oligodendroglial hyperplasia (OH), from focal cortical

dysplasia. I demonstrated that while PET, ADC, and MEG source imaging of focal slowing could help localise epileptogenic tissue containing OH, only ADC was capable of differentiating between OH and FCD type II. This remains a relatively small case series and future studies will need to replicate this work with greater sample sizes, but the results suggest that OH may radiologically differ from other malformations of cortical development in at least some aspects. Given the over 50% of children who become seizure free after a histologically-negative resection [203] further work is clearly needed to provide additional mechanistical explanations of epilepsy in these patients. An approach combining both carefully labelled surgical pathology and advanced pre-operative imaging could contribute to furthering this objective. Correlation of ex-vivo imaging of surgical specimens to histology could also help develop a better understanding of the imaging features of the various sequences used in the presurgical evaluation.

In conclusion, in this thesis I presented a group of studies with the overarching aim of assisting in some aspects of decision-making in neurosurgery. I made new contributions to applications of machine learning techniques in neuro-oncology and provided software and methodological developments that could aid in the presurgical evaluation for children with drug-resistant epilepsy. These studies together offer new hypotheses and directions of investigation that could lead to more quantitative tools to guide neurosurgical decision-making and improved patient outcomes. In future work, I hope to expand on this body of research with larger prospective and controlled studies, as well as by continuing to develop software applications that will aid in translating these findings to real-world practice.

List of publications

Published

1. **Moreau JT**, Hankinson TC, Baillet S, Dudley RWR. Individual-patient prediction of meningioma malignancy and survival using the Surveillance, Epidemiology, and End Results database. *npj Digital Medicine*. 2020;3(1):12. www.nature.com/articles/s41746-020-0219-5

2. Eid H, Crevier-Sorbo G, **Moreau JT**, Saint-Martin C, Elzawawi MS, Mousa WA, Dudley RWR, Wilson N. Eight-Year Experience With 3-T Intraoperative MRI Integration in Focal Pediatric Epilepsy Surgery: Impact on Extent of Resection, Residual Volumes, and Seizure Outcomes. *AJR*. 2020 Mar 24;1–8. www.ajronline.org/doi/abs/10.2214/AJR.19.22336

3. Niso G, Gorgolewski KJ, Bock E, Brooks TL, Flandin G, Gramfort A, Henson RN, Jas M, Litvak V, **Moreau JT**, Oostenveld R, Schoffelen J-M, Tadel F, Wexler J, Baillet S. MEG-BIDS, the brain imaging data structure extended to magnetoencephalography. *Sci Data*. 2018 Jun 19;5:180110. www.nature.com/articles/sdata2018110

4. Das S, Glatard T, Rogers C, Saigle J, Paiva S, MacIntyre L, Safi-Harab M, Rousseau M-E, Stirling J, Khalili-Mahani N, MacFarlane D, Kostopoulos P, Rioux P, Madjar C, Lecours-Boucher X, Vanamala S, Adalat R, Mohaddes Z, Fonov VS, Milot S, Leppert I, Degroot C, Durcan TM, Campbell T, **Moreau J**, Dagher A, Collins DL, Karamchandani J, Bar-Or A, Fon EA, Hoge R, Baillet S, Rouleau G, Evans AC. Cyberinfrastructure for Open Science at the Montreal Neurological Institute. *Front Neuroinform*. 2017;10:53. www.frontiersin.org/articles/10.3389/fninf.2016.00053

5. Das S, Glatard T, MacIntyre LC, Madjar C, Rogers C, Rousseau ME, Rioux P, MacFarlane D, Mohades Z, Gnanasekaran R, Makowski C, Kostopoulos P, Adalat R, Khalili-Mahani N, Niso G, **Moreau JT**, Evans AC. The MNI data-sharing and processing ecosystem. *Neuroimage*. 2016 Jan 1;124(Pt B):1188–95. www.sciencedirect.com/science/article/pii/S1053811915008009

6. Niso G*, Rogers C*, **Moreau JT**, Chen LY, Madjar C, Das S, Bock E, Tadel F, Evans AC, Jolicoeur P, Baillet S. OMEGA: The Open MEG Archive. *Neuroimage*. 2016 Jan 1;124(Pt B):1182–7. www.sciencedirect.com/science/article/pii/S1053811915003183

Under review

1. **Moreau JT**, Baillet S, Dudley RWR. Biased intelligence: on the subjectivity of digital objectivity.

2. **Moreau JT**, Saint-Martin C, Baillet S, Dudley RWR. MNI SISCOM: An open-source tool for computing subtraction ictal single-photon emission CT coregistered to MRI.

3. **Moreau JT**, Simard-Tremblay E, Albrecht S, Rosenblatt B, Baillet S, Dudley RWR. Overnight Ictal Magnetoencephalography.

4. **Moreau JT**, Vinaik R, Simard-Tremblay E, Albrecht S, Saint-Martin C, Rosenblatt B, Baillet S, Dudley RWR. Localisation of oligodendroglial hyperplasia and differentiation from focal cortical dysplasia type II with multimodal imaging.

Conferences proceedings

1. Schur S, **Moreau J**, Atkinson J, Farmer JP, Hall J, Olivier A, Dubeau F, Bernasconi A, Bernasconi N, Gotman J, Baillet S, Dudley R. A preliminary study on how a

new multi-modal pre-surgical evaluation strategy has impacted postsurgical outcomes for poorly-defined focal epilepsy in children. In: Abstracts from the 42nd Annual Meeting of the American Society of Pediatric Neurosurgeons. *J. Neurosurg. Pediatr.* 2019;23(3):261–410. www.thejns.org/pediatrics/view/journals/j-neurosurg-pediatr/23/3/article-p1.xml

2. **Moreau JT**, Tomaszewski P, Simard-Tremblay E, Farmer JP, Atkinson J, Rosenblatt B, Baillet S, Dudley RWR. Imaging the temporal spread of seizures for surgical planning with ictal magnetoencephalography in children with drug-resistant epilepsy. In: 46th Annual Meeting of International Society for Pediatric Neurosurgery, Tel Aviv, Israel, 7-11 October, 2018. *Childs Nerv Syst.* 2018;34:1997–2122. www.doi.org/10.1007/s00381-018-3912-9

International Conferences

1. **Moreau JT**, Simard-Tremblay E, Rosenblatt B, Baillet S, Dudley RWR. Overnight ictal magnetoencephalography in children with drug-resistant epilepsy. Oral session presented at: International Society for the Advancement of Clinical MEG; 2019 Sep 11-14; Toronto, ON, Canada.

2. **Moreau JT**, Tomaszewski P, Simard-Tremblay E, Farmer JP, Atkinson J, Rosenblatt B, Baillet S, Dudley RWR. Magnetoencephalography in Mild Malformations of Cortical Development with Oligodendroglial Hyperplasia. Poster session presented at: The 21st International Conference on Biomagnetism; 2018 Aug 26-30; Philadelphia, USA.

3. Niso G, Tadel F, Bock E, **Moreau JT**, del-Pozo F, Baillet S. Characterization of The OMEGA populations brain activity. Poster session presented at: The 21st International Conference on Biomagnetism; 2018 Aug 26-30; Philadelphia, USA.
4. **Moreau J**, Tomaszewski P, Farmer JP, Atkinson J, Rosenblatt B, Baillet S, Dudley R. The value of "negative" MEG studies: Defining the functional deficit zone using spontaneous MEG in children with intractable epilepsy. Poster session presented at: The 20th International Conference on Biomagnetism; 2016 Oct 1-6; Seoul, Korea.
5. Niso G, **Moreau J**, Bock E, Tadel F, Oostenveld R, Schoffelen JM, Gramfort A, Gorgolewski KJ, Baillet S. An MEG extension to BIDS: Brain Imaging Data Structure - a solution to organize, describe and share neuroimaging data. Poster session presented at: The 20th International Conference on Biomagnetism; 2016 Oct 1-6; Seoul, Korea.

National Conferences

1. **Moreau J**. Intracranial recording for focal epilepsy in children: Practical Tutorial on Analyzing Grid and SEEG data in Brainstorm. Oral session presented at: Canadian League Against Epilepsy (CLAE) Scientific Meeting; 2018 Sep 21-23; St. John's, NL.
2. **Moreau J**, Vinaik R, Simard-Tremblay E, Rosenblatt B, Saint-Martin C, Albrecht S, Baillet S, Dudley R. T1/T2 Ratio MRI and Diffusion Imaging of Oligodendrocyte Hyperplasia and Focal Cortical Dysplasia in Children with Drug-Resistant Epilepsy. Poster session presented at: Canadian League Against Epilepsy (CLAE) Scientific Meeting; 2018 Sep 21-23; St. John's, NL.

3. **Moreau J**, Tomaszewski P, Rosenblatt B, Baillet S, Dudley R. Ictal Magnetoencephalography in Children Undergoing Presurgical Evaluation for Intractable Epilepsy. Poster session presented at: Canadian League Against Epilepsy (CLAE) Scientific Meeting; 2017 Oct 13-15; Vancouver, BC.
4. Tomaszewski P, Dudley R, **Moreau J**, Baillet S, Wintermark P. Arterial Spin Labeling (ASL) Perfusion MRI in the Pre-Surgical Evaluation of Pediatric Epilepsy: Lesional vs. Non-Lesional Cases. Poster session presented at: Canadian League Against Epilepsy (CLAE) Scientific Meeting; 2017 Oct 13-15; Vancouver, BC.
5. **Moreau J**, Tomaszewski P, Farmer JP, Atkinson J, Rosenblatt B, Baillet S, Dudley R. Valeur ajouté de la magnétoencéphalographie pour l'évaluation pré-chirurgicale d'enfants souffrant d'épilepsie réfractaire: Expérience avec les premiers 18 cas de l'Hôpital de Montréal pour enfants. Oral session presented at: Congrès Annuel de l'Association de Neurochirurgie Du Québec (ANCQ); 2016 Nov 11-12; Estérel, QC.
6. Tomaszewski P, Dudley R, **Moreau J**, Wintermark P, Baillet S. Arterial Spin Labeling (ASL) in the Pre-Surgical Evaluation of Pediatric Epilepsy. Poster session presented at: Canadian League Against Epilepsy (CLAE) Scientific Meeting; 2016 Oct 14-16; Quebec City, QC.

Local Conferences

1. **Moreau JT**, Saint-Martin C, Baillet S, Dudley RWR. MNI SISCOM: An open-source tool for computing subtraction ictal single-photon emission CT coregistered to MRI. Oral session presented at: Preston Robb MCH Neurosciences Day; 2019 Dec 11; Montreal, QC.

2. **Moreau J**, Vinaik R, Simard-Tremblay E, Farmer JP, Atkinson J, Rosenblatt B, Saint-Martin C, Albrecht S, Baillet S, Dudley R. Multimodal imaging of oligodendrocyte hyperplasia and focal cortical dysplasia in children with drug-resistant epilepsy. Oral session presented at: 10th Annual H. Bruce Williams Pediatric Surgical Research Day; 2019 Jun 6; Montreal, QC.
3. **Moreau JT**, Hankinson TC, Baillet S, Dudley RWR. Individual-patient prediction of meningioma malignancy and survival using the surveillance, epidemiology and end results database. Oral session presented at: Preston Robb MCH Neurosciences Day; 2018 Nov 21; Montreal, QC.
4. **Moreau J**, Simard-Tremblay E, Baillet S, Dudley R. Predicting Functional Motor Outcomes Following Hemispherectomy: a Systematic Review and Meta-analysis. Oral session presented at: 9th Annual H. Bruce Williams Pediatric Surgical Research Day; 2018 Jun 14; Montreal, QC.
5. **Moreau J**, Tomaszewski P, Farmer JP, Atkinson J, Rosenblatt B, Baillet S, Dudley R. Functional Imaging with Magnetoencephalography for the Presurgical Evaluation of Children with Intractable Epilepsy. Oral session presented at: 8th Annual H. Bruce Williams Pediatric Surgical Research Day; 2017 Jun 15; Montreal, QC.
6. **Moreau J**, Tomaszewski P, Farmer JP, Atkinson J, Rosenblatt B, Baillet S, Dudley R. Added value of magnetoencephalography in the presurgical evaluation of children with intractable epilepsy: experience with the first 18 cases at the Montreal Children's Hospital. Oral session presented at: 3rd Annual MNI Epilepsy Day; Montreal, QC. 2017 Apr 6; Montreal, QC.
7. **Moreau J**, Tomaszewski P, Farmer JP, Atkinson J, Rosenblatt B, Baillet S, Dudley R. Imaging Epilepsy in Motion: Novel contributions of MEG and Magnetic Source Imaging to the Presurgical Evaluation in Paediatric Intractable Epilepsy.

Oral session presented at: MNI Neurosurgical Research Day; 2016 Jun 17; Montreal, QC.

8. **Moreau J**, Tomaszewski P, Farmer JP, Atkinson J, Rosenblatt B, Baillet S, Dudley R. Magnetoencephalography Without Spikes: Can MEG Still Provide Useful Information When no Epileptiform Events are Recorded? Oral session presented at: 7th Annual H. Bruce Williams Pediatric Surgical Research Day; 2016 Jun 2; Montreal, QC.

9. **Moreau JT**, Farah A, Bock E, Hall J, Dubeau F, Baillet S, Dudley RW. The use of magnetoencephalography (MEG) and robot-guided stereo-EEG (SEEG) after failed focal epilepsy surgery in children. Oral session presented at: 40th Annual Preston Robb Montreal Children's Hospital Neurosciences Day; 2015 Dec 2; Montreal, QC.

References

1. O'Brien TJ, So EL, Mullan BP, Hauser MF, Brinkmann BH, Bohnen NI, et al. Subtraction ictal SPECT co-registered to MRI improves clinical usefulness of SPECT in localizing the surgical seizure focus. Neurology. 1998 Feb;50(2):445–54.

2. Kirkman MA. The role of imaging in the development of neurosurgery. J Clin Neurosci. 2015 Jan;22(1):55–61.

3. Duncan JS, Winston GP, Koepp MJ, Ourselin S. Brain imaging in the assessment for epilepsy surgery. Lancet Neurol. 2016 Apr;15(4):420–33.

4. Bisdas S, Roder C, Ernemann U, Tatagiba MS. Intraoperative MR Imaging in Neurosurgery. Clin Neuroradiol. 2015 Oct;25 Suppl 2:237–44.

5. Busso VO, McAuliffe JJ. Intraoperative neurophysiological monitoring in pediatric neurosurgery. Paediatr Anaesth. 2014 Jul;24(7):690–7.

6. Orringer DA, Golby A, Jolesz F. Neuronavigation in the surgical management of brain tumors: current and future trends. Expert Rev Med Devices. 2012 Sep;9(5):491–500.

7. Azagury DE, Dua MM, Barrese JC, Henderson JM, Buchs NC, Ris F, et al. Image-guided surgery. Curr Probl Surg. 2015 Dec;52(12):476–520.

8. Topol EJ. High-performance medicine: the convergence of human and artificial intelligence. Nat Med. 2019 Jan;25(1):44–56.

9. Senders JT, Staples PC, Karhade AV, Zaki MM, Gormley WB, Broekman MLD, et al. Machine Learning and Neurosurgical Outcome Prediction: A Systematic Review. World Neurosurg. 2018 Jan;109:476-486.e1.

10. Rajkomar A, Dean J, Kohane I. Machine Learning in Medicine. N Engl J Med. 2019 Apr 4;380(14):1347–58.

11. Langen K-J, Galldiks N, Hattingen E, Shah NJ. Advances in neuro-oncology imaging. Nat Rev Neurol. 2017 May;13(5):279–89.

12. Kelleher JD, Namee BM, D'Arcy A. Fundamentals of Machine Learning for Predictive Data Analytics: Algorithms, Worked Examples, and Case Studies. MIT Press; 2015. 595 p.

13. Parikh RB, Kakad M, Bates DW. Integrating Predictive Analytics Into High-Value Care: The Dawn of Precision Delivery. JAMA. 2016 Feb 16;315(7):651–2.

14. Copeland J. Artificial Intelligence: A Philosophical Introduction. John Wiley & Sons; 2015. 328 p.

15. Mc Cauley N. The use of expert systems in the healthcare industry. Information & Management. 1992;22:2277235.

16. Coats PK. Why Expert Systems Fail. Financial Management. 1988;17(3):77–86.

17. Hendler J. Avoiding Another AI Winter. IEEE Intell Syst. 2008 Mar;23(2):2–4.

18. LeCun Y, Bengio Y, Hinton G. Deep learning. Nature. 2015 May 28;521(7553):436–44.

19. Deo RC. Machine Learning in Medicine. Circulation. 2015 Nov 17;132(20):1920–30.

20. Mitra P, Murthy CA, Pal SK. Unsupervised feature selection using feature similarity. IEEE Trans Pattern Anal Mach Intell. 2002 Mar;24(3):301–12.

21. Sing DC, Metz LN, Dudli S. Machine Learning-Based Classification of 38 Years of Spine-Related Literature Into 100 Research Topics. Spine . 2017 Jun 1;42(11):863–70.

22. Wang X, Wang D, Yao Z, Xin B, Wang B, Lan C, et al. Machine Learning Models for Multiparametric Glioma Grading With Quantitative Result Interpretations. Front Neurosci. 2018;12:1046.

23. Hale AT, Stonko DP, Wang L, Strother MK, Chambless LB. Machine learning analyses can differentiate meningioma grade by features on magnetic resonance imaging. Neurosurg Focus. 2018 Nov 1;45(5):E4.

24. Sachdeva J, Kumar V, Gupta I, Khandelwal N, Ahuja CK. Multiclass Brain Tumor Classification Using GA-SVM. In: 2011 Developments in E-systems Engineering. 2011. p. 182–7.

25. Capper D, Jones DTW, Sill M, Hovestadt V, Schrimpf D, Sturm D, et al. DNA methylation-based classification of central nervous system tumours. Nature. 2018 Mar 22;555(7697):469–74.

26. Hollon TC, Pandian B, Adapa AR, Urias E, Save AV, Khalsa SSS, et al. Near real-time intraoperative brain tumor diagnosis using stimulated Raman histology and deep neural networks. Nat Med. 2020 Jan;26(1):52–8.

27. Abbasi B, Goldenholz DM. Machine learning applications in epilepsy. Epilepsia [Internet]. 2019 Sep 3; Available from: http://dx.doi.org/10.1111/epi.16333

28. Jin B, Krishnan B, Adler S, Wagstyl K, Hu W, Jones S, et al. Automated detection of focal cortical dysplasia type II with surface-based magnetic resonance imaging postprocessing and machine learning. Epilepsia. 2018 May;59(5):982–92.

29. Ahmedt-Aristizabal D, Fookes C, Dionisio S, Nguyen K, Cunha JPS, Sridharan S. Automated analysis of seizure semiology and brain electrical activity in presurgery evaluation of epilepsy: A focused survey. Epilepsia. 2017 Nov;58(11):1817–31.

30. Hong S-J, Kim H, Schrader D, Bernasconi N, Bernhardt BC, Bernasconi A. Automated detection of cortical dysplasia type II in MRI-negative epilepsy. Neurology. 2014 Jul 1;83(1):48–55.

31. Baud MO, Kleen JK, Anumanchipalli GK, Hamilton LS, Tan Y-L, Knowlton R, et al. Unsupervised Learning of Spatiotemporal Interictal Discharges in Focal Epilepsy. Neurosurgery [Internet]. 2017 Oct 10; Available from: http://dx.doi.org/10.1093/neuros/nyx480

32. Winkler-Schwartz A, Yilmaz R, Mirchi N, Bissonnette V, Ledwos N, Siyar S, et al. Machine Learning Identification of Surgical and Operative Factors Associated With Surgical Expertise in Virtual Reality Simulation. JAMA Netw Open. 2019 Aug 2;2(8):e198363.

33. Muhlestein WE, Akagi DS, Kallos JA, Morone PJ, Weaver KD, Thompson RC, et al. Using a Guided Machine Learning Ensemble Model to Predict Discharge Disposition following Meningioma Resection. J Neurol Surg B Skull Base. 2018 Apr;79(2):123–30.

34. Hollon TC, Parikh A, Pandian B, Tarpeh J, Orringer DA, Barkan AL, et al. A machine learning approach to predict early outcomes after pituitary adenoma surgery. Neurosurg Focus. 2018 Nov 1;45(5):E8.

35. Hale AT, Stonko DP, Brown A, Lim J, Voce DJ, Gannon SR, et al. Machine-learning analysis outperforms conventional statistical models and CT classification systems

in predicting 6-month outcomes in pediatric patients sustaining traumatic brain injury. Neurosurg Focus. 2018 Nov 1;45(5):E2.

36. Titano JJ, Badgeley M, Schefflein J, Pain M, Su A, Cai M, et al. Automated deep-neural-network surveillance of cranial images for acute neurologic events. Nat Med. 2018 Sep;24(9):1337–41.

37. Buchlak QD, Esmaili N, Leveque J-C, Farrokhi F, Bennett C, Piccardi M, et al. Machine learning applications to clinical decision support in neurosurgery: an artificial intelligence augmented systematic review. Neurosurg Rev [Internet]. 2019 Aug 17; Available from: http://dx.doi.org/10.1007/s10143-019-01163-8

38. Senders JT, Zaki MM, Karhade AV, Chang B, Gormley WB, Broekman ML, et al. An introduction and overview of machine learning in neurosurgical care. Acta Neurochir . 2018 Jan;160(1):29–38.

39. Sarkiss CA, Germano IM. Machine Learning in Neuro-Oncology: Can Data Analysis from 5,346 Patients Change Decision Making Paradigms? World Neurosurg [Internet]. 2019 Jan 23; Available from: http://dx.doi.org/10.1016/j.wneu.2019.01.046

40. Silver D, Huang A, Maddison CJ, Guez A, Sifre L, van den Driessche G, et al. Mastering the game of Go with deep neural networks and tree search. Nature. 2016 Jan 28;529(7587):484–9.

41. Mao R, Zhu H, Zhang L, Chen A. A New Method to Assist Small Data Set Neural Network Learning. In: Sixth International Conference on Intelligent Systems Design and Applications. 2006. p. 17–22.

42. Banks MA. Sizing up big data. Nat Med. 2020 Jan;26(1):5–6.

43. Obermeyer Z, Emanuel EJ. Predicting the Future - Big Data, Machine Learning, and Clinical Medicine. N Engl J Med. 2016 Sep 29;375(13):1216–9.

44. Rajkomar A, Oren E, Chen K, Dai AM, Hajaj N, Hardt M, et al. Scalable and accurate deep learning with electronic health records. npj Digital Medicine. 2018 May 8;1(1):18.

45. Niso G, Rogers C, Moreau JT, Chen L-Y, Madjar C, Das S, et al. OMEGA: The Open MEG Archive. Neuroimage. 2016 Jan 1;124(Pt B):1182–7.

46. Das S, Glatard T, MacIntyre LC, Madjar C, Rogers C, Rousseau M-E, et al. The MNI data-sharing and processing ecosystem. Neuroimage. 2016 Jan 1;124(Pt B):1188–95.

47. Das S, Glatard T, Rogers C, Saigle J, Paiva S, MacIntyre L, et al. Cyberinfrastructure for Open Science at the Montreal Neurological Institute. Front Neuroinform. 2016;10:53.

48. Niso G, Gorgolewski KJ, Bock E, Brooks TL, Flandin G, Gramfort A, et al. MEG-BIDS, the brain imaging data structure extended to magnetoencephalography. Sci Data. 2018 Jun 19;5:180110.

49. Cabitza F, Rasoini R, Gensini GF. Unintended Consequences of Machine Learning in Medicine. JAMA. 2017 Aug 8;318(6):517–8.

50. Beam AL, Kohane IS. Big Data and Machine Learning in Health Care. JAMA. 2018 Apr 3;319(13):1317–8.

51. Fröhlich H, Balling R, Beerenwinkel N, Kohlbacher O, Kumar S, Lengauer T, et al. From hype to reality: data science enabling personalized medicine. BMC Med. 2018 Aug 27;16(1):150.

52. Rigby MJ. Ethical Dimensions of Using Artificial Intelligence in Health Care. AMA Journal of Ethics. 2019 Feb 1;21(2):121–4.

53. Schiff D, Borenstein J. How Should Clinicians Communicate With Patients About the Roles of Artificially Intelligent Team Members? AMA J Ethics. 2019 Feb 1;21(2):E138-145.

54. Price WN 2nd, Cohen IG. Privacy in the age of medical big data. Nat Med. 2019 Jan;25(1):37–43.

55. Cios KJ, Moore GW. Uniqueness of medical data mining. Artif Intell Med. 2002 Sep;26(1–2):1–24.

56. Mikk KA, Sleeper HA, Topol EJ. The Pathway to Patient Data Ownership and Better Health. JAMA. 2017 Oct 17;318(15):1433–4.

57. Rodwin MA. The case for public ownership of patient data. JAMA. 2009 Jul 1;302(1):86–8.

58. Guerrini R. Epilepsy in children. Lancet. 2006 Feb 11;367(9509):499–524.

59. Spencer S, Huh L. Outcomes of epilepsy surgery in adults and children. Lancet Neurol. 2008 Jun;7(6):525–37.

60. Moosa ANV, Wyllie E. Cognitive Outcome After Epilepsy Surgery in Children. Semin Pediatr Neurol. 2017;24(4):331–9.

61. Berg AT, Zelko FA, Levy SR, Testa FM. Age at onset of epilepsy, pharmacoresistance, and cognitive outcomes: a prospective cohort study. Neurology. 2012 Sep 25;79(13):1384–91.

62. Kwan P, Schachter SC, Brodie MJ. Drug-resistant epilepsy. N Engl J Med. 2011 Sep 8;365(10):919–26.

63. Crawford B, McBurney K. Neuroanatomy Coronal Brain Slices [Internet]. Available from: http://www.neuroanatomy.ca/coronals.html

64. Rosenow F, Lüders H. Presurgical evaluation of epilepsy. Brain. 2001 Sep;124(Pt 9):1683–700.

65. Bartolomei F, Lagarde S, Wendling F, McGonigal A, Jirsa V, Guye M, et al. Defining epileptogenic networks: Contribution of SEEG and signal analysis. Epilepsia [Internet]. 2017 May 20; Available from: http://dx.doi.org/10.1111/epi.13791

66. Stefan H, Lopes da Silva FH. Epileptic neuronal networks: methods of identification and clinical relevance. Front Neurol. 2013 Mar 1;4:8.

67. Holmes MD, Tucker DM. Identifying the epileptic network. Front Neurol. 2013 Jul 1;4:84.

68. Gil F, Padilla N, Soria-Pastor S, Setoain X, Boget T, Rumiá J, et al. Beyond the Epileptic Focus: Functional Epileptic Networks in Focal Epilepsy. Cereb Cortex [Internet]. 2019 Dec 21; Available from: http://dx.doi.org/10.1093/cercor/bhz243

69. Alkawadri R, Burgess RC, Kakisaka Y, Mosher JC, Alexopoulos AV. Assessment of the Utility of Ictal Magnetoencephalography in the Localization of the Epileptic Seizure Onset Zone. JAMA Neurol. 2018 Oct 1;75(10):1264–72.

70. Ryvlin P, Cross JH, Rheims S. Epilepsy surgery in children and adults. Lancet Neurol. 2014 Nov;13(11):1114–26.

71. Penfield W, Jasper H. Epilepsy and the functional anatomy of the human brain. 1954;896. Available from: https://psycnet.apa.org/fulltext/1955-01377-000.pdf

72. Penfield W, Milner B. Memory deficit produced by bilateral lesions in the hippocampal zone. AMA Arch Neurol Psychiatry. 1958 May;79(5):475–97.

73. Dwivedi R, Ramanujam B, Chandra PS, Sapra S, Gulati S, Kalaivani M, et al. Surgery for Drug-Resistant Epilepsy in Children. N Engl J Med. 2017 Oct 26;377(17):1639–47.

74. Widjaja E, Jain P, Demoe L, Guttmann A, Tomlinson G, Sander B. Seizure outcome of pediatric epilepsy surgery: Systematic review and meta-analyses. Neurology [Internet]. 2020 Jan 29; Available from: http://dx.doi.org/10.1212/WNL.0000000000008966

75. Maragkos GA, Geropoulos G, Kechagias K, Ziogas IA, Mylonas KS. Quality of Life After Epilepsy Surgery in Children: A Systematic Review and Meta-Analysis. Neurosurgery. 2019 Dec 1;85(6):741–9.

76. Shorvon SD. A history of neuroimaging in epilepsy 1909-2009. Epilepsia. 2009 Mar;50 Suppl 3:39–49.

77. Hounsfield GN. Computerized transverse axial scanning (tomography): Part 1. Description of system. BJR Suppl. 1973 Dec 1;46(552):1016–22.

78. Gastaut H. Conclusions: computerized transverse axial tomography in epilepsy. Epilepsia. 1976 Sep;17(3):337–8.

79. Glasser O. WC Roentgen and the discovery of the Roentgen rays. AJR Am J Roentgenol. 1995;165(5):1033–40.

80. Dandy WE. VENTRICULOGRAPHY FOLLOWING THE INJECTION OF AIR INTO THE CEREBRAL VENTRICLES. Ann Surg. 1918 Jul;68(1):5–11.

81. Dandy WE. RONTGENOGRAPHY OF THE BRAIN AFTER THE INJECTION OF AIR INTO THE SPINAL CANAL. Ann Surg. 1919 Oct;70(4):397–403.

82. Berger H. Über das elektroenkephalogramm des menschen. Archiv für psychiatrie und nervenkrankheiten. 1929;87(1):527–70.

83. Haas LF. Hans Berger (1873-1941), Richard Caton (1842-1926), and electroencephalography. J Neurol Neurosurg Psychiatry. 2003 Jan;74(1):9.

84. Brownell GL, Sweet WH. Localization of brain tumors with positron emitters. Nucleonics. 1953;11(11):40–5.

85. Sweet WH, Brownell GL. Localization of intracranial lesions by scanning with positron-emitting arsenic. J Am Med Assoc. 1955 Apr 2;157(14):1183–8.

86. Mansfield P, Maudsley AA. Medical imaging by NMR. Br J Radiol. 1977 Mar;50(591):188–94.

87. Martinez-Rios C, McAndrews MP, Logan W, Krings T, Lee D, Widjaja E. MRI in the evaluation of localization-related epilepsy. J Magn Reson Imaging. 2016 Jul;44(1):12–22.

88. Deleo F, Thom M, Concha L, Bernasconi A, Bernhardt BC, Bernasconi N. Histological and MRI markers of white matter damage in focal epilepsy. Epilepsy Res. 2018 Feb;140:29–38.

89. Rüber T, David B, Elger CE. MRI in epilepsy: clinical standard and evolution. Curr Opin Neurol. 2018 Apr;31(2):223–31.

90. Morgan VL, Englot DJ, Rogers BP, Landman BA, Cakir A, Abou-Khalil BW, et al. Magnetic resonance imaging connectivity for the prediction of seizure outcome in temporal lobe epilepsy. Epilepsia [Internet]. 2017 Apr 27; Available from: http://dx.doi.org/10.1111/epi.13762

91. Gaxiola-Valdez I, Singh S, Perera T, Sandy S, Li E, Federico P. Seizure onset zone localization using postictal hypoperfusion detected by arterial spin labelling MRI. Brain. 2017 Nov 1;140(11):2895–911.

92. Blauwblomme T, Boddaert N, Chémaly N, Chiron C, Pages M, Varlet P, et al. Arterial Spin Labeling MRI: a step forward in non-invasive delineation of focal cortical dysplasia in children. Epilepsy Res. 2014 Dec;108(10):1932–9.

93. Sierra-Marcos A, Carreño M, Setoain X, López-Rueda A, Aparicio J, Donaire A, et al. Accuracy of arterial spin labeling magnetic resonance imaging (MRI) perfusion in detecting the epileptogenic zone in patients with drug-resistant neocortical epilepsy: comparison with electrophysiological data, structural MRI, SISCOM and FDG-PET. Eur J Neurol. 2016 Jan;23(1):160–7.

94. Boscolo Galazzo I, Mattoli MV, Pizzini FB, De Vita E, Barnes A, Duncan JS, et al. Cerebral metabolism and perfusion in MR-negative individuals with refractory

focal epilepsy assessed by simultaneous acquisition of 18F-FDG PET and arterial spin labeling. NeuroImage: Clinical. 2016;11:648–57.

95. Pan JW, Kuzniecky RI. Utility of magnetic resonance spectroscopic imaging for human epilepsy. Quant Imaging Med Surg. 2015 Apr;5(2):313–22.

96. Khoo HM, von Ellenrieder N, Zazubovits N, He D, Dubeau F, Gotman J. The spike onset zone: The region where epileptic spikes start and from where they propagate. Neurology. 2018 Aug 14;91(7):e666–74.

97. Khoo HM, Hao Y, von Ellenrieder N, Zazubovits N, Hall J, Olivier A, et al. The hemodynamic response to interictal epileptic discharges localizes the seizure-onset zone. Epilepsia [Internet]. 2017 Mar 15; Available from: http://dx.doi.org/10.1111/epi.13717

98. Moeller F, Stephani U, Siniatchkin M. Simultaneous EEG and fMRI recordings (EEG-fMRI) in children with epilepsy. Epilepsia. 2013 Jun;54(6):971–82.

99. De Ciantis A, Barba C, Tassi L, Cosottini M, Tosetti M, Costagli M, et al. 7T MRI in focal epilepsy with unrevealing conventional field strength imaging. Epilepsia. 2016 Mar;57(3):445–54.

100. Sarikaya I. PET studies in epilepsy. Am J Nucl Med Mol Imaging. 2015 Oct 12;5(5):416–30.

101. Perissinotti A, Setoain X, Aparicio J, Rubí S, Fuster BM, Donaire A, et al. Clinical Role of Subtraction Ictal SPECT Coregistered to MR Imaging and 18F-FDG PET in Pediatric Epilepsy. J Nucl Med. 2014 Jul 1;55(7):1099–105.

102. Lam J, DuBois JM, Rowley J, González-Otárula KA, Soucy J-P, Massarweh G, et al. In vivo metabotropic glutamate receptor type 5 abnormalities localize the epileptogenic zone in mesial temporal lobe epilepsy. Ann Neurol. 2019 Feb;85(2):218–28.

103. Chugani HT, Kumar A, Kupsky W, Asano E, Sood S, Juhász C. Clinical and histopathologic correlates of 11C-alpha-methyl-L-tryptophan (AMT) PET abnormalities in children with intractable epilepsy. Epilepsia. 2011 Sep;52(9):1692–8.

104. Juhász C, Chugani DC, Muzik O, Shah A, Asano E, Mangner TJ, et al. Alpha-methyl-L-tryptophan PET detects epileptogenic cortex in children with intractable epilepsy. Neurology. 2003 Mar 25;60(6):960–8.

105. Van Paesschen W. Ictal SPECT. Epilepsia. 2004;45 Suppl 4:35–40.

106. Juhász C, John F. Utility of MRI, PET, and ictal SPECT in presurgical evaluation of non-lesional pediatric epilepsy. Seizure [Internet]. 2019 May 11; Available from: http://dx.doi.org/10.1016/j.seizure.2019.05.008

107. Chen T, Guo L. The role of SISCOM in preoperative evaluation for patients with epilepsy surgery: A meta-analysis. Seizure. 2016 Oct;41:43–50.

108. von Oertzen TJ, Mormann F, Urbach H, Reichmann K, Koenig R, Clusmann H, et al. Prospective use of subtraction ictal SPECT coregistered to MRI (SISCOM) in presurgical evaluation of epilepsy. Epilepsia. 2011 Dec;52(12):2239–48.

109. Ahnlide J-A, Rosén I, Lindén-Mickelsson Tech P, Källén K. Does SISCOM contribute to favorable seizure outcome after epilepsy surgery? Epilepsia. 2007 Mar;48(3):579–88.

110. Lee J-J, Lee SK, Choi JW, Kim D-W, Park KI, Kim BS, et al. Ictal SPECT using an attachable automated injector: clinical usefulness in the prediction of ictal onset zone. Acta radiol. 2009 Dec;50(10):1160–8.

111. Kim S, Holder DL, Laymon CM, Tudorascu DL, Deeb EL, Panigrahy A, et al. Clinical value of the first dedicated, commercially available automatic injector for ictal brain SPECT in presurgical evaluation of pediatric epilepsy: comparison with manual injection. J Nucl Med. 2013 May;54(5):732–8.

112. Baillet S, Mosher JC, Leahy RM. Electromagnetic brain mapping. Signal Processing Magazine, IEEE. 2001 Nov;18(6):14–30.

113. Baillet S. Magnetoencephalography for brain electrophysiology and imaging. Nat Neurosci. 2017 Feb 23;20(3):327–39.

114. Hillebrand A, Barnes GR. A quantitative assessment of the sensitivity of whole-head MEG to activity in the adult human cortex. Neuroimage. 2002 Jul;16(3 Pt 1):638–50.

115. Zulma S. Tovar-Spinoza, Ayako Ochi, James T. Rutka, Cristina Go, Hiroshi Otsubo. The role of magnetoencephalography in epilepsy surgery. Neurosurg Focus. 2008;25(3):E16.

116. Hansen P, Kringelbach M, Salmelin R. MEG: An Introduction to Methods. New York: Oxford University Press; 2010.

117. Stefan H, Hummel C, Scheler G, Genow A, Druschky K, Tilz C, et al. Magnetic brain source imaging of focal epileptic activity: a synopsis of 455 cases. Brain. 2003 Nov;126(Pt 11):2396–405.

118. Englot DJ, Nagarajan SS, Imber BS, Raygor KP, Honma SM, Mizuiri D, et al. Epileptogenic zone localization using magnetoencephalography predicts seizure freedom in epilepsy surgery. Epilepsia. 2015 Jun;56(6):949–58.

119. Duez L, Tankisi H, Hansen PO, Sidenius P, Sabers A, Pinborg LH, et al. Electromagnetic source imaging in presurgical workup of patients with epilepsy: A prospective study. Neurology. 2019 Feb 5;92(6):e576–86.

120. Talairach J, Bancaud J, Bonis A, Szikla G, Tournoux P. Functional stereotaxic exploration of epilepsy. Confin Neurol. 1962;22:328–31.

121. Wyler AR, Ojemann GA, Lettich E, Ward AA Jr. Subdural strip electrodes for localizing epileptogenic foci. J Neurosurg. 1984 Jun;60(6):1195–200.

122. Youngerman BE, Khan FA, McKhann GM. Stereoelectroencephalography in epilepsy, cognitive neurophysiology, and psychiatric disease: safety, efficacy, and place in therapy. Neuropsychiatr Dis Treat. 2019 Jun 28;15:1701–16.

123. Cardinale F, Cossu M. Letter to the Editor: SEEG has the lowest rate of complications. J Neurosurg. 2015 Feb 1;122(2):475–8.

124. De Benedictis A, Trezza A, Carai A, Genovese E, Procaccini E, Messina R, et al. Robot-assisted procedures in pediatric neurosurgery. Neurosurg Focus. 2017 May;42(5):E7.

125. Mullin JP, Shriver M, Alomar S, Najm I, Bulacio J, Chauvel P, et al. Is SEEG safe? A systematic review and meta-analysis of stereo-electroencephalography-related complications. Epilepsia [Internet]. 2016 Feb 21; Available from: http://dx.doi.org/10.1111/epi.13298

126. Arya R, Mangano FT, Horn PS, Holland KD, Rose DF, Glauser TA. Adverse events related to extraoperative invasive EEG monitoring with subdural grid electrodes: a systematic review and meta-analysis. Epilepsia. 2013 May;54(5):828–39.

127. Yan H, Katz JS, Anderson M, Mansouri A, Remick M, Ibrahim GM, et al. Method of invasive monitoring in epilepsy surgery and seizure freedom and morbidity: A systematic review. Epilepsia. 2019 Sep;60(9):1960–72.

128. Remick M, Ibrahim GM, Mansouri A, Abel TJ. Patient phenotypes and clinical outcomes in invasive monitoring for epilepsy: An individual patient data meta-analysis. Epilepsy Behav. 2020 Jan;102:106652.

129. Toth M, Papp KS, Gede N, Farkas K, Kovacs S, Isnard J, et al. Surgical outcomes related to invasive EEG monitoring with subdural grids or depth electrodes in adults: A systematic review and meta-analysis. Seizure. 2019 Aug;70:12–9.

130. Ostrom QT, Gittleman H, Liao P, Vecchione-Koval T, Wolinsky Y, Kruchko C, et al. CBTRUS Statistical Report: Primary brain and other central nervous system tumors diagnosed in the United States in 2010-2014. Neuro Oncol. 2017 Nov 6;19(suppl_5):v1–88.

131. Porter KR, McCarthy BJ, Freels S, Kim Y, Davis FG. Prevalence estimates for primary brain tumors in the United States by age, gender, behavior, and histology. Neuro Oncol. 2010 Jun;12(6):520–7.

132. Aizer AA, Bi WL, Kandola MS, Lee EQ, Nayak L, Rinne ML, et al. Extent of resection and overall survival for patients with atypical and malignant meningioma. Cancer. 2015 Dec 15;121(24):4376–81.

133. Dudley RWR, Torok MR, Randall S, Béland B, Handler MH, Mulcahy-Levy JM, et al. Pediatric versus adult meningioma: comparison of epidemiology, treatments, and outcomes using the Surveillance, Epidemiology, and End Results database. J Neurooncol. 2018 May;137(3):621–9.

134. Overview of the SEER Program [Internet]. [cited 2018 Jun 30]. Available from: https://seer.cancer.gov/about/overview.html

135. Ohba S, Abe M, Hasegawa M, Hirose Y. Intraparenchymal Meningioma: Clinical, Radiologic, and Histologic Review. World Neurosurg. 2016 Aug;92:23–30.

136. Yuan Y, Su W, Zhu M. Threshold-free measures for assessing the performance of medical screening tests. Front Public Health. 2015 Apr 20;3:57.

137. Cai H, Yuan Y, Zhou QM, Li B. APtools: Average Positive Predictive Values (AP) for Binary Outcomes and Censored Event Times [Internet]. 2018. Available from: https://CRAN.R-project.org/package=APtools

138. Uno H, Cai T, Pencina MJ, D'Agostino RB, Wei LJ. On the C-statistics for evaluating overall adequacy of risk prediction procedures with censored survival data. Stat Med. 2011 May 10;30(10):1105–17.

139. Harrell FE Jr, Lee KL, Mark DB. Multivariable prognostic models: issues in developing models, evaluating assumptions and adequacy, and measuring and reducing errors. Stat Med. 1996 Feb 28;15(4):361–87.

140. Shukla N, Hagenbuchner M, Win KT, Yang J. Breast cancer data analysis for survivability studies and prediction. Comput Methods Programs Biomed. 2018 Mar;155:199–208.

141. Kate RJ, Nadig R. Stage-specific predictive models for breast cancer survivability. Int J Med Inform. 2017 Jan;97:304–11.

142. Lotfnezhad Afshar H, Ahmadi M, Roudbari M, Sadoughi F. Prediction of breast cancer survival through knowledge discovery in databases. Glob J Health Sci. 2015 Jan 26;7(4):392–8.

143. Wang X, Hershman DL, Neugut AI. Using machine learning, general regression, and Cox proportional hazards regression to predict the effectiveness of treatment in patients with breast cancer. AMIA Annu Symp Proc. 2006;1133.

144. Shin H, Nam Y. A coupling approach of a predictor and a descriptor for breast cancer prognosis. BMC Med Genomics. 2014 May 8;7 Suppl 1:S4.

145. Lynch CM, van Berkel VH, Frieboes HB. Application of unsupervised analysis techniques to lung cancer patient data. PLoS One. 2017 Sep 14;12(9):e0184370.

146. Lynch CM, Abdollahi B, Fuqua JD, de Carlo AR, Bartholomai JA, Balgemann RN, et al. Prediction of lung cancer patient survival via supervised machine learning classification techniques. Int J Med Inform. 2017 Dec;108:1–8.

147. Woo C-W, Chang LJ, Lindquist MA, Wager TD. Building better biomarkers: brain models in translational neuroimaging. Nat Neurosci. 2017 Feb 23;20(3):365–77.

148. Kshettry VR, Ostrom QT, Kruchko C, Al-Mefty O, Barnett GH, Barnholtz-Sloan JS. Descriptive epidemiology of World Health Organization grades II and III intracranial meningiomas in the United States. Neuro Oncol. 2015 Aug;17(8):1166–73.

149. Westwick HJ, Shamji MF. Effects of sex on the incidence and prognosis of spinal meningiomas: a Surveillance, Epidemiology, and End Results study. J Neurosurg Spine. 2015 Sep;23(3):368–73.

150. Amsbaugh M, Ugiliweneza B, Burton E, Skirboll S, Woo S, Boakye M. Patterns of Care and Outcomes of Adjuvant Radiotherapy for Meningiomas: A Surveillance, Epidemiology, and End Results and Medicare Linked Analysis. Cureus. 2016 Apr 12;8(4):e567.

151. Dolecek TA, Dressler EVM, Thakkar JP, Liu M, Al-Qaisi A, Villano JL. Epidemiology of meningiomas post-Public Law 107-206: The Benign Brain Tumor Cancer Registries Amendment Act. Cancer. 2015 Jul 15;121(14):2400–10.

152. Garzon-Muvdi T, Yang W, Lim M, Brem H, Huang J. Atypical and anaplastic meningioma: outcomes in a population based study. J Neurooncol [Internet]. 2017 Apr 20; Available from: http://dx.doi.org/10.1007/s11060-017-2436-6

153. Chen C, Liaw A, Breiman L, Others. Using random forest to learn imbalanced data. University of California, Berkeley. 2004;110:1–12.

154. Cox DR. Regression Models and Life-Tables. J R Stat Soc Series B Stat Methodol. 1972;34(2):187–220.

155. Davidson-Pilon C, Kalderstam J, Zivich P, Kuhn B, Fiore-Gartland A, Moneda L, et al. CamDavidsonPilon/lifelines: v0.20.3 [Internet]. 2019. Available from: https://zenodo.org/record/2604107

156. Dietterich TG. Ensemble Methods in Machine Learning. In: Multiple Classifier Systems. Springer Berlin Heidelberg; 2000. p. 1–15.

157. Yan P-F, Yan L, Hu T-T, Xiao D-D, Zhang Z, Zhao H-Y, et al. The Potential Value of Preoperative MRI Texture and Shape Analysis in Grading Meningiomas: A Preliminary Investigation. Transl Oncol. 2017 Aug;10(4):570–7.

158. Qureshi H, Sertel O, Rajpoot N, Wilson R, Gurcan M. Adaptive Discriminant Wavelet Packet Transform and Local Binary Patterns for Meningioma Subtype Classification. In: Medical Image Computing and Computer-Assisted Intervention – MICCAI 2008. Springer Berlin Heidelberg; 2008. p. 196–204.

159. Nowosielski M, Galldiks N, Iglseder S, Kickingereder P, von Deimling A, Bendszus M, et al. Diagnostic challenges in meningioma. Neuro Oncol. 2017 Nov 29;19(12):1588–98.

160. Cerami E, Gao J, Dogrusoz U, Gross BE, Sumer SO, Aksoy BA, et al. The cBio cancer genomics portal: an open platform for exploring multidimensional cancer genomics data. Cancer Discov. 2012 May;2(5):401–4.

161. Clark K, Vendt B, Smith K, Freymann J, Kirby J, Koppel P, et al. The Cancer Imaging Archive (TCIA): maintaining and operating a public information repository. J Digit Imaging. 2013 Dec;26(6):1045–57.

162. Bycroft C, Freeman C, Petkova D, Band G, Elliott LT, Sharp K, et al. The UK Biobank resource with deep phenotyping and genomic data. Nature. 2018 Oct;562(7726):203–9.

163. Miller KL, Alfaro-Almagro F, Bangerter NK, Thomas DL, Yacoub E, Xu J, et al. Multimodal population brain imaging in the UK Biobank prospective epidemiological study. Nat Neurosci. 2016 Nov;19(11):1523–36.

164. Gagnon J, Leggett JA, Richard C, Lussier M-T. Facilitating informed consent for EMR research in Quebec. Can Fam Physician. 2014 Jan;60(1):90.

165. Keshavjee K, Williamson T, Martin K, Truant R, Aliarzadeh B, Ghany A, et al. Getting to usable EMR data. Can Fam Physician. 2014 Apr;60(4):392.

166. Owens B. Family doctors call for guaranteed access to EMR data for research and quality improvement. CMAJ. 2018 Jan 15;190(2):E60–1.

167. Jensen PB, Jensen LJ, Brunak S. Mining electronic health records: towards better research applications and clinical care. Nat Rev Genet. 2012 May 2;13(6):395–405.

168. Dudley RWR, Torok MR, Gallegos DR, Mulcahy-Levy JM, Hoffman LM, Liu AK, et al. Pediatric low-grade ganglioglioma: epidemiology, treatments, and outcome analysis on 348 children from the surveillance, epidemiology, and end results database. Neurosurgery. 2015 Mar;76(3):313–9; discussion 319; quiz 319–20.

169. Dudley RWR, Torok MR, Gallegos D, Liu AK, Handler MH, Hankinson TC. Pediatric choroid plexus tumors: epidemiology, treatments, and outcome analysis on 202 children from the SEER database. J Neurooncol. 2015 Jan;121(1):201–7.

170. Hankinson TC, Fields EC, Torok MR, Beaty BL, Handler MH, Foreman NK, et al. Limited utility despite accuracy of the national SEER dataset for the study of craniopharyngioma. J Neurooncol. 2012 Nov;110(2):271–8.

171. Hankinson TC, Dudley RWR, Torok MR, Patibandla MR, Dorris K, Poonia S, et al. Short-term mortality following surgical procedures for the diagnosis of pediatric brain tumors: outcome analysis in 5533 children from SEER, 2004-2011. J Neurosurg Pediatr. 2016 Mar;17(3):289–97.

172. Noone A-M, Lund JL, Mariotto A, Cronin K, McNeel T, Deapen D, et al. Comparison of SEER Treatment Data With Medicare Claims. Med Care. 2016 Sep;54(9):e55-64.

173. Stessin AM, Schwartz A, Judanin G, Pannullo SC, Boockvar JA, Schwartz TH, et al. Does adjuvant external-beam radiotherapy improve outcomes for nonbenign meningiomas? A Surveillance, Epidemiology, and End Results (SEER)-based analysis. J Neurosurg. 2012 Oct;117(4):669–75.

174. Collins GS, Reitsma JB, Altman DG, Moons KGM. Transparent Reporting of a multivariable prediction model for Individual Prognosis or Diagnosis (TRIPOD): the TRIPOD statement. Ann Intern Med. 2015 Jan 6;162(1):55–63.

175. Ripley BD. Pattern Recognition and Neural Networks. Cambridge University Press; 2007. 403 p.

176. Pedregosa F, Varoquaux G, Gramfort A, Michel V, Thirion B, Grisel O, et al. Scikit-learn: Machine Learning in Python. J Mach Learn Res. 2011;12(Oct):2825–30.

177. Lemaître G, Nogueira F, Aridas CK. Imbalanced-learn: A Python Toolbox to Tackle the Curse of Imbalanced Datasets in Machine Learning. J Mach Learn Res. 2017;18(17):1–5.

178. Raschka S. MLxtend: Providing machine learning and data science utilities and extensions to Python's scientific computing stack. JOSS. 2018 Apr 22;3(24):638.

179. Breiman L. Random Forests. Mach Learn. 2001 Oct 1;45(1):5–32.

180. Platt JC. Probabilistic Outputs for Support Vector Machines and Comparisons to Regularized Likelihood Methods. In: ADVANCES IN LARGE MARGIN CLASSIFIERS. 1999.

181. Bergstra J, Bengio Y. Random Search for Hyper-Parameter Optimization. J Mach Learn Res. 2012;13(Feb):281–305.

182. Liu M, Xu C, Luo Y, Xu C, Wen Y, Tao D. Cost-Sensitive Feature Selection by Optimizing F-Measures. IEEE Trans Image Process. 2018 Mar;27(3):1323–35.

183. Ozenne B, Subtil F, Maucort-Boulch D. The precision--recall curve overcame the optimism of the receiver operating characteristic curve in rare diseases. J Clin Epidemiol. 2015 Aug;68(8):855–9.

184. Heagerty PJ, Lumley T, Pepe MS. Time-dependent ROC curves for censored survival data and a diagnostic marker. Biometrics. 2000;56(2):337–44.

185. Pölsterl S, Navab N, Katouzian A. Fast Training of Support Vector Machines for Survival Analysis. In: Machine Learning and Knowledge Discovery in Databases. Springer International Publishing; 2015. p. 243–59.

186. CB Insights. The Complete List of Unicorn Companies [Internet]. 2020 [cited 2020 Jan 22]. Available from: https://www.cbinsights.com/research-unicorn-companies

187. Blumenthal D. Why Google's Move into Patient Information Is a Big Deal. Harvard Business Review [Internet]. 2019 Nov 26 [cited 2020 Jan 26]; Available from: https://hbr.org/2019/11/why-googles-move-into-patient-information-is-a-big-deal

188. Hendricks-Sturrup RM, Prince AER, Lu CY. Direct-to-Consumer Genetic Testing and Potential Loopholes in Protecting Consumer Privacy and Nondiscrimination. JAMA. 2019 May 21;321(19):1869–70.

189. GlaxoSmithKline. GSK and 23andMe sign agreement to leverage genetic insights for the development of novel medicines [Internet]. 2018 [cited 2020 Jan 26]. Available from: https://www.gsk.com/en-gb/media/press-releases/gsk-and-23andme-sign-agreement-to-leverage-genetic-insights-for-the-development-of-novel-medicines/

190. Liu X, Faes L, Kale AU, Wagner SK, Fu DJ, Bruynseels A, et al. A comparison of deep learning performance against health-care professionals in detecting diseases from medical imaging: a systematic review and meta-analysis. The Lancet Digital Health. 2019 Oct 1;1(6):e271–97.

191. Spector M, Hals T. Exclusive: OxyContin maker Purdue is "Pharma Co X" in U.S. opioid kickback probe - sources. Reuters [Internet]. 2020 Jan 28 [cited 2020 Jan 30]; Available from: https://www.reuters.com/article/us-purdue-pharma-investigation-opioids-e-idUSKBN1ZR2RY

192. McKinney SM, Sieniek M, Godbole V, Godwin J, Antropova N, Ashrafian H, et al. International evaluation of an AI system for breast cancer screening. Nature. 2020 Jan;577(7788):89–94.

193. Reddy CL, Mitra S, Meara JG, Atun R, Afshar S. Artificial Intelligence and its role in surgical care in low-income and middle-income countries. The Lancet Digital Health. 2019 Dec 1;1(8):e384–6.

194. Moreau JT, Hankinson TC, Baillet S, Dudley RWR. Individual-patient prediction of meningioma malignancy and survival using the Surveillance, Epidemiology, and End Results database. npj Digital Medicine. 2020 Jan 30;3(1):12.

195. Penny WD, Friston KJ, Ashburner JT, Kiebel SJ, Nichols TE. Statistical Parametric Mapping: The Analysis of Functional Brain Images. Elsevier; 2011. 656 p.

196. Martí Fuster B, Esteban O, Planes X, Aguiar P, Crespo C, Falcon C, et al. FocusDET, a new toolbox for SISCOM analysis. Evaluation of the registration accuracy using Monte Carlo simulation. Neuroinformatics. 2013 Jan;11(1):77–89.

197. Li X, Morgan PS, Ashburner J, Smith J, Rorden C. The first step for neuroimaging data analysis: DICOM to NIfTI conversion. J Neurosci Methods. 2016 May 1;264:47–56.

198. Abraham A, Pedregosa F, Eickenberg M, Gervais P, Mueller A, Kossaifi J, et al. Machine learning for neuroimaging with scikit-learn. Front Neuroinform. 2014 Feb 21;8:14.

199. Kazemi NJ, Worrell GA, Stead SM, Brinkmann BH, Mullan BP, O'Brien TJ, et al. Ictal SPECT statistical parametric mapping in temporal lobe epilepsy surgery. Neurology. 2010 Jan 5;74(1):70–6.

200. Bagic A, Funke ME, Ebersole J, ACMEGS Position Statement Committee. American Clinical MEG Society (ACMEGS) position statement: the value of magnetoencephalography (MEG)/magnetic source imaging (MSI) in noninvasive presurgical evaluation of patients with medically intractable localization-related epilepsy. J Clin Neurophysiol. 2009 Aug;26(4):290–3.

201. Rampp S, Stefan H, Wu X, Kaltenhäuser M, Maess B, Schmitt FC, et al. Magnetoencephalography for epileptic focus localization in a series of 1000 cases. Brain. 2019 Oct 1;142(10):3059–71.

202. Pellegrino G, Hedrich T, Chowdhury R, Hall JA, Lina J-M, Dubeau F, et al. Source localization of the seizure onset zone from ictal EEG/MEG data. Hum Brain Mapp. 2016 Jul;37(7):2528–46.

203. Blumcke I, Spreafico R, Haaker G, Coras R, Kobow K, Bien CG, et al. Histopathological Findings in Brain Tissue Obtained during Epilepsy Surgery. N Engl J Med. 2017 Oct 26;377(17):1648–56.

204. Schurr J, Coras R, Rössler K, Pieper T, Kudernatsch M, Holthausen H, et al. Mild Malformation of Cortical Development with Oligodendroglial Hyperplasia in Frontal Lobe Epilepsy: A New Clinico-Pathological Entity. Brain Pathol. 2017 Jan;27(1):26–35.

205. Mata-Mbemba D, Iimura Y, Hazrati L-N, Ochi A, Otsubo H, Snead OC 3rd, et al. MRI, Magnetoencephalography, and Surgical Outcome of Oligodendrocytosis versus Focal Cortical Dysplasia Type I. AJNR Am J Neuroradiol. 2018 Dec;39(12):2371–7.

206. Sakuma S, Halliday WC, Nomura R, Ochi A, Otsubo H. Increased population of oligodendroglia-like cells in pediatric intractable epilepsy. Neurosci Lett. 2014 Apr 30;566:188–93.

207. Sakuma S, Halliday WC, Nomura R, Baba S, Sato Y, Okanari K, et al. Increased subcortical oligodendroglia-like cells in pharmacoresistant focal epilepsy in children correlate with extensive epileptogenic zones. Epilepsia. 2016 Dec;57(12):2031–8.

208. Hartlieb T, Winkler P, Coras R, Pieper T, Holthausen H, Blümcke I, et al. Age-related MR characteristics in mild malformation of cortical development with oligodendroglial hyperplasia and epilepsy (MOGHE). Epilepsy Behav. 2019 Feb;91:68–74.

209. Garganis K, Kokkinos V, Zountsas B, Dinopoulos A, Coras R, Blümcke I. Temporal lobe "plus" epilepsy associated with oligodendroglial hyperplasia (MOGHE). Acta Neurol Scand. 2019 Oct;140(4):296–300.

210. Verentzioti A, Blumcke I, Alexoudi A, Patrikelis P, Siatouni A, Korfias S, et al. Epileptic Patient with Mild Malformation of Cortical Development with Oligodendroglial Hyperplasia and Epilepsy (MOGHE): A Case Report and Review of the Literature. Case Rep Neurol Med. 2019 Jun 9;2019:9130780.

211. Bankhead P, Loughrey MB, Fernández JA, Dombrowski Y, McArt DG, Dunne PD, et al. QuPath: Open source software for digital pathology image analysis. Sci Rep. 2017 Dec 4;7(1):16878.

212. Han X, Kwitt R, Aylward S, Bakas S, Menze B, Asturias A, et al. Brain extraction from normal and pathological images: A joint PCA/Image-Reconstruction approach. Neuroimage. 2018 Aug 1;176:431–45.

213. Fischl B. FreeSurfer. Neuroimage. 2012 Aug 15;62(2):774–81.

214. Ganzetti M, Wenderoth N, Mantini D. Whole brain myelin mapping using T1- and T2-weighted MR imaging data. Front Hum Neurosci. 2014 Sep 2;8:671.

215. Tadel F, Baillet S, Mosher JC, Pantazis D, Leahy RM. Brainstorm: a user-friendly application for MEG/EEG analysis. Comput Intell Neurosci. 2011 Apr 13;2011:879716.

216. Jenkinson M, Beckmann CF, Behrens TEJ, Woolrich MW, Smith SM. FSL. Neuroimage. 2012 Aug 15;62(2):782–90.

217. Hamilton BE, Nesbit GM. MR imaging identification of oligodendroglial hyperplasia. AJNR Am J Neuroradiol. 2009 Aug;30(7):1412–3.

218. Koeller KK, Rushing EJ. Oligodendroglioma and its variants: radiologic-pathologic correlation. Radiographics. 2005 Nov;25(6):1669–88.

219. Khalid L, Carone M, Dumrongpisutikul N, Intrapiromkul J, Bonekamp D, Barker PB, et al. Imaging characteristics of oligodendrogliomas that predict grade. AJNR Am J Neuroradiol. 2012 May;33(5):852–7.